

Origins of cell-to-cell variability in apoptosis

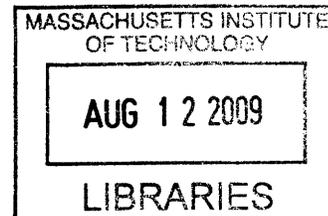
By

Sabrina Leigh Spencer

M.S. Human Genetics
University of Michigan, 2003

B.S. Biology
The George Washington University, 2001

B.A. French Language and Literature
The George Washington University, 2001



ARCHIVES

Submitted to the Computational and Systems Biology Program in partial fulfillment of the requirements for the degree of

**Doctor of Philosophy in Computational and Systems Biology
at the
Massachusetts Institute of Technology**

June 2009

©2009 Massachusetts Institute of Technology. All rights reserved.

Signature of Author: _____

Certified by: _____

Accepted by: _____

A I A

[Signature] Computational and Systems Biology Program
May 15, 2009

[Signature]

Peter K. Sorger
Professor of Systems Biology
Professor of Biological Engineering
Thesis Supervisor

Christopher Burge
Associate Professor of Biology
Director, Computational and Systems Biology Graduate Program

Thesis Committee

Douglas A. Lauffenburger
Whitaker Professor of Biological Engineering, Chemical Engineering, and Biology
(Massachusetts Institute of Technology)
Thesis Committee Chair

Peter K. Sorger
Professor of Biological Engineering (Massachusetts Institute of Technology)
and Professor of Systems Biology (Harvard Medical School)
Thesis Supervisor

Alexander van Oudenaarden
Professor of Physics (Massachusetts Institute of Technology)
Thesis Committee Member

Anthony Letai
Assistant Professor of Medicine, Dana-Farber Cancer Institute (Harvard Medical School)
Thesis Committee Member

Origins of cell-to-cell variability in apoptosis

by
Sabrina Leigh Spencer

Submitted to the Computational and Systems Biology Program on May 15, 2009,
in partial fulfillment of the requirements for the degree of
Doctor of Philosophy in Computational and Systems Biology

Abstract

Diversity within a population of organisms is typically ascribed to genetic differences. However, even members of a genetically identical group of cells or organisms in identical environments can exhibit variability in state and phenotype. One striking example of such heterogeneity is revealed when a genetically identical population of human cells is exposed to saturating doses of a death-inducing drug called TRAIL – many cells in the population will undergo apoptosis, a form of controlled cell death, but a fraction of cells always survives the treatment.

The goal of this thesis was to understand the origins of variability in both the timing and the probability of death in TRAIL-induced apoptosis. To this end, both experimental and computational methods were implemented. Experiments examining the response of sister cells to TRAIL provided strong evidence that variability in initial conditions played a key role, and ruled out genetic, stochastic, and cell cycle effects as possible causes of heterogeneity in response. A detailed analysis of the relative contributions of three segments of the TRAIL pathway revealed that the majority of the variability in time-to-death arose upstream of mitochondrial outer membrane permeabilization (MOMP), with little contribution from downstream reactions. More specifically, the rate of cleavage of initiator caspase substrates was highly predictive of a cell's death time. However, to determine whether (as opposed to when) a cell will die, variation in the MOMP threshold became critical. This dependency was indicated by observation of the height of the MOMP threshold in surviving and dying cells and by modulation of this threshold via overexpression of anti-apoptotic regulators of MOMP. Simulations of cell-to-cell variability in TRAIL-induced apoptosis confirmed that the endogenous variability in apoptotic regulators was sufficient to produce the observed variability in death time. However, knowledge of the concentration of individual proteins did not allow prediction of death time because variation in other proteins masked the underlying trends. The ability to simulate heterogeneity in cellular response also led to the development of novel, biologically intuitive methods of sensitivity analysis, which revealed that sensitivities shift depending on whether knowledge of covariance in initial conditions is included.

The ability to predict sensitivity and resistance of tumors to TRAIL would be clinically valuable, as TRAIL is currently in clinical trials as an anti-cancer therapy. The results described here represent progress toward understanding the “fractional killing” of tumor cells following exposure to chemotherapy, and for understanding variability in mammalian signaling pathways in general.

Supervisor: Peter Sorger, Ph.D.

Title: Professor of Systems Biology, Harvard Medical School

Professor of Biological Engineering, Massachusetts Institute of Technology

Acknowledgements

I am very grateful to have had the opportunity to complete this thesis amidst wonderful colleagues. The work presented in this thesis would not have been possible without the resources, ideas, and group put in place by my thesis advisor, Peter Sorger. Peter's lab has been an exciting, diverse, and creative place to do biology where I had full freedom to pursue my own ideas with support when I needed it. Peter's love of science is truly inspiring and I thank him for making my time as a PhD student successful, exciting, and fun.

I would also like to thank my thesis committee members individually. First, Doug Lauffenburger has lent his encouragement and advice since I came to MIT and I thank him for serving as the chair of my committee. Second, I would like to thank Alexander van Oudenaarden, who advised me early on in my PhD on topics relating to noise in gene expression. Third, I would like to thank Tony Letai, who advised me after our lab moved to Harvard Medical School on topics relating to apoptosis and on general academic decisions. I also thank Tony for bringing the topic of fractional kill to my attention, which increased the potential clinical implications of my work.

I would like to acknowledge two institutes for helping me to make the transition from biology to systems biology. The opportunity to attend the Santa Fe Institute's summer program in 2003 allowed me to make contact with others who were interested in modeling biological systems and solidified my desire to pursue topics in the developing field of systems biology. I would also like to thank MIT for creating a PhD program in Computational and Systems Biology at just the right moment for me, as well as the admissions committee who accepted me into their first class.

I am deeply indebted to my four co-authors and collaborators in the Sorger Lab. John Albeck has been like a second mentor to me, always providing useful advice and serving as a sounding board. I will certainly miss scheming about science with him. Recently, I have also collaborated closely with Suzanne Gaudet, who was wonderful to work with during the sister paper resubmissions and on the material in Chapter 3. I would also like to thank my colleagues Debbie Flusberg and John Burke, with whom I have enjoyed many enlightening conversations. I have been very privileged to have these four talented scientists as co-authors and collaborators.

Many members of the Sorger Lab have contributed to my thesis in various ways. Thanks to Paul Jasper, Jeremy Muhlich, Leo Alexopoulos, Floris Fojjer, Julio Saez-Rodriguez, Bree Aldridge, Hung Nguyen, Bjorn Millard, Eugenio Marco-Rubio, Carlos Lopez, Will Chen, and Holger Conzelmann. I would especially like to thank my class-mate and bay-mate Laura Sontag-Kleiman for the good times and science conversations as we moved through classes, quals, rotations, teaching, and research together at MIT and Harvard. I also want to acknowledge Tom Norman, Ron Milo, German Enciso, Johan Paulsson, and Becky Ward in the Department of Systems Biology at Harvard for insightful comments and conversations. I am grateful to have spent 2.5 years in the Department of Systems Biology, an almost magical place where science is always fun and collaborations across disciplines are the norm. It is a very special place indeed, and I will miss it.

I enjoyed various extracurricular activities during my PhD from skiing, to Harvard Ballet Company classes, Graduate Student Council, and the MIT ballroom dance team. However, my experiences between June 2005 and June 2006 dancing salsa and serving in the Sidney Pacific student government will be the most fondly remembered. Sidney Pacific was a wonderful home

to me and my experience at MIT was much richer for having lived there for 4.5 years. My friends, most connected to Sidney Pacific in some way, these last five years have kept life fun. In addition to my colleagues listed above, I would especially like to thank Lucy Wong, Obrad Scepanovic, Matt Eddy, Ali Motamedi, Ali Rahimi, Iason Chatzakis, Ivan Skopovi, Neville Sanjana, Cortina McCurry, Rosaria Chiang, Scott Carter, and Brandon Roy for many fond memories, some early on at MIT and others more recently.

I would also like to thank my boyfriend Leeland for being part of my life these last few years. Leeland has been a calming, Canadian presence in my otherwise more erratic lifestyle. I have appreciated his patience, advice, and companionship as I pursued the research in this thesis throughout all the ups and downs.

Finally, I must thank my parents. They have supported me all these years through my varying artistic, literary, and scientific pursuits. Growing up, Dad was always there to help me solve tricky math problems and Mims was always there to proofread my three-part French essays. I am very lucky to have two parents whose knowledge so elegantly spanned the sciences and the humanities. My parents taught me to be curious, to ask questions, and to love learning. They have supplied countless pieces of advice and their wisdom has served me well on many occasions. They have offered encouragement in all of my endeavors from my early science experiments racing earthworms down the hallway to my most recent effort, this PhD thesis. I thank them for the infinite gifts they have given me.

Boston, MA
May, 2009

Table of Contents

| | |
|---|-----------|
| 1 INTRODUCTION | 13 |
| 1.1 Specific Aims | 14 |
| 1.2 Cell-to-cell variability | 15 |
| 1.2.1 <i>Origins of noise in gene expression in prokaryotes and lower eukaryotes ..</i> | <i>15</i> |
| 1.2.2 <i>Variability in the behavior of mammalian cells</i> | <i>19</i> |
| 1.2.3 <i>Modeling cell-to-cell variability</i> | <i>22</i> |
| 1.3 Apoptosis | 23 |
| 1.3.1 <i>The TRAIL-mediated apoptosis pathway</i> | <i>24</i> |
| 1.3.2 <i>TRAIL's natural role in the organism</i> | <i>28</i> |
| 1.3.3 <i>TRAIL as a chemotherapy</i> | <i>28</i> |
| 1.3.4 <i>Monitoring the dynamics of apoptotic events in single cells</i> | <i>31</i> |
| 2 NON-GENETIC ORIGINS OF CELL-TO-CELL VARIABILITY IN TRAIL-INDUCED APOPTOSIS..... | 37 |
| 2.1 Results | 38 |
| 2.2 Discussion..... | 47 |
| 2.3 Methods | 48 |
| 2.3.1 <i>Methods summary</i> | <i>48</i> |
| 2.3.2 <i>Supplementary methods</i> | <i>50</i> |
| 2.4 Supplementary figures | 54 |
| 3 SIMULATING A POPULATION OF TRAIL-TREATED CELLS WITH A POPULATION OF MODELS..... | 65 |
| 3.1 Introduction..... | 66 |
| 3.2 Results..... | 69 |
| 3.2.1 <i>Modeling a population of cells with a population of models</i> | <i>69</i> |
| 3.2.2 <i>Forward propagation of variability in initial conditions to timing of death</i> | <i>72</i> |
| 3.2.3 <i>Correlations in initial conditions reduce variance in death time.....</i> | <i>74</i> |
| 3.2.4 <i>A biologically driven sensitivity analysis.....</i> | <i>75</i> |
| 3.2.5 <i>Reverse prediction of death time given incomplete knowledge of initial conditions.....</i> | <i>79</i> |
| 3.3 Discussion..... | 82 |
| 3.4 Methods..... | 85 |

| | | |
|------------|---|------------|
| 3.5 | Supplementary figures | 88 |
| 4 | CROSSING THE THRESHOLD FOR MITOCHONDRIAL OUTER MEMBRANE PERMEABILIZATION | 97 |
| 4.1 | Observation and modulation of the threshold for MOMP | 98 |
| 4.1.1 | <i>Monitoring the approach to the MOMP threshold in surviving and dying cells.</i> | <i>98</i> |
| 4.1.2 | <i>Co-drugging lowers the threshold for MOMP.....</i> | <i>103</i> |
| 4.2 | Memory of TRAIL treatment in surviving cells and induced transient resistance..... | 104 |
| 4.2.1 | <i>TRAIL treatment induces transient resistance in surviving cells</i> | <i>104</i> |
| 4.2.2 | <i>Transient resistance is due to changes downstream of receptors and initiator caspases but upstream of effector caspases.....</i> | <i>106</i> |
| 4.3 | Pore formation converts a gradual buildup of pro-apoptotic signal into a switch-like commitment to death..... | 107 |
| 4.3.1 | <i>MOMP is complete by the time dying cells have assembled relatively few pores</i> | <i>108</i> |
| 4.4 | Future directions..... | 111 |
| 5 | CONCLUSIONS | 113 |
| 5.1 | Summary of major contributions..... | 113 |
| 5.2 | Relevance of this work..... | 114 |
| 5.2.1 | <i>Evolutionary advantages and disadvantages of variability.....</i> | <i>114</i> |
| 5.2.2 | <i>Cancer stem cells</i> | <i>117</i> |
| 5.2.3 | <i>Fractional killing of tumors</i> | <i>119</i> |
| 5.3 | Future Directions | 122 |
| 5.4 | Closing thoughts | 124 |
| 6 | REFERENCES | 127 |

List of Tables

Table 1: Initial conditions and synthesis/degradation rates 63
Table 2: Kinetic rate parameters 64

List of Figures

Chapter 1

Figure 1.1. Intrinsic and extrinsic noise.

Figure 1.2. Protein level dynamics and mixing times in individual cells.

Figure 1.3. The TRAIL-induced apoptosis pathway.

Figure 1.4. A composite picture of effector and initiator caspases in single cells.

Chapter 2

Figure 2.1. Time-to-death is highly correlated between HeLa sister cells but correlation decays as a function of time since division.

Figure 2.2. Endogenous variation in the concentrations of apoptotic regulators is sufficient to explain variability in T_d .

Figure 2.3. A single time-dependent process upstream of MOMP predicts time-to-death.

Figure 2.4. No single protein predicts T_d under normal conditions but overexpression can increase predictability.

Supplementary Figure 2.1. Variability in death time with and without cycloheximide.

Supplementary Figure 2.2. Time of MOMP is correlated in sister MCF10A cells treated with TRAIL plus cycloheximide.

Supplementary Figure 2.3. Cell fate is correlated in sister HeLa cells treated with TRAIL alone.

Supplementary Figure 2.4. Distribution of death time for HeLa sister cells, with and without cycloheximide.

Supplementary Figure 2.5. Comparison of sister cell experiments performed in parallel, with and without cycloheximide.

Supplementary Figure 2.6. Fitting of IC-RP trajectories.

Supplementary Figure 2.7. Contribution of k_{IC} vs. θ .

Supplementary Figure 2.8. Computational analysis suggests that Bid overexpression reduces T_d mean and dispersion.

Supplementary Figure 2.9. Quantitative immunoblots for Bid-GFP and endogenous Bid in HeLa cells.

Chapter 3

Figure 3.1. Measurement of variability in protein levels in the TRAIL-induced apoptosis network.

Figure 3.2. Propagation of variability in initial conditions to produce variability in t_{PARP} .

Figure 3.3. Correlations in protein levels affect the distribution of death times.

Figure 3.4. Effect of knock-down and overexpression of protein levels on t_{MOMP} .

Figure 3.5. The levels of single or double proteins are not detectably different in untreated cells and TRAIL survivors.

Figure 3.6. Knowledge of the initial level of a single protein is not predictive of a cell's death time.

Supplementary Figure 3.1. Validation of antibodies used for measuring protein distributions by flow cytometry.

Supplementary Figure 3.2. Comparison of antibodies to the five proteins described in Methods with their relevant isotype controls.

Supplementary Figure 3.3. Test of protein level distributions for log-normality.

Supplementary Figure 3.4. Quantitative immunoblots for endogenous Bcl-2 and GFP-Bcl-2 in HeLa cells.

Supplementary Figure 3.5. Quantitative immunoblots for endogenous Bcl-x_L and GFP-Bcl-x_L in HeLa cells.

Supplementary Figure 3.6. Increasing Bcl-2 and Bcl-x_L levels cause a slight increase in t_{MOMP} .

Supplementary Figure 3.7. Sensitivity to doubling the level of Bcl-2.

Supplementary Figure 3.8. Selection of cells that survive a 2.5 hr treatment with 50 ng/ml TRAIL plus cycloheximide and comparison of duplicate samples.

Chapter 4

Figure 4.1. The approach to the MOMP threshold in surviving and dying cells.

Figure 4.2. Cycloheximide lowers the MOMP threshold in HeLa cells treated with TRAIL.

Figure 4.3. Transient resistance to TRAIL-induced apoptosis in cells which survive an initial challenge.

Figure 4.4. Transient TRAIL-resistance is not due to receptor desensitization.

Figure 4.5. Formation of GFP-Bax and GFP-Bak puncta in synchrony with MOMP in HeLa cells.

Chapter 1

1 Introduction

The description of apoptosis 37 years ago (Kerr, Wyllie et al. 1972) and the subsequent identification of the core set of regulatory genes in *C. elegans* (Ellis and Horvitz 1986) inspired the modern era of apoptosis research, but the critical role of cell death in development and homeostasis of multicellular organisms had been appreciated for over 100 years (Clarke and Clarke 1995). In a healthy adult human, billions of cells die each hour in the intestine and bone marrow; this loss of cells must be balanced by an equal number of cell divisions to maintain constant body size (Vaux and Korsmeyer 1999; Alberts, Johnson et al. 2002). An imbalance in the amount of apoptosis relative to the level of proliferation can result in diseases such as neurodegenerative and auto-immune disorders in the case of too much apoptosis or cancer in the case of too little apoptosis. In fact, the discovery that the anti-apoptotic protein Bcl-2 is often over-expressed in cancer was the first indication that cancer is a result not only of over-active proliferation but also of suppressed apoptosis (Vaux, Cory et al. 1988; Hockenbery, Nunez et al. 1990). The ultimate goal of cancer treatment is to induce apoptosis in cancer cells while leaving normal cells unaffected (Letai 2008). However, cancer cells can be refractory to chemotherapy for a variety of reasons including genetic mutations causing resistance to the drug or

ineffectiveness of the drug if a cell is passing through a certain phase of the cell cycle (Skeel 2003). These two explanations are the most frequently quoted for why some cells live and some cells die in response to chemotherapy. However, beyond these two explanations, there are a number of other factors that can also contribute to partial chemotherapy resistance, such as heterogeneity in the tumor microenvironment and local interaction with stromal cells. Largely unaddressed is whether natural fluctuations in the levels or activity states of proteins and other biomolecules produce sufficient variation from cell to cell to have an impact on a cell's fate after an apoptotic trigger. It is this question that my thesis addresses.

1.1 Specific Aims

The overall goal of this thesis was to examine the causes of non-genetic variability in apoptosis at the single cell level. The first aim was experimental in nature, and focused primarily on the origins of heterogeneity in the timing of TRAIL-induced apoptosis. These experiments involved tracking cell pedigrees with time-lapse imaging to determine whether cells with similar initial conditions would die at similar times. Live-cell microscopy of apoptotic events, monitored with fluorescent reporters, was used to determine which biochemical reactions were primarily involved in generating this variability in death time. Lastly, the levels of various proteins involved in cell death were varied to assess their impact on the timing of apoptosis.

The second aim computationally addressed how variability in the levels of apoptotic regulators propagated through the network to produce heterogeneity in the apoptotic response. A population of cells was modeled with a population of models, with variability in each 'cell' produced by sampling from measured distributions of protein levels. Using this framework, the sensitivities of apoptotic regulators, the impact of correlations in initial conditions, and the

degree to which knowledge of individual protein levels allows prediction of cellular death time were assessed.

The third aim was again experimental in nature and examined the differences between cells that survive TRAIL treatment and cells that succumb. Cells that survived a first TRAIL stimulation were re-challenged with TRAIL and assessed for their ability to resist this second treatment as well as the duration of any refractory period. Next, the biochemical reactions governing the approach to the ‘point of no return’ (mitochondrial outer membrane permeabilization - MOMP) were monitored in single cells to identify the features of cells that do and do not cross this threshold. Finally, the reactions at the MOMP threshold that convert a gradual buildup of pro-apoptotic signals to a switch-like commitment to death were examined.

1.2 Cell-to-cell variability

Diversity within a population of organisms is typically ascribed to genetic differences. However, even members of a genetically identical group of cells or organisms in identical environments can exhibit variability in state and phenotype. Only in the last decade have the origins of non-genetic variability begun to be addressed in mechanistic terms. A thorough review of this topic was recently published (Raj and van Oudenaarden 2008); here I highlight the literature relevant to this thesis.

1.2.1 Origins of noise in gene expression in prokaryotes and lower eukaryotes

“Non-genetic individuality” in bacterial chemotaxis was first reported over 30 years ago (Spudich and Koshland 1976), but it was not until the late 1990s that theoretical work on stochastic gene expression prompted interest in the sources of this noise (McAdams and Arkin 1997; Arkin, Ross et al. 1998). This theoretical work modeled stochastic chemical kinetics to

show that protein numbers could fluctuate significantly and that these fluctuations could contribute to the apparently stochastic decision to activate the lytic or lysogenic pathway of lambda phage (McAdams and Arkin 1997; Arkin, Ross et al. 1998).

The first experiment to analyze the sources of noise in gene expression involved tagging two copies of the same promoter with a fluorescent protein in *E. coli* – one with cyan fluorescent protein (CFP) and one with yellow fluorescent protein (YFP) (Elowitz, Levine et al. 2002). This system allowed the authors to distinguish between “extrinsic noise” (fluctuations that affect both copies of the gene equally in the same cell, but may vary from cell to cell) and “intrinsic noise” (fluctuations caused by the inherent stochasticity in transcription and translation). If cell-to-cell variability in protein levels were due only to intrinsic fluctuations, the CFP and YFP levels would not be correlated in a single cell; if noise were only due to extrinsic fluctuations, CFP and YFP levels would be tightly correlated. The authors found that both sources of noise contributed to produce cell-to-cell variability in gene expression (Fig. 1.1).

The van Oudenaarden group predicted (Thattai and van Oudenaarden 2001) and showed experimentally (Ozbudak, Thattai et al. 2002) that the variability in protein expression level in a population would be anti-correlated with the rate of transcription, but would be unaffected by the rate of translation because proteins are produced rapidly in “bursts” from a single transcript. Subsequent studies in eukaryotes (initially yeast and later higher eukaryotes) found that the sources of noise were different from those in prokaryotes in several ways (Blake, M et al. 2003; Raser and O'Shea 2004; Becskei, Kaufmann et al. 2005; Blake, Balazsi et al. 2006). The observed differences were compatible with models encoding transcriptional bursts in which a gene randomly switches between transcriptional activity and inactivity. A likely explanation is

chromatin remodeling, for which there is suggestive but no direct evidence (Raj and van Oudenaarden 2008).

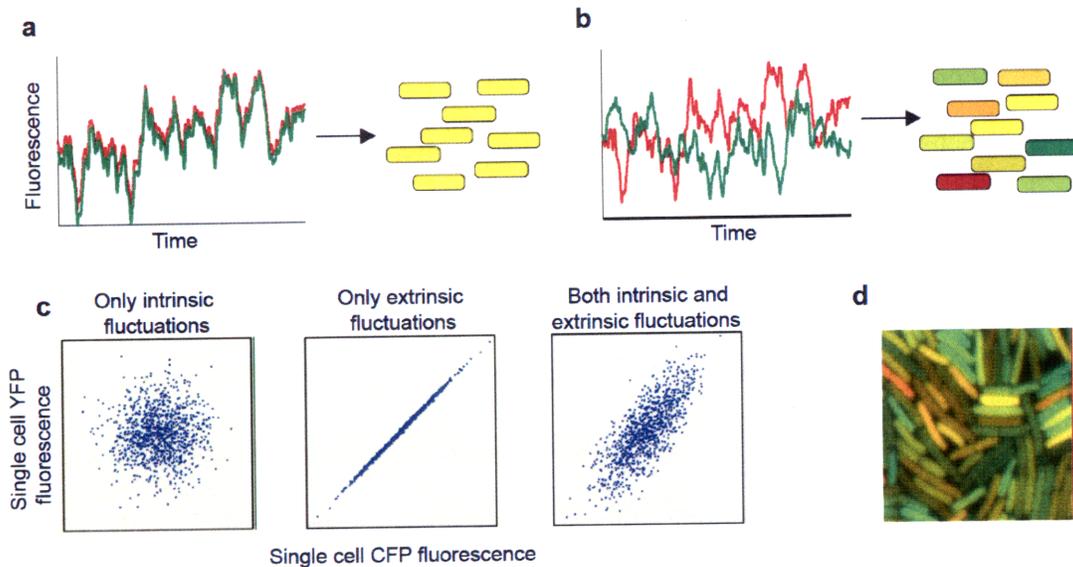


Figure 1.1. Intrinsic and extrinsic noise can be measured and distinguished with two genes (*cfp*, shown in green; *yfp* shown in red) controlled by identical regulatory sequences. Cells with the same amount of each protein appear yellow, whereas cells expressing more of one fluorescent protein than the other appear red or green. **a**, In the absence of intrinsic noise, the two fluorescent proteins fluctuate in a correlated fashion over time in a single cell (left). Thus, in a population, each cell will have the same amount of both proteins, although that amount will differ from cell to cell because of extrinsic noise (right). **b**, Expression of the two genes may become uncorrelated in individual cells because of intrinsic noise (left), giving rise to a population in which some cells express more of one fluorescent protein than the other (right). **c**, Expected cell-to-cell variations when fluctuations are intrinsic, extrinsic, or both. **d**, *E. coli* showing significant amounts of intrinsic noise. CFP and YFP fluorescence images were combined in the green and red channels, respectively. **a**, **b** and **d** are reprinted from *Science*, 297(5584), Elowitz MB, Levine AJ, Siggia ED, Swain PS. "Stochastic gene expression in a single cell", 1183-6, (2002), with permission from Elsevier. **c** is reprinted from *Cell*, 135(2), Raj A, van Oudenaarden A. "Nature, nurture, or chance: stochastic gene expression and its consequences", 216-26, (2008), with permission from AAAS.

Noise in gene expression in yeast is primarily extrinsic in origin, with contributions from cell size, cell cycle state, variations in common upstream factors, and location of the gene being transcribed (Raser and O'Shea 2004; Becskei, Kaufmann et al. 2005; Newman, Ghaemmaghami et al. 2006; Volfson, Marciniak et al. 2006). In support of this, one study quantified the various sources of noise on the yeast mating pheromone response pathway and found that most of the variability was due to pre-existing differences between cells that propagate the signal (Colman-Lerner, Gordon et al. 2005). In multicellular eukaryotes, despite the larger cell size and

increased number of molecules, cell-to-cell variability can be considerable. Reports studying *Dictyostelium* and Chinese hamster ovary cells have found that transcriptional bursts are infrequent but long-lasting, producing high variation from cell to cell in mRNA number (Chubb, Trecek et al. 2006; Raj and van Oudenaarden 2008).

Another important consideration is the role of network architecture on noise propagation, minimization, and amplification. Noise in an upstream regulator was found to propagate to a downstream gene, adding to the intrinsic noise inherent in the downstream gene's output (Pedraza and van Oudenaarden 2005). Negative and positive feedback loops are common network motifs found in biology. Negative feedback can reduce the effects of noise in a system, bringing the signal back to the set point by correcting deviation from that set point (Becskei and Serrano 2000; Austin, Allen et al. 2006; Dublanche, Michalodimitrakis et al. 2006). Positive feedback can have the opposite effect, acting to amplify small fluctuations, potentially flipping a switch from an "on" to an "off" state. Cooperativity can act to maintain a given state, buffering it against small fluctuations which could flip its state, and providing a long-term protein-level memory. This bistability has been observed in networks containing positive feedback loops, such as spontaneous entry into competence (a transiently differentiated state where DNA can be taken up from the environment) in *Bacillus subtilis* (Suel, Garcia-Ojalvo et al. 2006; Suel, Kulkarni et al. 2007).

In the last decade, much has been learned about the causes of noise in gene expression. There is now increasing interest in assessing whether cell-to-cell differences in protein levels resulting from noisy gene expression have important physiological consequences for cells, or whether cells have evolved to be robust to these fluctuations.

1.2.2 Variability in the behavior of mammalian cells

Studies of variability in mammalian cells are less common, and variability at the gene and protein levels is rarely linked to variability in phenotypic outcome, although it is known that cells can vary widely in their responses to physiological stimuli. Since the start of this thesis work (June 2005), several research papers have been published on the topic of variability in mammalian cells.

A pioneering study measured fluctuations in the levels of 20 endogenous proteins over time in living human cells (Sigal, Milo et al. 2006). The proteins were tagged with YFP at their endogenous locus and tracked by live cell microscopy under normal growth conditions for several generations. This method allowed dynamic observation of protein level heterogeneity and examined whether cells that have higher than average protein levels eventually become lower. This mixing occurred for all proteins, and the half-life for mixing time was found to range between 0.8 cell generations for proteins with narrowly distributed expression and 2.5 cell generations for proteins with broadly distributed expression (Fig. 1.2). This persistent memory of protein levels could result in ‘outlier’ cells and may underlie variability in cell behavior. The observed long-lasting memory suggests that several cell cycles might be needed for a population of cells to reach a certain multidimensional state where all cells will be fully affected by a certain drug or signal; this finding is relevant to the results in Chapter 4.

Other studies have examined variability in cell behavior after some perturbation. For example, live cell microscopy has been used to study the oscillatory dynamics of the tumor suppressor p53 after DNA damage (Lahav, Rosenfeld et al. 2004; Geva-Zatorsky, Rosenfeld et al. 2006). These studies found that identical cells respond very differently to DNA damage – some cells had zero pulses of p53, while others oscillated for three days (more than 10 peaks) (Lahav, Rosenfeld et al. 2004; Geva-Zatorsky, Rosenfeld et al. 2006). Single-cell imaging of

NF κ B localization after stimulation with tumor necrosis factor alpha (TNF α) also revealed asynchronous oscillations (Nelson, Ihekweba et al. 2004).

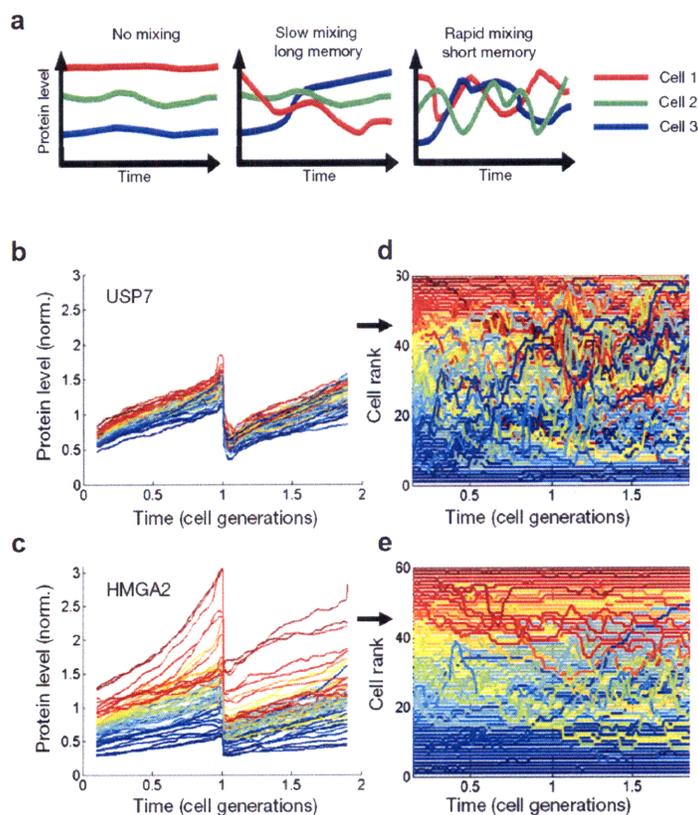


Figure 1.2. a, Possible mixing dynamics of a protein in a population of cells. b, c, Dynamics of cells expressing YFP-tagged USP7 and HMGA2 across two cell generations. Each line represents the protein level of one cell, normalized to the population mean. d, e, Ranks of 60 randomly selected cells for USP7 and HMGA2 through two cell generations, where 1 is the lowest and 60 is the highest protein level in the population at the given time point. Lines are colour-coded for rank at the start of the first cell cycle, with red being high relative to the mean and blue low. From these data, the auto-correlations of protein level ranks are calculated. Reprinted by permission from Macmillan Publishers Ltd: *Nature*, 444(7119), Sigal A, Milo R, Cohen A, Geva-Zatorsky N, Klein Y, Liron Y, Rosenfeld N, Danon T, Perzov N, Alon U. "Variability and memory of protein levels in human cells", 643-6, (2006).

Flow cytometry was used in three recent studies to observe the effects of endogenous variability in protein levels. In one study, variability in the activation of a clonal population of T cells could be linked to endogenous variability in the levels of two proteins, CD8 and SHP-1 (Feinerman, Veiga et al. 2008). Another study found significant heterogeneity in the levels of the stem cell marker, Sca-1 (Chang, Hemberg et al. 2008). Sorting for cells with low and high Sca-1 levels revealed that the level of this protein governs the propensity to differentiate into the erythroid or myeloid lineage (Chang, Hemberg et al. 2008). A second independent but related report observed noteworthy heterogeneity in the expression levels of the stem cell master regulator, Nanog (Chambers, Silva et al. 2007). This group observed a reduced capacity for self-

renewal in embryonic stem cells sorted to have low Nanog levels and an increased propensity to differentiate in cells sorted to have high Nanog levels (Chambers, Silva et al. 2007).

The first studies to note that apoptosis proceeds at different rates in different cells were published in 2000 (Goldstein, Kluck et al. 2000; Tyas, Brophy et al. 2000). One report noted that stronger apoptotic stimuli induce earlier death but found no correlation between the time of onset of apoptosis and the duration of the apoptotic process (Goldstein, Kluck et al. 2000). Both of these results were later confirmed by our group in a dynamic study of apoptosis in single cells using live-cell reporters of apoptotic events (Albeck, Burke et al. 2008a; Albeck, Burke et al. 2008b). Another study characterized the response of 15 cell lines to three different classes of antimetabolic drugs and found significant inter- as well as intra-line variation, with cells within any given cell line exhibiting multiple behaviors in response to treatment (Gascoigne and Taylor 2008). A recent paper identified two proteins whose levels rise in cells that survive treatment with the cancer drug camptothecin and decrease in cells that died, thereby correlating variability arising *subsequent* to treatment with cell fate (Cohen, Geva-Zatorsky et al. 2008). However, the cause of this bifurcation in protein levels was not addressed, preventing *a priori* prediction of which cells will live and which will die.

In summary, the origins of variability in protein levels have been well described in prokaryotes and yeast, the time-scale of protein level fluctuations in unperturbed human cells has been characterized, and variability has been observed in several signaling pathways including DNA damage, T cell activation, differentiation, and apoptosis. However, no study has examined whether pre-treatment protein-level variability has any cell fate consequences in the context of apoptosis.

1.2.3 Modeling cell-to-cell variability

As it becomes feasible to study single cells rather than the average behavior of a population, new modeling frameworks will be required to describe this heterogeneity. Continuous deterministic models are appropriate when the number of reactants is large, but will become inaccurate when the number of reactants falls below ~ 10 , as molecular populations change by discrete integer amounts. The dynamics of such a biological system can be modeled using a stochastic Markov jump process where any change to the system occurs discretely after a random period of time (Wilkinson 2009). This type of process is generally simulated with a stochastic simulation algorithm (Gillespie 1977), which was notably applied to stochastic gene expression (McAdams and Arkin 1997; Arkin, Ross et al. 1998).

In mammalian cells, however, the number of reactants in protein signal transduction pathways is rarely low enough to require stochastic simulations and yet mammalian cells can still vary in phenotype and response. As described in Section 1.2.1, cells are subject to sources of variability other than noise in kinetic biochemical reactions (intrinsic noise). For example, cells may behave differently from one another because they have different initial conditions (RNA or protein levels, activity states, or localizations) at the start of the experiment. This type of variability has previously been referred to as “extrinsic noise” (see Section 1.2.1), but in this work will be referred to as variability in initial conditions. This type of pre-existing variability can be modeled using deterministic equations with random sampling of a distribution of initial conditions, thereby taking into account differences in the starting state of each cell. There is currently no literature which uses a deterministic framework with random sampling of initial conditions to model a population of cells, allowing one to examine how this input variability propagates through a network to produce cell-to-cell variability in a biological response. Such research is the topic of Chapter 3.

1.3 Apoptosis

The apoptotic form of cell death is defined by the controlled activation of caspases; it is often contrasted with necrotic death of cells due to injury causing rupture of the cells and a strong inflammatory response. A hallmark feature of apoptosis is that the cell is internally dismantled into membrane-bound fragments (“apoptotic bodies”) in a controlled fashion that recruits macrophages to engulf apoptotic cells without causing an inflammatory response from the organism (Leist and Jaattela 2001). Apoptosis plays a key role in the development of multicellular organisms as well as in the homeostasis of adult organisms. During development, cells that are produced in excess are eliminated via apoptosis and thus this process is critical for the proper sculpting of organs and tissues (Meier, Finch et al. 2000). An oft-cited example of the role of apoptosis in animal development is the formation of free and independent digits by apoptosis of the interlinking tissue (Zou and Niswander 1996; Zuzarte-Luis and Hurlle 2002). Another example is the control of the size and connectivity of the developing brain, where more than half of the neurons that are initially created die by apoptosis (Hutchins and Barger 1998).

The key role of apoptosis in the biology of organisms implicates this process in a number of diseases and pathologies. A decrease in the required amount of apoptosis can result in diseases such as cancer, auto-immune diseases, and the spreading of viral infections. In contrast, neurodegenerative disorders, AIDS, and ischemic diseases are caused or enhanced by excessive apoptosis (Fadeel, Orrenius et al. 1999). The role of apoptosis in the development of cancer is especially relevant for this thesis. Cells with severely damaged DNA that cannot be repaired or cells with inappropriate mitogenic signaling are instructed to die by apoptosis. If they fail to do so, cancer may develop and in fact, evasion of apoptosis is a hallmark of cancer (Hanahan and

Weinberg 2000). The first oncogene found to cause cancer by preventing apoptosis rather than promoting proliferation was Bcl-2, an anti-apoptotic protein found to be overexpressed by chromosomal translocation in follicular lymphoma and other cancers (Vaux, Cory et al. 1988; Hockenbery, Nunez et al. 1990).

There are two major signaling pathways that lead to apoptosis in mammalian cells – the intrinsic pathway, and the extrinsic or receptor-mediated pathway studied in this thesis. Intrinsic apoptosis is triggered by signals originating inside the cell, such as DNA damage, oxidative stress, and starvation (Kaufmann and Earnshaw 2000; Wang 2001). Some of these signals converge on the tumor suppressor p53, which can stimulate expression of a variety of apoptosis-inducing genes causing a change in the balance of pro- and anti-apoptotic factors. This leads to permeabilization of the mitochondria, followed by effector caspase activation and death of the cell (Miyashita and Reed 1995; Vousden and Lu 2002). In receptor-mediated apoptosis, a protein signaling network controls the transmission of a death signal from receptors on the cell surface to effector caspases that cause cell death, as described below.

1.3.1 The TRAIL-mediated apoptosis pathway

The TRAIL-induced apoptosis pathway is triggered by the binding of TNF-related apoptosis inducing ligand (TRAIL) to its receptors on the cell surface (Fig. 1.3, green arrow). TRAIL is a member of the TNF (tumor necrosis factor) family of death ligands which include TRAIL, FasL, and TNF α , each of which binds to a unique receptor(s). There are two receptors for the TRAIL ligand, DR4 and DR5, which trimerize upon ligand binding. This event triggers assembly of the death-inducing signaling complex (DISC), which recruits several adaptor proteins, including Fadd (Fas-associated death domain) and FLIP (cellular FLICE-inhibitory protein) (Kischkel, Hellbardt et al. 1995; Medema, Scaffidi et al. 1997). Fadd recruits initiator

caspases 8 and 10 (hereafter referred to as C8), which are activated by conformational changes resulting from induced dimerization (Boatright, Renatus et al. 2003; Donepudi, Mac Sweeney et al. 2003). Autocatalytic processing of C8 then occurs and the resulting mature C8 dimer is released into the cytosol (Chang, Xing et al. 2003). The activation of C8 is regulated by FLIP, a protein that is structurally similar to C8 but lacks catalytic activity (Irmeler, Thome et al. 1997). At low levels, FLIP can act as an enhancer of C8 activation by acting as a dimerization partner for C8; at high concentrations, FLIP can act as a “dominant-negative” by competing for C8 binding at the DISC (Chang, Xing et al. 2002; Boatright, Deis et al. 2004).

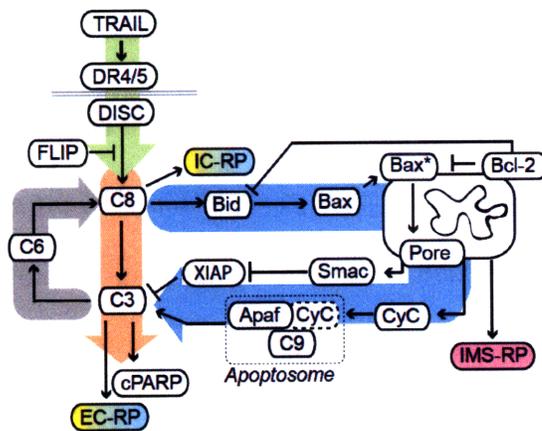


Figure 1.3. The TRAIL-induced apoptosis pathway. Green arrow, TRAIL-receptor binding and activation of the DISC. Orange arrow, initiator caspase cleavage of effector caspases. Blue arrow, the mitochondrial outer membrane permeabilization pathway. Gray arrow, potential positive feedback through caspase-6. Reporter proteins IC-RP, EC-RP, and IMS-RP are indicated. See text for details.

Activated C8 can directly cleave and activate effector caspases 3 and 7 (hereafter C3; Fig 1.3, orange arrow), which are normally present in the cell as inactive pro-caspase homodimers (Pop, Chen et al. 2001). The activating cleavage by C8 enables a conformational change allowing it to form a heterotetramer that opens the active site (Bose, Pop et al. 2003). However, active C3 is held in check by XIAP (X-linked inhibitor of apoptosis) until the mitochondrial pathway is triggered. XIAP is a potent inhibitor of caspases-3, and -7 with inhibition constants of 0.7 and 0.2 nM, respectively (Deveraux, Takahashi et al. 1997). XIAP also contains a RING domain which mediates degradation of active effector caspases via its E3-ubiquitin ligase

activity (Suzuki, Nakabayashi et al. 2001); XIAP can also regulate its own levels by auto-ubiquitination (Yang, Fang et al. 2000).

The mitochondrial pathway can be thought of as a feedforward loop (Fig. 1.3, blue arrow) controlled by pro- and anti-apoptotic Bcl-2-family proteins. In most cell types (often referred to as “type II”), including those examined in this thesis, the feedforward amplification provided by the mitochondrial pathway is required for death. This pathway is activated because C8 also cleaves Bid to activated tBid, a member of the “activator” class of pro-apoptotic Bcl-2 proteins, so called because they in turn activate “effectors” Bax and homolog Bak by induced conformational change (Wei, Lindsten et al. 2000; Wei, Zong et al. 2001; Kuwana, Mackey et al. 2002; Letai, Bassik et al. 2002). Active Bax translocates to the mitochondria, where it multimerizes and acts to form pores in the mitochondrial outer membrane; Bak is naturally present in the mitochondrial outer membrane (Kuwana, Mackey et al. 2002). The pro-apoptotic activity of “activators” and “effectors” is antagonized, however, by the anti-apoptotic Bcl-2 family proteins (including Bcl-2, Bcl-x_L, and Mcl-1) (Oltvai, Milliman et al. 1993; Cheng, Wei et al. 2001). These proteins act as a buffer for activated tBid, Bax, and Bak. When these proteins overwhelm the buffer, pores are formed and MOMP, or mitochondrial outer membrane permeabilization, occurs. In effect, the levels of pro-apoptotic tBid, Bax, and Bak and the anti-apoptotic Bcl-2 (and homologs) set a threshold for MOMP, which is considered to be the “point of no return” in apoptosis (Keeble and Gilmore 2007). This threshold can also be indirectly altered by proteins of the “sensitizer” class, which are structurally similar to the “activator” class, but which cannot directly activate Bax and Bak (Letai, Bassik et al. 2002). Rather, “sensitizers” (such as Bad, Noxa, and BMF) bind to free anti-apoptotic Bcl-2 family proteins, distracting them

from interacting with Bax and Bak, and effectively lowering the threshold for MOMP (Letai, Bassik et al. 2002).

Once MOMP occurs, a potent mixture of pro-apoptotic proteins, including cytochrome *c* and Smac are released from the mitochondrial intermembrane space in an “all-or-none” fashion. Cytochrome *c* forms the apoptosome complex with Apaf-1 and caspase-9, which activates additional C3 (Li, Nijhawan et al. 1997; Rodriguez and Lazebnik 1999; Kim, Du et al. 2005). This activation is aided by Smac’s inhibition of XIAP, freeing C3 from its XIAP-inhibited state (Du, Fang et al. 2000; Verhagen, Ekert et al. 2000). A positive feedback loop mediated by caspase-6 serves to amplify the death signal under certain conditions (Fig 1.3, gray arrow), although this feedback does not seem to be important in the HeLa cells used in this thesis (Albeck, Burke et al. 2008b).

C3 goes on to kill the cell by destroying its genome and proteome. The genome is dismantled via C3 cleavage of ICAD (inhibitor of caspase-activated DNAses). ICAD is typically bound to CAD, holding the DNase activity of CAD in check. When ICAD is cleaved by caspases, CAD is released and creates double-strand breaks in the DNA, fragmenting the genome (Liu, Li et al. 1998; Inohara, Koseki et al. 1999). Another important category of C3 substrates are DNA repair enzymes such as PARP (poly-ADP-ribose polymerase). Cleavage of PARP is often used as a marker for C3 activity (Kaufmann 1989; Tewari, Quan et al. 1995; Fischer, Janicke et al. 2003). A third category of C3 substrates relevant to this thesis includes structural proteins, such as cytokeratins and nuclear lamins, whose cleavage results in the characteristic apoptotic morphology of cell deformation and shrinking (Fischer, Janicke et al. 2003).

1.3.2 TRAIL's natural role in the organism

TRAIL is a ligand native to the human body that is highly expressed by natural killer cells, and may be induced on other leukocytes (Griffith, Wiley et al. 1999; Smyth, Cretney et al. 2001; Takeda, Hayakawa et al. 2001). The presumed biological function of TRAIL is the immune surveillance of tumors, as it has been shown to act as a tumor suppressor in mouse experimental tumor models. For example, two studies showed that TRAIL is important for suppressing sarcomas induced by the chemical carcinogen methylcholanthrene either by administering a neutralizing anti-TRAIL antibody (Takeda, Smyth et al. 2002) or by performing the study in TRAIL-deficient mice (Cretney, Takeda et al. 2002). A third study observed *spontaneous* lymphoid malignancies over the life-span of TRAIL-deficient mice (Zerafa, Westwood et al. 2005).

However, given the incidence of cancer, many tumors must be able to evade immune surveillance. There are a variety of mechanisms by which cancer cells do this; specific to the TRAIL pathway, several genetic lesions have been associated with human tumor onset and progression. The TRAIL receptors DR4 and DR5 maps to human chromosome 8p21-22, a region that is frequently lost in tumors (Johnstone, Frew et al. 2008). Mutations in DR5 have been identified in a proportion of various human tumors, including breast, lung, head and neck, and non-Hodgkin lymphoma (Lee, Shin et al. 1999; Fisher, Virmani et al. 2001; Lee, Shin et al. 2001; Shin, Kim et al. 2001), and there is some (weaker) evidence for mutations in DR4, caspase-8, and Flip causing cancer predisposition (Johnstone, Frew et al. 2008).

1.3.3 TRAIL as a chemotherapy

A main goal of cancer treatment via radiation and chemotherapy is to induce the death of cancer cells by apoptosis. Cancer cells often 'harbor the seeds of their own destruction': the very

oncogenic mutations that allow them to aberrantly proliferate also have the potential to trigger the apoptotic program (Lowe, Cepero et al. 2004). Thus, cancer cells can be particularly sensitive to therapies that re-establish the pro-apoptotic signaling that these abnormal cells have found a way to suppress. Cancer cells may be closer to crossing the threshold for initiation of apoptosis than normal cells, so drugs like ABT-737 (which relieve Bcl-2, Bcl-w, and Bcl-x_L's inhibition of pro-apoptotic Bcl-2 family members) are likely to be effective strategies for cancer cells that are "primed" for death (Letai 2008).

The enthusiasm over TRAIL as a cancer treatment is a result of early observations that it preferentially kills cancer cells over normal cells, and is safe to administer systemically, unlike death ligands FasL and TNF α (Walczak, Miller et al. 1999; Bouralexis, Findlay et al. 2005). Many papers have been published citing various factors responsible for the respective resistance and sensitivity of normal and cancer cells to TRAIL; other studies have compared sensitive and resistant cancer cell lines, producing a similarly long list of critical factors (reviewed in ref. Zhang and Fang 2005). Briefly, expression of three antagonistic TRAIL decoy receptors (DcR1, DcR2, and osteoprotegerin) was initially thought to be responsible for resistance to TRAIL by competing with DR4 or DR5 for TRAIL binding (Degli-Esposti, Dougall et al. 1997; Degli-Esposti, Smolak et al. 1997; Pan, Ni et al. 1997; Sheridan, Marsters et al. 1997; Emery, McDonnell et al. 1998). However, levels of DR4, DR5, and decoy receptors fail to explain all cases of sensitivity or resistance. For example, some studies suggested that the ratio of expression of DR4/5 and decoy receptors determine TRAIL sensitivity (Pan, Ni et al. 1997; Sheridan, Marsters et al. 1997; Kim, Fisher et al. 2000; Ichikawa, Liu et al. 2001; Wang, Engels et al. 2004), but this ratio did not correlate with the sensitivity of hepatocytes to TRAIL (Jo, Kim et al. 2000). One study of melanoma cell lines reported a TRAIL-resistant line expressing

mRNA for DR5 but not for DcR1 and DcR2 and three TRAIL-sensitive lines expressing DcR1, DcR2, or both (Griffith, Wiley et al. 1999). Another study of 18 neuroblastoma cell lines found five that were sensitive to TRAIL but nevertheless expressed DcR1, DcR2, or both (Eggert, Grotzer et al. 2001). Components of the DISC can also play a role in TRAIL resistance. Several types of cancer cells show resistance to TRAIL that correlates with down-regulation or absence of C8 expression (Teitz, Wei et al. 2000; Eggert, Grotzer et al. 2001; Fulda, Kufer et al. 2001; Hopkins-Donaldson, Ziegler et al. 2003; Yang, Merchant et al. 2003). FLIP expression and the C8:FLIP ratio have been reported to correlate with TRAIL resistance in several different tumors, including melanoma, hepatocellular carcinoma, Burkitt's lymphoma, and B-cell chronic lymphocytic leukemia (Tepper and Seldin 1999; Okano, Shiraki et al. 2003). Lastly, downstream factors that are not unique to receptor-mediated apoptosis have also been implicated in TRAIL resistance. These include Bcl-x_L and IAPs (Hinz, Trauzold et al. 2000; Zhang, Zhang et al. 2001; Ng and Bonavida 2002; Ng, Zisman et al. 2002), as well as survival signaling through NF- κ B and the MAP kinase pathway (Zhang and Fang 2005). When considered together, these studies reveal that the selectivity of TRAIL is much more complex than originally thought, as each apparently critical factor is defeated by a few cell lines that break the proposed rule. Single-gene explanations are not likely to explain sensitivity to death-inducing agents as all of these proteins play a role to a greater or lesser extent depending on their concentrations and other aspects of cell physiology. A systems-level measurement should have better success at predicting TRAIL sensitivity.

The capacity of TRAIL to trigger apoptosis preferentially in cancer cells has motivated the development of several TRAIL-related cancer therapies, which are currently in Phase I and Phase II clinical trials. Amgen and Genentech have co-developed a recombinant TRAIL;

Amgen, Genentech, and Human Genome Sciences have separately developed monoclonal antibodies to DR5 (AMG 655, apomab, and lexatumumab, respectively); Human Genome Sciences has developed a monoclonal antibody targeting DR4 (mapatumumab) (Ashkenazi and Herbst 2008). In general, Phase I trials have established that these TRAIL receptor agonists are well-tolerated in patients. Phase II trials are currently evaluating the therapeutic benefit of these drugs as single agents or in combination with other targeted cancer therapies such as bortezomib (a proteasome inhibitor), rituximab (monoclonal antibody against CD20), and bevacizumab (monoclonal antibody against vascular endothelial growth factor) (Ashkenazi and Herbst 2008).

TRAIL receptor agonists can synergize with other drugs to kill TRAIL-resistant cells *in vitro*, perhaps by reducing the heterogeneity in TRAIL-resistant cells to obtain a more complete response. One attempt involves stimulation of the TRAIL pathway with a DNA damaging agent to activate the p53 response. Other efforts involve inhibition of survival pathways such as the NF- κ B pathway or the PI3K-Akt pathway, both of which connect to the TRAIL signaling network. Although numerous studies have measured upregulation of pro-apoptotic factors or downregulation anti-apoptotic factors during combination treatment, there is little consensus as to how different chemotherapies synergize with TRAIL (Johnstone, Frew et al. 2008). Efforts to understand the molecular mechanisms of this synergy would benefit from a dynamic systems-level approach; Chapter 4 touches on one such effort.

1.3.4 Monitoring the dynamics of apoptotic events in single cells

Apoptosis is a dynamic process whose reaction rates are critical to understanding the design principles of the apoptotic network as well as cells' sensitivity or resistance to death. Biochemical assays that involve lysing a population of cells at a single time point obscure the heterogeneity in the apoptotic response of individual cells, as the contents of both living and

dead cells are measured in aggregate. Quantifying and predicting the sensitivity or resistance of normal cells as well as different cancer cell types is essential for clinical studies of TRAIL and other chemotherapies. The fraction of dead cells at a certain time and the final fraction of surviving cells are related to the rate at which cells die (S.L.S., unpublished observations). The molecular mechanisms behind these relationships can best be gleaned by live-cell imaging with reporters of apoptotic events.

Previous work using live-cell reporters of apoptosis found that cytochrome *c* and Smac release from the mitochondria during MOMP is always a rapid, all-or-nothing event (requiring ~10 minutes); this event precedes rapid, all-or-nothing caspase-3 activation by 10-15 minutes (Goldstein, Waterhouse et al. 2000; Tyas, Brophy et al. 2000; Rehm, Dussmann et al. 2002; Rehm, Dussmann et al. 2003; Goldstein, Munoz-Pinedo et al. 2005; Munoz-Pinedo, Guio-Carrion et al. 2006). Much less is known, however, about the pre-MOMP period, which is quite variable and can last between 0.5 and 12 hours in individual cells undergoing the same treatment. As MOMP is a binary uni-directional event, the pre-MOMP decision phase must involve the building toward some threshold of pro-apoptotic signaling which must be crossed in order to trigger MOMP.

Recent work from our group involved building and making use of live-cell reporters to understand the network logic linking initiator caspase activation to MOMP and subsequent effector caspase activation (Albeck, Burke et al. 2008a). The authors used Förster resonance energy transfer (FRET) to build sensors for caspase activation by linking CFP to YFP with amino acids selective for initiator (IC-RP) or effector (EC-RP) caspase cleavage sites. A reporter for MOMP was built by fusing a red fluorescent protein (RFP) to the mitochondrial import sequence of Smac; this reporter is biochemically inactive as it lacks an IAP-binding

motif. Using combinations of these reporters, the authors found that initiator caspase activity, but not effector caspase activity, is present during the pre-MOMP delay (Fig. 1.4). Combining mathematical modeling with perturbation (over-expression or siRNA) of the network proteins revealed that XIAP's inhibitory activity of effector caspases is critical for restraining effector caspase activity during the pre-MOMP delay. This result was experimentally validated by knocking down XIAP levels (to reduce its ability to restrain effector caspases) and by over-expressing Bcl-2 or knocking down Bid (to block MOMP). Under these conditions, the pre-MOMP delay in effector caspase activation was eliminated – instead of being an all-or-nothing switch, effector caspase activity began to rise slowly soon after TRAIL addition. The possible consequences of partial effector caspase substrate cleavage in cells that eventually survive include partial genome and proteome degradation, which have the potential to produce genomically unstable pre-cancerous cells.

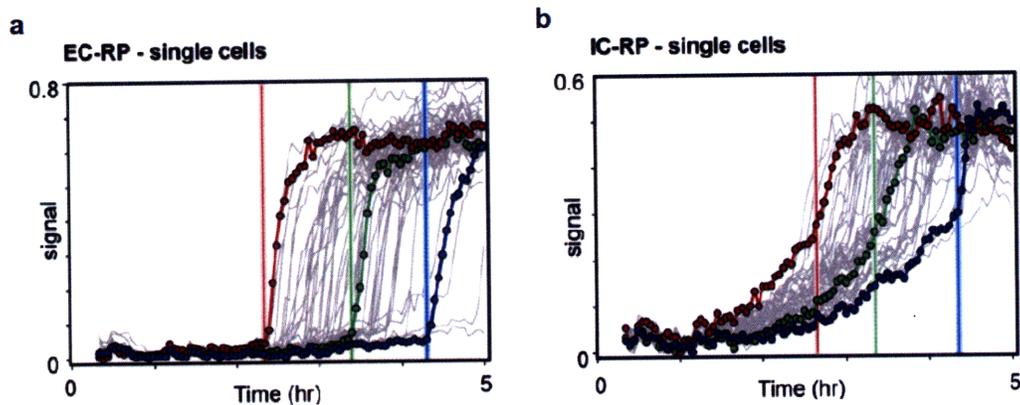


Figure 1.4. A composite picture of effector and initiator caspases in single cells. **a, b,** Time courses of cells expressing IMS-RP and either EC-RP (**a**) or IC-RP (**b**), treated with 50 ng/ml TRAIL and 2.5 ug/ml cycloheximide. Fifty individual cells are shown for each reporter (gray lines), with three cells exhibiting early, late, or intermediate times of death highlighted in red, blue, and green; vertical bars indicate the time of IMS-RP release for each highlighted cell. Reprinted from *Mol Cell*, 30(1), Albeck JG, Burke JM, Aldridge BB, Zhang M, Lauffenburger DA, Sorger PK. "Quantitative analysis of pathways controlling extrinsic apoptosis in single cells", 11-25, (2008), with permission from Elsevier.

A second study from the Sorger laboratory examined the unusual variable delay, snap-action switch involved in receptor-mediated apoptosis (Albeck, Burke et al. 2008b). This involved building a differential equation model of the pathway summarized in Fig 1.3, which was manually calibrated to single-cell experimental data to accurately reproduce the behavior of normal and perturbed cells. The model describes a single cell's trajectory through the pathway upon TRAIL stimulation and contains 58 species (18 having non-zero initial conditions and 40 additional species representing cleaved, complexed, or differentially localized forms of the initial species) which interact via 28 reactions described by 70 rate constants. The authors found that MOMP is the point at which the graded TRAIL - C8 activation - active Bax signal is converted to a snap-action response. By building multiple miniature models of the switch with increasing realism and complexity, the authors found that simple competitive binding between an activator (active Bax) and an inhibitor (Bcl-2) is not sufficient to create a snap-action switch under any set of realistic biophysical assumptions. Rather, switch-like behavior requires additional Bcl-2 family members, physical separation of Smac and cytochrome *c* from their binding partners in the cytosol, and multimerization of Bax into functional complexes. When pores finally form, Smac and cytochrome *c* are rapidly released due to the very steep concentration gradient involved in moving these proteins from the mitochondrial inter-membrane space to the cytosol. In summary, transition from graded to switch-like kinetics was found to be a result of maintenance of a very tight "off" state during the pre-MOMP delay followed by a low impedance "on" state.

In all of these single-cell studies of apoptosis, cell-to-cell variability in various apoptotic events is noticeable, but the origins of this variability and the possible physiological consequences are not addressed. The building of the live-cell reporters and mathematical model described above as well as the detailing of the network features responsible for certain

characteristics of apoptotic cell death laid the foundation for this thesis, which addresses the origins and consequences of cell-to-cell variability in apoptosis.

Chapter 2

2 Non-genetic origins of cell-to-cell variability in TRAIL-induced apoptosis

This chapter is based upon:

Non-genetic origins of cell-to-cell variability in TRAIL-induced apoptosis

Nature, Advanced online publication, Epub Date 12 April 2009

DOI: 10.1038/nature08012

Sabrina L. Spencer*, Suzanne Gaudet*, John G. Albeck, John M. Burke, Peter K. Sorger

(* These authors contributed equally to this work.)

In microorganisms, noise in gene expression gives rise to cell-to-cell variability in protein concentrations (McAdams and Arkin 1997; Elowitz, Levine et al. 2002; Ozbudak, Thattai et al. 2002; Blake, M et al. 2003; Colman-Lerner, Gordon et al. 2005; Golding, Paulsson et al. 2005; Rosenfeld, Young et al. 2005). In mammalian cells, protein levels also vary (Sigal, Milo et al. 2006; Chang, Hemberg et al. 2008; Feinerman, Veiga et al. 2008) and individual cells differ widely in responsiveness to uniform physiological stimuli (Goldstein, Kluck et al. 2000; Lahav,

Rosenfeld et al. 2004; Geva-Zatorsky, Rosenfeld et al. 2006; Albeck, Burke et al. 2008a; Albeck, Burke et al. 2008b). In the case of apoptosis mediated by TRAIL (TNF related apoptosis-inducing ligand) it is common for some cells in a clonal population to die while others survive – a striking divergence in cell fate. Among cells that die, the time between TRAIL exposure and caspase activation is highly variable. Here we image sister cells expressing reporters of caspase activation and mitochondrial outer membrane permeabilisation (MOMP) following exposure to TRAIL. We show that naturally occurring differences in the levels or states of proteins regulating receptor-mediated apoptosis are the primary causes of cell-to-cell variability in the timing and probability of death. Protein state is transmitted from mother to daughter, giving rise to transient heritability in fate, but protein synthesis promotes rapid divergence so that sister cells soon become no more similar to each other than pairs of cells chosen at random. Our results have implications for understanding “fractional killing” of tumor cells following exposure to chemotherapy, and for variability in mammalian signal transduction in general.

2.1 Results

TRAIL elicits a heterogeneous phenotypic response in both sensitive and relatively resistant cell lines: some cells die within 45 min, others 8-12 hr later, and yet others live indefinitely (Supplementary Fig. 2.1). During the variable delay between TRAIL addition and MOMP, upstream initiator caspases are active but downstream effector caspases are not (Albeck, Burke et al. 2008a; Albeck, Burke et al. 2008b). Possible sources of cell-to-cell variability in responses to TRAIL include genetic or epigenetic differences, stochastic fluctuations in biochemical reactions involving low copy number components (“intrinsic noise” (Elowitz, Levine et al. 2002)), differences in cell cycle phase, and natural variation in the concentrations of

key reactants. To distinguish among these and other possibilities, we used live-cell microscopy to compare the timing and probability of death in sister cells exposed to TRAIL. Were phenotypic variability caused by genetic or epigenetic differences, sister cells should behave identically. In contrast, were stochastic fluctuations in reactions triggered by TRAIL to predominate, sister cells should be no more similar to each other than pairs of cells selected at random. The influence of cell cycle state on apoptosis should be readily observable from time-lapse imaging of asynchronous cultures. Finally, variability arising from differences in protein levels (or in activity or modification state) should produce a highly distinctive form of inheritance in which newly born sister cells are very similar, because they inherit similar numbers of abundant factors from their mother (Golding, Paulsson et al. 2005; Rosenfeld, Young et al. 2005), but then diverge as new proteins are made and levels drift (Sigal, Milo et al. 2006; Kaufmann, Yang et al. 2007). With this in mind, we examined apoptosis in HeLa cells and in non-transformed MCF10A mammary epithelial cells in the presence and absence of protein synthesis inhibitors.

Pairs of sister cells expressing a fluorescent reporter of MOMP (IMS-RP; (Albeck, Burke et al. 2008a)) born during a 20-30 hr period were identified by time-lapse microscopy. TRAIL and the protein synthesis inhibitor cycloheximide were then added and filming continued for another 8 hr. The TRAIL to MOMP interval (T_d) was calculated for each cell (Fig. 2.1a). Among recently divided sisters (< 7 hr between division and death), T_d was highly correlated ($R^2 = 0.93$, Fig. 2.1b) whereas T_d was uncorrelated ($R^2 = 0.04$) for recently divided cells chosen at random. Time since division (Fig. 2.1c) and position in the dish (data not shown) did not correlate with T_d , ruling out a role for cycle state and cell-cell interactions under our experimental conditions. However, as time since division increased, sister-to-sister correlation in

T_d decayed exponentially with a half-life of ~ 11 hr so that sisters lost memory of shared ancestry within 50 hours or about 2 cell generations ($R^2 \leq 0.05$, the same as random pairs of cells; Fig. 2.1d,e). Similar results were obtained with MCF10A cells (Supplementary Fig. 2.2).

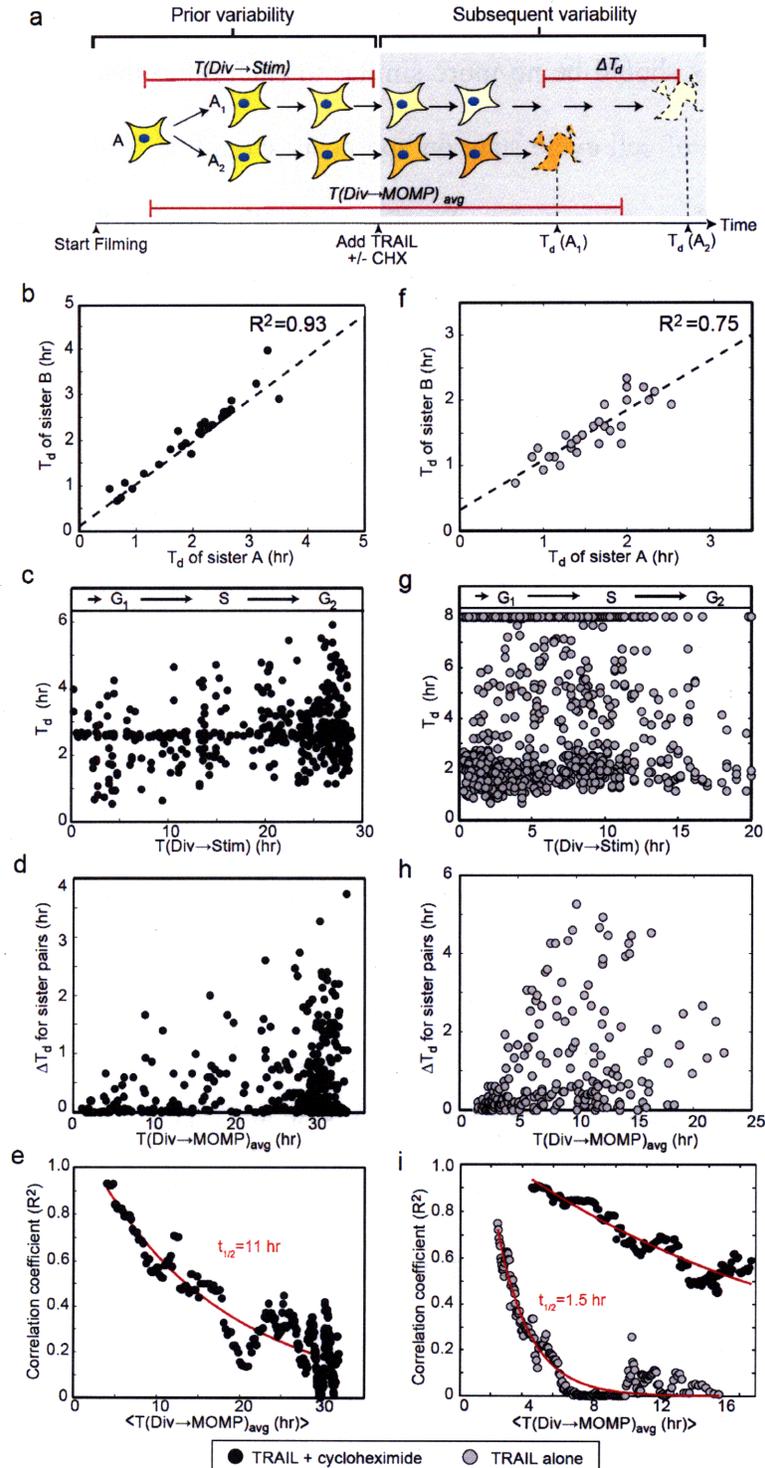


Figure 2.1. Time-to-death is highly correlated between HeLa sister cells but correlation decays as a function of time since division. **a**, Schematic of experimental design. ΔT_d represents the difference in time of MOMP between sisters; $T(\text{Div} \rightarrow \text{MOMP})_{\text{avg}}$ the time between cytokinesis of the mother and the average time of MOMP in daughter cells; $T(\text{Div} \rightarrow \text{Stim})$ the time between cytokinesis and TRAIL addition. The shading of each cell depicts concentrations/states of relevant proteins. **b** and **f**, Similarity in T_d among pairs of recently divided sister cells ($T(\text{Div} \rightarrow \text{MOMP})_{\text{avg}} < 7$ hr for (b) and < 3.5 hr for (f)). **c** and **g**, T_d as a function of $T(\text{Div} \rightarrow \text{Stim})$, a proxy for cell cycle state ($R^2 < 0.03$). **d** and **h**, ΔT_d as a function of $T(\text{Div} \rightarrow \text{MOMP})_{\text{avg}}$. **e** and **i**, Decay in the correlation of T_d between sister pairs as a function of $T(\text{Div} \rightarrow \text{MOMP})_{\text{avg}}$. In (i), black circles represent data for cells treated with TRAIL plus cycloheximide imaged in parallel with the TRAIL alone treatment (Supplementary Fig. 2.5).

High correlation among recently born sisters shows that variability in T_d arises from differences that exist prior to TRAIL exposure and rules out stochastic fluctuations in signaling reactions. Rapid decorrelation also rules out genetic mutation or conventional epigenetic differences (which typically last $10\text{-}10^5$ cell divisions (Rando and Verstrepen 2007)). However, transient heritability is precisely what we expected for cell-to-cell differences arising from variations in the concentrations or states of proteins that are partitioned binomially at cell division.

Whereas all TRAIL-treated HeLa cells eventually died in the presence of cycloheximide, in its absence a fraction always survived (presumably due to induction of survival pathways (Chaudhary, Eby et al. 1997)). When the fates of sister cells were compared, both lived or both died in almost all cases (chi-square test, $p=7 \times 10^{-19}$, Supplementary Fig. 2.3). Variability in T_d across the population was large (Fig. 2.1g and Supplementary Fig. 2.4), but recently born sisters were nevertheless correlated in T_d ($R^2=0.75$, Fig. 2.1f). Again, cell cycle phase was not correlated with fate or time-to-death (Fig. 2.1g). Decorrelation in T_d among sisters was an order of magnitude more rapid in the presence of protein synthesis than in its absence (~ 1.5 hr half-life, Fig. 2.1h,i and Supplementary Fig. 2.5). Thus, the length of time that T_d is heritable is very sensitive to rates of protein synthesis, both basal and TRAIL-induced.

Are the concentrations of proteins regulating TRAIL-induced apoptosis sufficiently different from cell to cell to account for variability in T_d ? Using flow cytometry, we measured

the distributions of five apoptotic regulators for which specific antibodies are available. All five proteins were log-normally distributed across the population with coefficients of variation between 0.21 and 0.28 for cells of similar size (Fig. 2.2a), consistent with data on other proteins (Sigal, Milo et al. 2006). To determine the impact of variability in protein levels on variability in time-to-death, we turned to an ordinary differential equation model of TRAIL-induced apoptosis (Albeck, Burke et al. 2008b). This model encapsulates the biochemistry of TRAIL-mediated death and recapitulates the dynamics of apoptosis under various conditions of protein depletion or over-expression (Albeck, Burke et al. 2008b). When variability in T_d arising from variance in protein levels was modeled, a good match was observed to experimental data (Fig. 2.2b-d) implying that measured differences in protein levels are sufficient to account for variability in T_d .

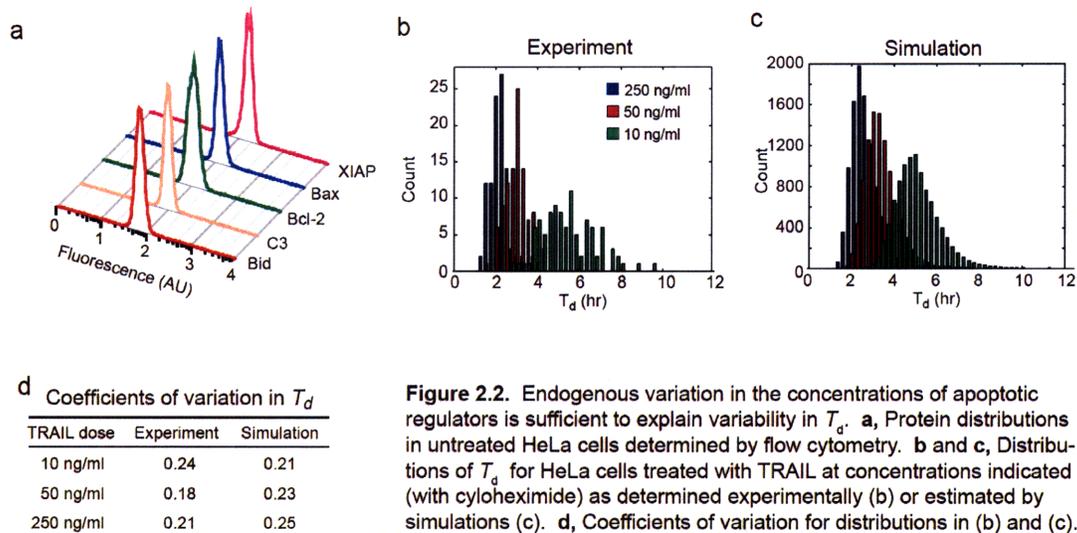


Figure 2.2. Endogenous variation in the concentrations of apoptotic regulators is sufficient to explain variability in T_d . **a**, Protein distributions in untreated HeLa cells determined by flow cytometry. **b** and **c**, Distributions of T_d for HeLa cells treated with TRAIL at concentrations indicated (with cycloheximide) as determined experimentally (**b**) or estimated by simulations (**c**). **d**, Coefficients of variation for distributions in (**b**) and (**c**).

Which steps in receptor-mediated apoptosis are responsible for variation in time-to-death? To address this question, we grouped reactions into three sets: those occurring before, during, or subsequent to MOMP (Fig. 2.3a – blue, grey, and orange). Before MOMP, TRAIL

binds and oligomerizes DR4/5 receptors, promoting assembly of death-inducing signaling complexes (DISCs) that then activate initiator pro-caspases-8 and -10 (C8/10) (Fuentes-Prior and Salvesen 2004). Active C8/10 cleaves Bid to tBid (Li, Zhu et al. 1998; Luo, Budihardjo et al. 1998), which activates the pore-forming proteins Bax and Bak (Youle and Strasser 2008). C8/10 also processes effector pro-caspases-3 and -7 (C3/7) but C3/7 activity is held in check by XIAP until MOMP (Fuentes-Prior and Salvesen 2004). MOMP itself involves self-assembly of activated Bax/Bak into transmembrane pores, a process antagonized by anti-apoptotic Bcl-2 proteins (Youle and Strasser 2008). When levels of activated tBid, Bax, and Bak exceed a threshold set by inhibitory Bcl-2 proteins, pores form in the mitochondrial outer membrane, allowing cytochrome *c* and Smac to translocate into the cytosol (Youle and Strasser 2008). In post-MOMP reactions, cytosolic Smac neutralizes XIAP, relieving C3/7 inhibition and allowing cleavage of effector caspase substrates and consequent cell death (Fuentes-Prior and Salvesen 2004). In a parallel route to C3/C7 activation, cytosolic cytochrome *c* promotes apoptosome assembly and caspase-9 activation.

To determine which steps in TRAIL-induced apoptosis play the greatest role in determining variability in death time, we imaged cells expressing a reporter of either initiator or effector caspase activity (IC-RP or EC-RP) (Albeck, Burke et al. 2008a) in combination with IMS-RP. We found almost all variability in T_d to arise during the pre-MOMP interval (Fig. 2.3b). The timing of MOMP itself is determined by the rate at which tBid accumulates to a threshold set by the levels of Bcl-2 family proteins. This rate and threshold can be determined from the initial rate of IC-RP cleavage (k_{IC}) and the fraction of IC-RP cleaved (θ) at the time of MOMP, respectively. When k_{IC} and θ were measured in single TRAIL-treated cells, the timing of MOMP was found to be controlled by a variable rate of approach to a threshold of variable

height (Fig. 2.3c,d). However, variation in k_{IC} played a significantly greater role in determining T_d than variation in θ ($R^2=0.82$ vs. $R^2=0.22$; Fig. 2.3e,f, and Supplementary Fig. 2.7). Moreover, k_{IC} was very similar in recently born sister cells with similar T_d , but dissimilar in older sisters (Fig. 2.3g). We conclude that cell-to-cell variability in k_{IC} – and by implication the rate of conversion of Bid to tBid – is the primary determinant of variability in time-to-death under our experimental conditions.

Levels of multiple proteins set k_{IC} , including DR4/5 receptors, DISC components, C8, and Bid itself. Modelling suggested that knowing the concentration of any single protein upstream of Bid would have minimal value in predicting T_d – the impact of variation in all other proteins is too great (Fig. 2.4a). Live-cell analysis of FLIP, an important regulator of procaspase-8 binding to the DISC, was consistent with this prediction, as was analysis of other single proteins by flow cytometry (Fig. 2.4b and data not shown). However, modelling showed that with increasing over-production of Bid, measurement of its levels would be increasingly predictive of T_d (Fig. 2.4c, Supplementary Fig. 2.8). We therefore measured the relationship between dispersion in T_d and levels of Bid-GFP (Fig. 2.4d). A ~50-fold increase in Bid-GFP caused the variability in T_d to fall significantly, concomitant with a decrease in mean time-to-death from ~3 hr to ~45 min. Thus, only when over-expressed is the level of one protein predictive of T_d ; under normal circumstances, control is multivariate.

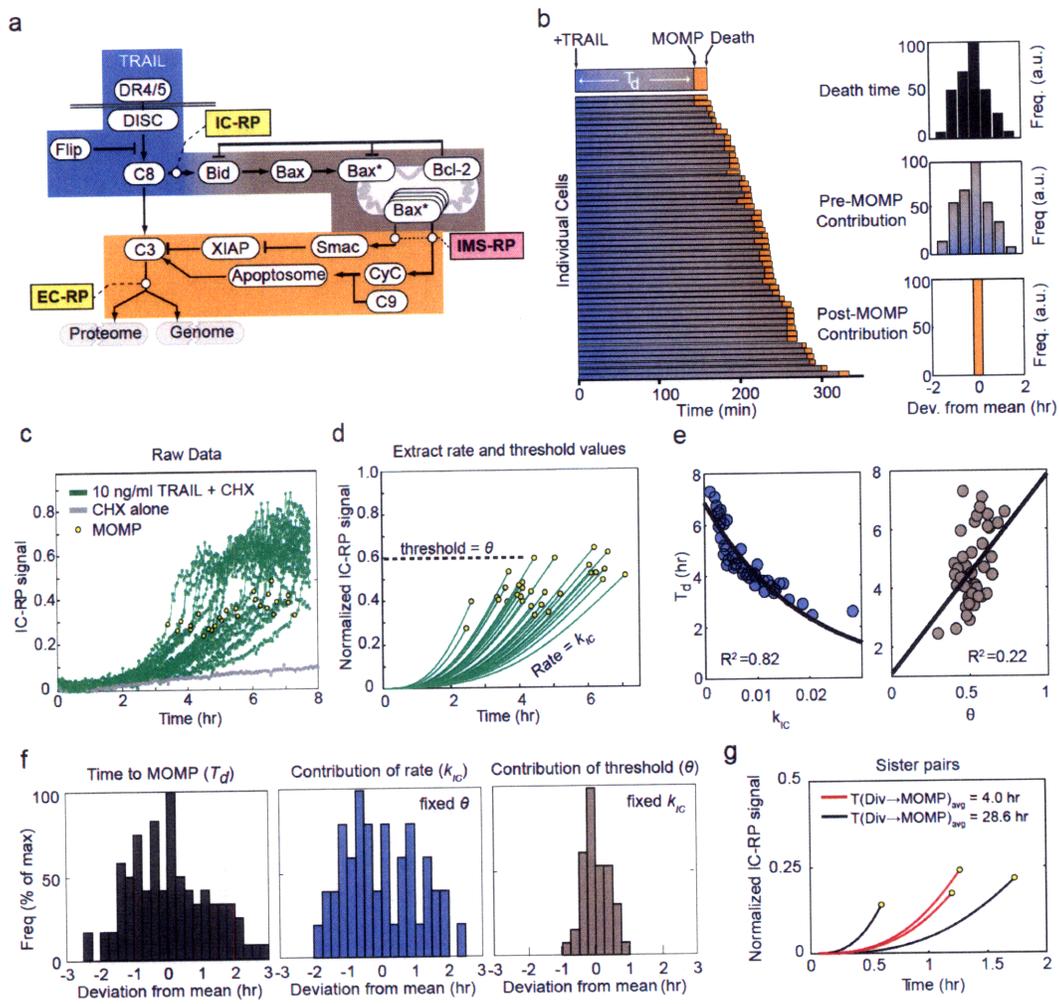


Figure 2.3. A single time-dependent process upstream of MOMP predicts time-to-death. **a**, Schematic of receptor-mediated apoptosis signalling with IC-RP, EC-RP, and IMS-RP indicated. The Bcl-2 protein family is represented in simplified form by Bid, Bax, and Bcl-2. Reactions occur before (blue), during (grey), or subsequent to MOMP (orange). **b**, Timing of apoptotic events in HeLa cells expressing IMS-RP and EC-RP and treated with TRAIL; blue-grey denotes the pre-MOMP interval and orange the interval between MOMP and half-maximal cleavage of EC-RP (a marker of death). Insets show death times computed from data (top) and contributions of pre-MOMP (middle) or post-MOMP (top) intervals. **c** and **d**, Raw and fitted trajectories for IC-RP cleavage in single TRAIL-treated HeLa cells co-expressing IMS-RP and IC-RP. Values for height of the MOMP threshold (θ) and rate of approach to the threshold (k_{IC}) were derived by fitting (Supplementary Fig. 2.6). **e**, Correlation between T_d and k_{IC} (left) or θ (right) for data in (d). **f**, Relative contributions of variability in k_{IC} (blue) or θ (grey) to variability in T_d (black; Supplementary Fig. 2.7). **g**, Trajectories of IC-RP cleavage in recently divided sister HeLa cells having similar T_d (red) and older sisters with differing T_d (black) treated with 50 ng/ml TRAIL.

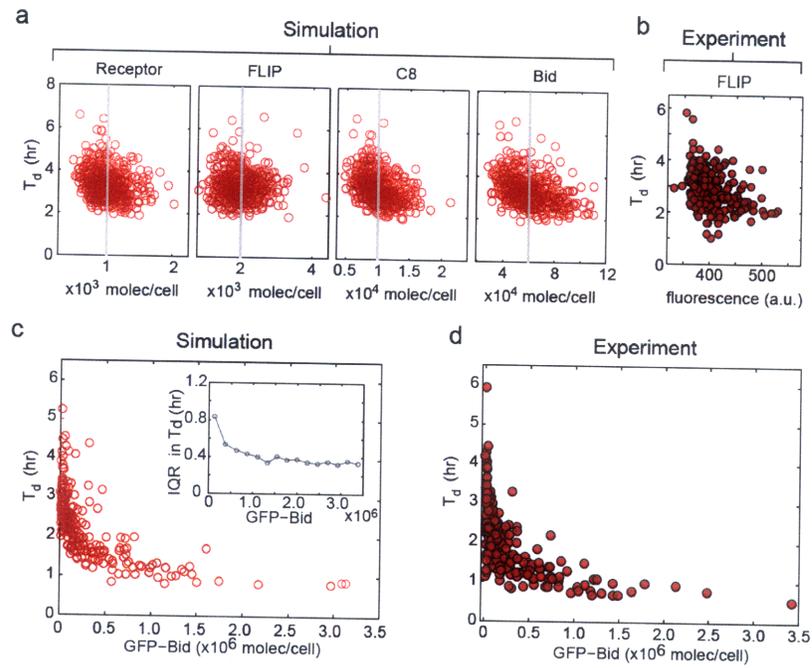


Figure 2.4. No single protein predicts T_d under normal conditions but over-expression can increase predictability. **a**, T_d as a function of four protein levels based on simulation. Grey lines denote mean protein concentration; each point represents a single simulated cell. **b**, Death time as a function of endogenous FLIP levels in H1299 cells. **c** and **d**, Effect of GFP-Bid over-expression on T_d in HeLa cells, as predicted by simulation (**c**) or observed in experiment (**d**). Inset shows reduction in dispersion of T_d with increasing Bid, as measured by interquartile range (IQR; Supplementary Fig. 2.8).

2.2 Discussion

Other studies (for example, ref. (Wagner, Punnoose et al. 2007)) address genetic factors determining the average sensitivity of cell lines to TRAIL whereas this paper examines non-genetic cell-to-cell variability within an individual cell line. We come to three primary conclusions. First, cell-to-cell variation in the timing and probability of death is transiently heritable. Cell cycle state, number of neighbouring cells, and stochastic fluctuations in TRAIL-induced signalling reactions do not play a major role under our conditions. Instead, variability in phenotype arises from cell-to-cell differences in protein levels that exist prior to TRAIL exposure (our experiments do not distinguish between cell-to-cell differences in total concentrations or in post-translationally modified forms). Second, the rate at which sisters lose memory of a shared past is an order of magnitude faster in the presence of protein translation than in its absence. This further implicates variability in protein levels as the origin of differences in phenotype. Third, knowing the concentration of individual proteins does not allow T_d to be predicted but measuring the rate of a single reaction does (Bid to tBid conversion in our experiments). These findings are likely to hold for other examples of ligand-induced apoptosis, however for intrinsic apoptosis, different proteins will control the rate of approach to MOMP and θ may dominate in certain contexts. Moreover, given the prevalence of multi-protein cascades in signal transduction, multivariate control over cell-to-cell variability is likely to be more common than the univariate control observed in other settings (Wagner, Punnoose et al. 2007; Chang, Hemberg et al. 2008; Cohen, Geva-Zatorsky et al. 2008).

Heritable, non-genetic determinants of phenotype are often referred to as “epigenetic” (Rando and Verstrepen 2007), but the transient heritability we observe is fundamentally different

in origin and duration. Given variability in growth rates and noise in gene expression, genetically identical cells will inevitably contain slightly different concentrations of most proteins. However, differences in protein concentrations do not necessarily affect phenotype, a property often referred to as robustness (Barkai and Leibler 1997). For example, the efficiency with which effector caspase substrates are cleaved does not vary from cell to cell (Albeck, Burke et al. 2008b). Given the importance of tight control over apoptosis, cell-to-cell variability in the timing and probability of death seems unlikely to reflect an inability of cells to achieve robust regulation. Instead, by transforming what is a binary decision at the single-cell level into a graded response at the population level, variability probably has an adaptive advantage. TRAIL is currently undergoing clinical trials as an anti-cancer drug (Ashkenazi and Herbst 2008) and our findings may have implications for the use of TRAIL and other apoptosis inducers as therapeutics. Many drugs exhibit “fractional killing” in which each round of therapy kills some but not all of the cells in a tumor (Berenbaum 1972). Traditionally, this is thought to reflect differences in genotype, cell cycle state, or the involvement of cancer stem cells, but our data demonstrate that dramatic variability can also arise from natural differences in protein levels. We propose that the efficiency of TRAIL-mediated killing of cancer cells could be increased by reducing the impact of cell-to-cell variability, perhaps through co-drugging.

2.3 Methods

2.3.1 Methods summary

Live-cell microscopy. Cells expressing IMS-RP and FRET reporters EC-RP or IC-RP were imaged as described (Albeck, Burke et al. 2008a). In Figure 2.1, cells were imaged for 20-30hr to determine time of division and identify sisters; then media containing 50 ng/ml TRAIL

plus 2.5 $\mu\text{g/ml}$ cycloheximide or 250 ng/ml TRAIL alone was added. The difference in TRAIL concentrations was designed to generate a similar range in T_d with and without cycloheximide (Supplementary Fig. 2.4). Cells were then imaged for 8 hr to determine the time of MOMP, by monitoring cytosolic translocation of IMS-RP. Unless otherwise noted, all treatments included 2.5 $\mu\text{g/ml}$ cycloheximide.

Data analysis. Correlation coefficients (R^2) were obtained by linear regression except where noted. Sister-sister correlation was determined by sorting pairs of cells on $T(\text{Div} \rightarrow \text{MOMP})_{\text{avg}}$ and calculating R^2 for the first 40 pairs. R^2 was then re-calculated for cells 2-41, 3-42, etc., and the results plotted as a function of the average $T(\text{Div} \rightarrow \text{MOMP})_{\text{avg}}$ for the 40 cells in question, denoted by “< >”. The results were fit to an exponential decay: $R^2 = 1.2e^{(-0.063T(\text{Div} \rightarrow \text{MOMP})_{\text{avg}})}$ for TRAIL plus cycloheximide, and $R^2 = 2.3e^{(-0.47T(\text{Div} \rightarrow \text{MOMP})_{\text{avg}})}$ for TRAIL alone. Half-lives were calculated as $\ln(2)/0.063 = 11$ hr, and $\ln(2)/0.47 = 1.5$ hr. Contributions to T_d of k_{IC} , θ , and pre- and post-MOMP intervals were obtained by fixing one parameter and allowing the other to vary over the observed range, then mean-centring the resulting distributions (Supplementary Fig. 2.7). Fitted IC-RP trajectories were obtained after subtracting a trajectory for cycloheximide alone (Fig. 2.3c) to control for photobleaching (Supplementary Fig. 2.6).

Modelling. The responses of cell populations were simulated using a trained ODE model (Albeck, Burke et al. 2008b) sampling from log-normally distributed protein concentrations with $\text{CV} \approx 0.25$ (see Supplemental Methods). In Figure 2.4, GFP-Bid (an experimental observable) was added to log-normally distributed endogenous Bid (unobservable); other proteins were sampled from lognormal distributions as before. Simulations were adjusted to match the distribution GFP-Bid achieved experimentally.

2.3.2 Supplementary methods

Cell culture and transfections. HeLa cells were maintained in DMEM (Mediatech, Inc.) supplemented with L-glutamine (Gibco), penicillin/streptomycin (Gibco) and 10% foetal bovine serum (Mediatech, Inc.). MCF10A cells were cultured as described (Debnath, Muthuswamy et al. 2003). H1299 cells containing FLIP tagged with YFP at the endogenous locus were obtained from the Kahn Dynamic Proteomics Project and maintained at 8% CO₂ in RPMI (Mediatech, Inc.) with 10% foetal bovine serum and penicillin/streptomycin. HeLa cells expressing IMS-RP (Albeck, Burke et al. 2008a) were transfected using FuGENE 6 (Roche) with pd4-Bid-EGFP (Clontech) to sample expression levels across a wide range. H1666 cells were maintained (and imaged) in RPMI supplemented with 10% FBS, L-Glutamine, penicillin/streptomycin, 1x ITES (Lonza Biosciences #17-839Z), 50 nM hydrocortisone, 10 uM phosphorylethanolamine, 0.1 nM Tri-iodothyronine, 10 mM HEPES, 0.5 mM sodium pyruvate, 2 g/L BSA, and 1 ng/mL EGF. Fresh primary liver cells were obtained from CellzDirect and plated on collagen type I. Cells were maintained (and imaged) in Eagle's Minimum Essential Medium supplemented with 10% FBS, L-Glutamine, 100 nM dexamethasone, 5 ug/mL human insulin, 5 ug/mL transferrin from human serum, 5 ug/mL sodium selenite, and 15 mM HEPES. SKBR3 cells were maintained (and imaged) in RPMI supplemented with 10% FBS, L-Glutamine, and penicillin/streptomycin.

Live-cell microscopy. HeLa cells expressing IMS-RP and FRET reporters EC-RP or IC-RP were imaged in a 37°C humidified chamber as described (Albeck, Burke et al. 2008a). For sister cell experiments, HeLa cells expressing IMS-RP were imaged (Albeck, Burke et al. 2008a) at 10-minute intervals for 20-30 hours in phenol red-free CO₂ independent medium (Invitrogen) with L-glutamine, penicillin/streptomycin, and 1% serum (Fig. 2.1b-e) or at ~5% CO₂ in phenol red-free DMEM with L-glutamine, penicillin/streptomycin, and 10% serum (Fig. 2.1f-i, see also Supplementary Fig. 2.5). The growth media was then replaced with the same media containing

TRAIL (Alexis Biochemicals ALX-201-115) with or without 2.5 $\mu\text{g/ml}$ cycloheximide (Sigma-Aldrich) and images were acquired at 3-minute intervals for an additional 8 hr. Cells still alive at the end of the 8 hr were considered to have survived the treatment. MFC10A were imaged as described (Albeck, Burke et al. 2008a) but in $\sim 5\%$ CO_2 in phenol red-free assay media (Debnath, Muthuswamy et al. 2003) without EGF or insulin to reduce cell migration. HeLa cells co-expressing IMS-RP and Bid-GFP and H1299 YFP-FLIP cells were imaged (Albeck, Burke et al. 2008a) in the same media as described above for Fig. 2.1b-e but at $20\times$ magnification with frames every 3 min or every 10 minutes, respectively. H1666, SKBR3, and primary liver cells were imaged in 96-well glass bottom plates (Matrical) on a Nikon TE2000E at $10\times$ magnification in a 37°C chamber with 5% CO_2 .

Image analysis. Sister-cell tracking was performed manually. To assess whether there is a cell cycle effect on death time, we plotted death time as a function of time since division, as a proxy for cell cycle phase. Because the distribution of time since division is not uniform, one might infer a cell cycle effect but, in fact, a cell cycle effect would appear as a slope in the data, which we do not observe. For sister cell experiments where CO_2 independent medium was used, there was more proliferation early in the divisions movie (and thus more points near "G2") because CO_2 independent medium does not support very long term proliferation (division slows down, but the cells are not dying). Importantly, the lack of cell cycle effect is also apparent for sister cell experiments performed in DMEM, the standard medium for HeLa cells (Supplementary Fig. 2.5). In these experiments, the cells proliferated continuously during the divisions movie. Cells that divided early in the divisions movie often divided again if they survived stimulation with TRAIL, producing "cousins" which were excluded from the analysis.

This resulted in fewer cells in the “G2” region, but this does not indicate a cell cycle effect, as the probability of surviving or dying is constant.

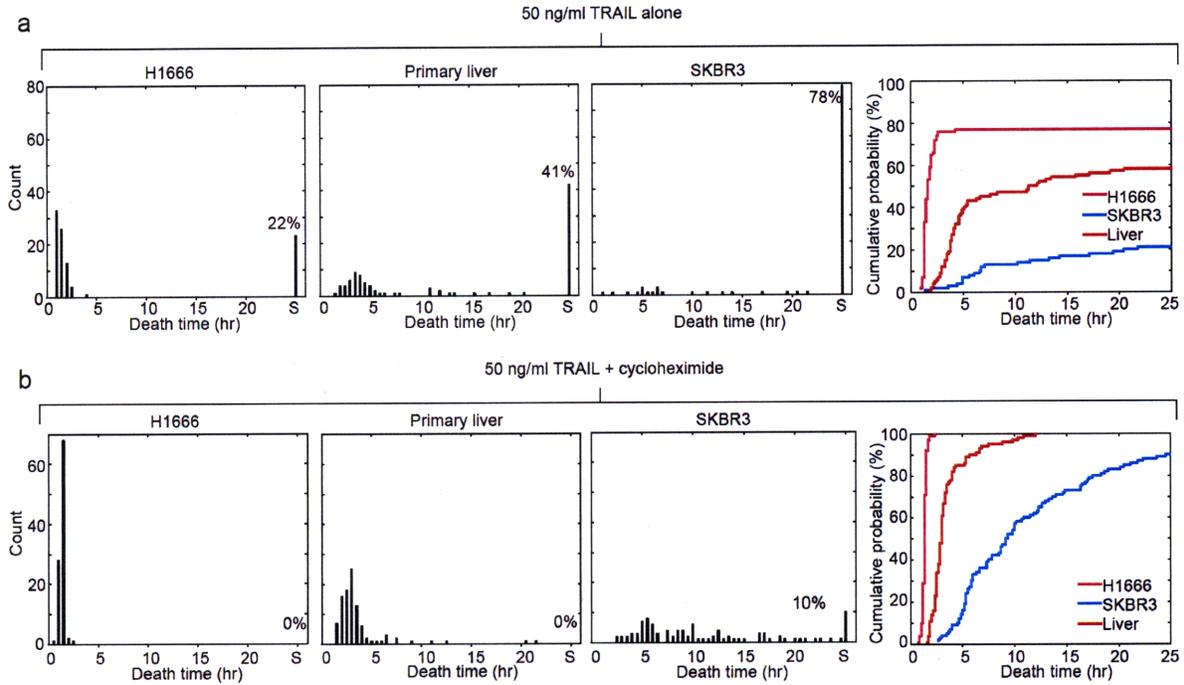
Analysis of IC-RP and EC-RP cleavage and IMS-RP translocation was performed as described (Albeck, Burke et al. 2008a). To derive estimates for k_{IC} and θ , individual cell trajectories were fit with an equation derived from mathematical reduction of the differential equation model for the pathway (J.M.B., J.G.A, S.L.S., D. Lauffenburger, P.K.S., manuscript in preparation; see also Supplementary Fig. 2.5). The equations for the fitted relationship between T_d and k_{IC} and between T_d and θ were as follows: $T_d = 6.9e^{(-53.7 k_{IC})}$ and $T_d = 6.8 \theta + 1.1$. FLIP-YFP fluorescence was quantified at $t = 0$ hr (time of TRAIL addition) by manually outlining the cell and measuring the average fluorescence intensity within the outline. For FLIP-YFP cells, time of death was scored as the first frame where a cell exhibited apoptotic morphology. Bid-GFP fluorescence was quantified at $t = 0$ hr by measuring the average fluorescence intensity from a representative area within the cell. To determine the absolute number of proteins/cell, the average Bid-GFP fluorescence intensity from these movies was set equal to the average number of GFP-tagged proteins per cell as measured by quantitative immunoblot (Supplementary Fig. 2.9).

Flow cytometry. The distributions of initial protein levels were measured in HeLa cells (fixed with paraformaldehyde and permeabilised with methanol) on a FACSCalibur (BD Biosciences). The antibodies were carefully validated by knockout or knockdown and/or by over-expression of GFP-tagged fusion proteins. The following antibodies were used: α -Bid (HPA000722, Atlas Antibodies), α -Bax (MAB4601, Chemicon International), α -Bcl-2 (SC7382, Santa Cruz Biotechnology), α -XIAP (610717, BD Biosciences), α -C3 (SC7272, Santa Cruz

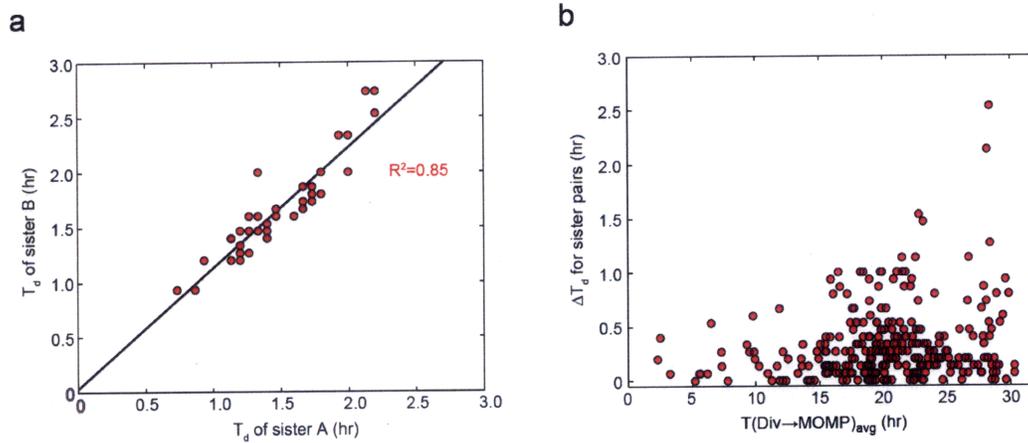
Biotechnology). The coefficient of variation (CV) of cells of similar size (as estimated by forward scatter) ranged from 0.21 to 0.28.

Modelling. The details of methods used will be described elsewhere. Briefly, a series of 10^4 simulations of the EARMv1.1 ordinary differential equation model (Albeck, Burke et al. 2008b) (modified to include general protein synthesis and degradation) were run in Jacobian (Numerica Technology). In previous work, only single values for each protein concentration were used (Albeck, Burke et al. 2008b). Here, for each run of the model (representing one cell), initial protein levels were independently sampled from log-normal distributions having mean values identical to those previously reported (Albeck, Burke et al. 2008b) (except for Bcl-2, whose mean was set to 30,000 molecules/cell), and coefficient of variation as measured by flow cytometry (Fig. 2.2a) or set to 0.25 for proteins that were not measured. Initial protein concentrations and parameter values are listed in Supplementary Tables 1 and 2.

2.4 Supplementary figures



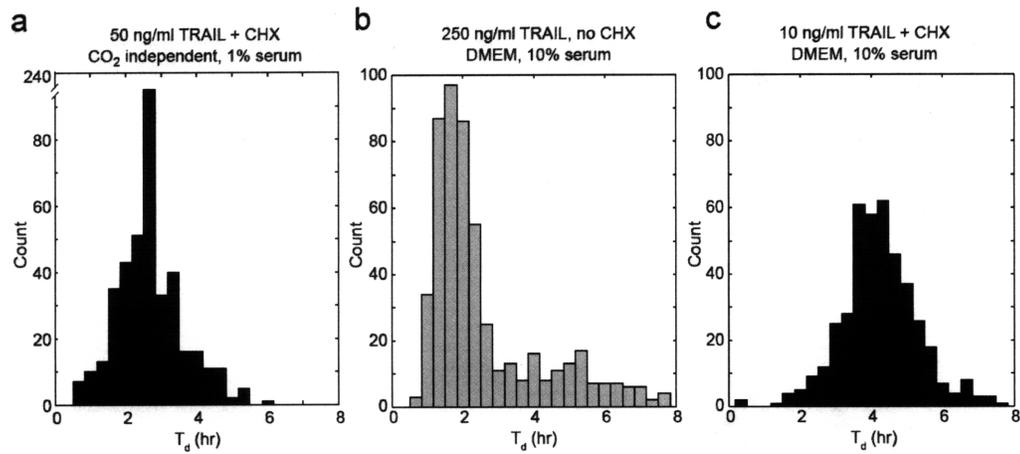
Supplementary Figure 2.1. Variability in death time with and without cycloheximide. The three cell types indicated were treated with 50 ng/ml TRAIL alone (top panels) or 50 ng/ml TRAIL + cycloheximide (bottom panels) and imaged by brightfield microscopy every 10 minutes for 25.5 hr. One hundred cells were analyzed for each distribution. Death time was scored as the first frame of apoptotic morphology. Cells surviving this 25.5 hr movie are labeled with an "S" and the percentage of survivors is indicated. H1666 cells were the most sensitive line examined, while SK-BR-3 cells were the most resistant. However, even H1666 show variability in cell fate when treated with TRAIL alone. Cumulative count was calculated from the distributions.



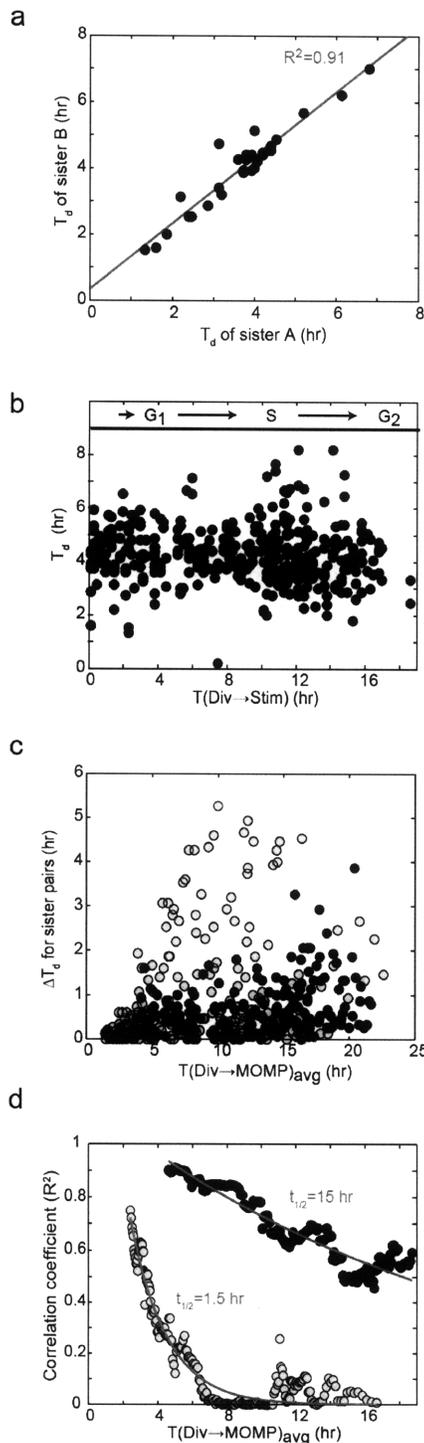
Supplementary Figure 2.2. Time of MOMP is correlated in sister MCF10A cells treated with TRAIL + CHX. The fluorescent reporter for MOMP (IMS-RP) was introduced into MCF10A cells. Cells were imaged with at 10x magnification for 28 hr (frames every 10 min) to determine division times and track pairs of sister cells. Subsequently, the growth media was replaced with media containing 50 ng/ml TRAIL plus 2.5 μ g/ml cycloheximide and cells were imaged (frames every 4 min) until all had died. **a**, Correlation in death time (T_d) between 40 pairs of recently divided sister cells ($T(\text{Div} \rightarrow \text{MOMP})_{\text{avg}} < 15.4$ hr). Each circle denotes a pair of sister cells. The correlation coefficient (R^2) was obtained by linear regression. **b**, Difference in T_d of sister cell pairs (ΔT_d) as a function of $T(\text{Div} \rightarrow \text{MOMP})_{\text{avg}}$.

| | | | |
|---------------------------------|-------------------------|-----------------------------|----------------|
| Number of cells that died: | 360 | | |
| Number of cells that survived: | 240 | | |
| Total number of cells analyzed: | 600 | | |
| Probability of dying: | 0.6 | | |
| Probability of surviving: | 0.4 | | |
| Fates of sister pairs: | <u>Live-Live</u> | <u>Live-Die or Die-Live</u> | <u>Die-Die</u> |
| Expected fraction: | 0.16 | 0.48 | 0.36 |
| Expected number: | 48 | 144 | 108 |
| Observed number: | 86 | 68 | 146 |
| Chi ² value = | 83.56 | | |
| Degrees of freedom = | 2 | | |
| p-value = | 7.16 x10 ⁻¹⁹ | | |

Supplementary Figure 2.3. Cell fate is correlated in sister HeLa cells treated with TRAIL alone. Table contains sister cells from the experiment depicted in Fig. 2.1f-i (250 ng/ml TRAIL). The number of cells that survived the treatment and the number that died were determined. The probability of surviving and the probability of dying were computed and used to determine the expected probability that a random pair of cells would either both live, both die, or have disparate fates (one lives, one dies). A Chi² test was used to compare the expected and observed numbers of pairs in each category. The highly statistically significant p-value indicates that sister pairs are much more likely to share the same fate (both live or both die) than would be expected for random pairs of cells.

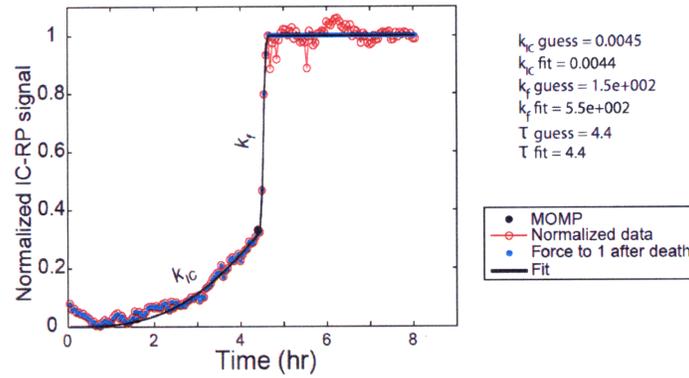


Supplementary Figure 2.4. Distributions of death time for HeLa sister cells, with and without cycloheximide. The distributions of MOMP times (T_d) of HeLa cells used for the sister cell experiments presented in Fig. 2.1 are plotted. **a**, Cells treated with 50 ng/ml TRAIL plus cycloheximide (CHX) in CO₂ independent medium with 1% serum (for Fig. 2.1b-e). **b**, Cells treated with 250 ng/ml TRAIL in the absence of CHX in DMEM with 10% serum (for Fig. 2.1f-i and Supplementary Fig. 2.5). **c**, Cells treated with 10 ng/ml TRAIL plus CHX in DMEM with 10% serum (for Fig. 2.1i and Supplementary Fig. 2.5).



Supplementary Figure 2.5. Comparison of sister cell experiments performed in parallel, with and without cycloheximide.

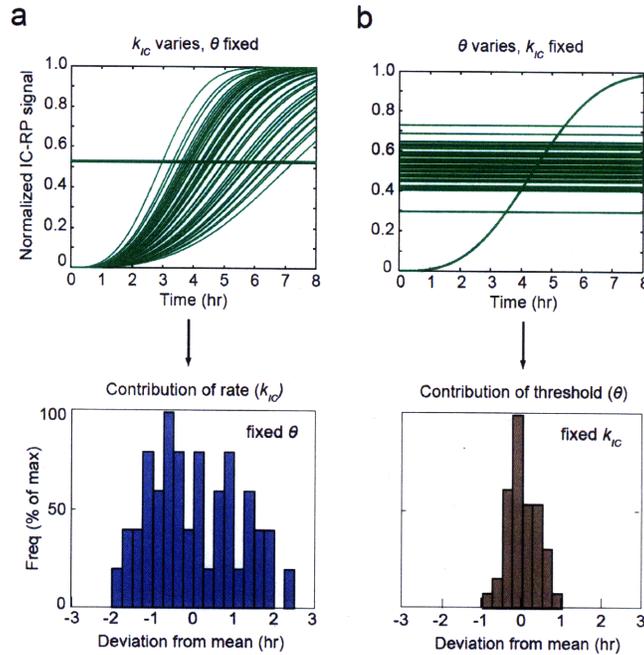
Comparison of sister cell decay times for cells imaged in DMEM with 10% serum and treated with 250 ng/ml TRAIL without cycloheximide (gray circles, data reproduced from Fig. 2.1f-i) or with 10 ng/ml TRAIL with 2.5 μ g/ml cycloheximide (black circles, data plotted or reproduced from Fig. 2.1i); these TRAIL doses were chosen based on Supplementary Fig. 2.3 to create populations of cells with similar ranges of death times. **a**, Correlation of T_d among 30 pairs of recently divided sister cells ($T(Div \rightarrow MOMP)_{avg} < 5$ hr). Each circle denotes a pair of sister cells. **b**, T_d as a function of time between division and stimulation, a proxy for cell cycle phase. Cell cycle phases are indicated as G1, S, G2, as approximated from time since division. No correlation was observed between cell cycle phase and T_d ($R^2 = 0.0008$). **c**, Difference in T_d of sister cell pairs (ΔT_d) as a function of $T(Div \rightarrow MOMP)_{avg}$. **d**, Decay in the correlation of sister cells for cells treated without cycloheximide (grey; reproduced from Fig. 2.1i) or with cycloheximide (black).



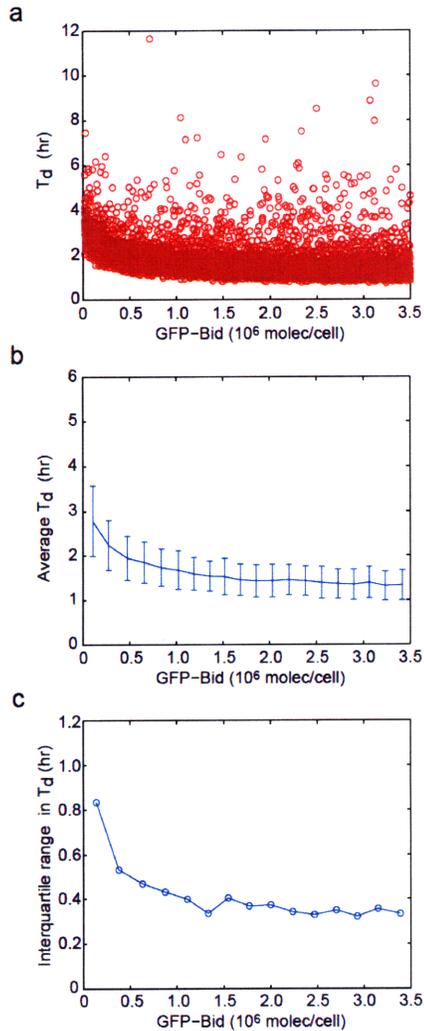
Supplementary Figure 2.6. Fitting of IC-RP trajectories. The cell shown was treated with 50 ng/ml TRAIL plus 2.5 μ g/ml CHX and imaged as described in Methods. For all of the cells in Fig. 2.3c, background-subtracted CFP and YFP images were divided to create a ratiometric image using ImageJ and custom plug-ins. For each cell, we then subtracted the minimum signal value across all time points. The cell was deemed “dead” at the first decrease in signal following MOMP. We normalized the trajectory by dividing by the signal’s value at this point. As the cell dies and lifts off the plate, the signal becomes noisy. We therefore force the signal to a value of one from this point on and fit to this modified trajectory (blue). To produce the trajectory in Fig. 2.3d, fitting was performed in MATLAB using the function ‘nlinfit’ with the following equation, mathematically derived to represent a single cell’s IC-RP trajectory (J.M.B., J.G.A., S.L.S., D. Lauffenburger, P.K.S., manuscript in preparation).

$$y = \begin{cases} 1 - e^{-k_{IC}t^3} & t < \tau \\ 1 - e^{-k_{IC}t^3 - k_f(t-\tau)^3} & t \geq \tau \end{cases}$$

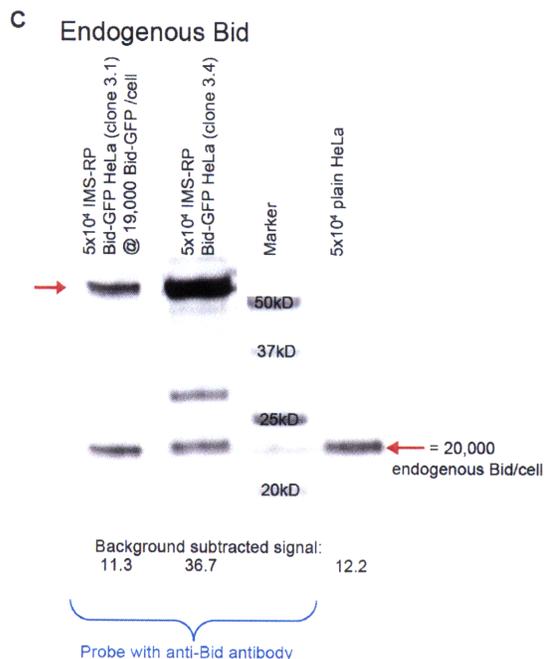
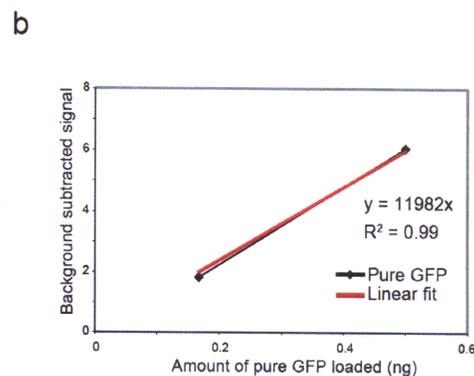
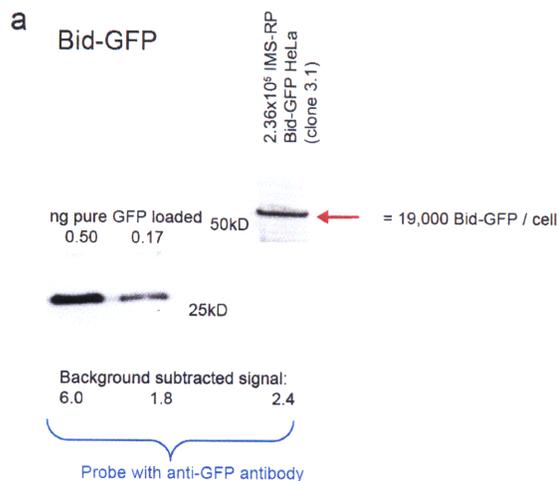
τ corresponds approximately to the time of MOMP. We found k_f to be invariant across dose and thus we focused only on k_{IC} in the body of the text.



Supplementary Figure 2.7. Contribution of k_{IC} vs. θ . For distributions shown in Fig. 2.3f, the relative contribution of variability in k_{IC} and θ to variability in T_d was assessed computationally by fixing one parameter at its mean value, allowing the other to vary over the observed range, and assessing the resulting distribution of T_d . The distributions were then mean-centered at 0. The effects of the two parameters contribute non-linearly to time of MOMP.



Supplementary Figure 2.8. Computational analysis suggests that Bid overexpression reduces T_d mean and dispersion. Simulations were performed to mimic overexpression of GFP-Bid. All initial protein concentrations were sampled from lognormal distributions as described in Methods, but an additional amount of Bid was added (GFP-Bid), by sampling from a uniform distribution. **a**, T_d as a function of GFP-Bid amount per cell for 10,000 simulations. **b**, Average T_d plotted as a function of GFP-Bid levels for 15 bins showing that Bid overexpression reduces average T_d . Error bars represent the interquartile range (75th percentile value - 25th percentile value). **c**, Dispersion in the values of T_d as a function of GFP-Bid levels. The dispersion in the distribution of T_d in 15 equal intervals of GFP-Bid expression was measured using the interquartile range to minimize the effect of outliers in the distribution. The variability in T_d decreases as GFP-Bid levels increase.



Supplementary Figure 2.9. Quantitative immunoblots for Bid-GFP and endogenous Bid in HeLa cells. Pure GFP protein (Biovision, #4999-100) and HeLa cell lysate were separated by 10% Tricine SDS-PAGE as indicated and transferred to a PVDF membrane, scanned on a LI-COR Odyssey scanner, and quantified digitally. **a**, The membrane was probed with mouse anti-GFP (Roche #11814460001) followed by IRDye 800-conjugated anti-mouse. **b**, From the standard curve, we calculate that a single IMS-RP Bid-GFP clone 3.1 HeLa cell has 8.51×10^{-10} g Bid-GFP. Using 27 kDa as the molecular weight of GFP, we find 19,000 Bid-GFP/cell. **c**, The membrane was probed with rabbit anti-Bid (Atlas Antibodies HPA000722) followed by AF680-conjugated anti-rabbit. Using the IMS-RP Bid-GFP clone 3.1 HeLa cells as a standard, we find that a single IMS-RP Bid-GFP clone 3.4 HeLa cell has 62,000 Bid-GFP/cell. We set the average (background subtracted) IMS-RP Bid-GFP clone 3.4 fluorescence intensity (70.9 relative fluorescence units, RFU) of the population of cells in the first frame of a movie equal to 62,000 (calculated above; $70.9 \text{ RFU} = 62,000 \text{ Bid-GFP/cell}$). This allows us to rescale the x-axis of Fig. 2.4d into units of Bid-GFP proteins per cell. Finally, using the IMS-RP Bid-GFP clone 3.1 HeLa cells as a standard and 21,995 as the molecular weight of Bid, we find 20,000 endogenous Bid/HeLa cell. The average of 3 such measurements yields 28,000 endogenous Bid/HeLa cell; s.e.m. = 5,000.

Supplementary Tables

Table 1: Initial conditions and synthesis/degradation rates.

See (Albeck, Burke et al. 2008b) for reaction equations; * indicates a unitless constant.

| | Initial conditions | HeLa Base case initial condition (molecules/cell) | Synthesis rate (molecules/s) | Degradation rate (1/s) | Coefficient of variation |
|----|----------------------|---|------------------------------|------------------------|--------------------------|
| 1 | Ligand | 1000* | 0 | 2.9E-6 | 0 |
| 2 | Receptor | 1000 | 0.00044 | 2.9E-6 | 0.25 |
| 3 | Ligand:Receptor | 0 | 0 | 2.9E-6 | N/A |
| 4 | Receptor* | 0 | 0 | 2.9E-6 | N/A |
| 5 | Flip | 2000 | 0.00087 | 2.9E-6 | 0.25 |
| 6 | Flip:Receptor* | 0 | 0 | 2.9E-6 | N/A |
| 7 | Caspase-8 | 10000 | 0.00435 | 2.9E-6 | 0.25 |
| 8 | Caspase-8:Receptor* | 0 | 0 | 2.9E-6 | N/A |
| 9 | Caspase-8* | 0 | 0 | 2.9E-6 | N/A |
| 10 | Bar | 1000 | 0.00044 | 2.9E-6 | 0.25 |
| 11 | Caspase-8*:Bar | 0 | 0 | 2.9E-6 | N/A |
| 12 | Caspase-3 | 10000 | 0.00435 | 2.9E-6 | 0.282 |
| 13 | Caspase-8*:Caspase-3 | 0 | 0 | 2.9E-6 | N/A |
| 14 | Caspase-3* | 0 | 0 | 2.9E-6 | N/A |
| 15 | Caspase-6 | 10000 | 0.00435 | 2.9E-6 | 0.25 |
| 16 | Caspase-3*:Caspase-6 | 0 | 0 | 2.9E-6 | N/A |
| 17 | Caspase-6* | 0 | 0 | 2.9E-6 | N/A |
| 18 | Caspase-6*:Caspase-8 | 0 | 0 | 2.9E-6 | N/A |
| 19 | XIAP | 100000 | 0.04350 | 2.9E-6 | 0.288 |
| 20 | XIAP:Caspase-3* | 0 | 0 | 2.9E-6 | N/A |
| 21 | PARP | 1000000 | 0.43500 | 2.9E-6 | 0.25 |
| 22 | Caspase-3*:PARP | 0 | 0 | 2.9E-6 | N/A |
| 23 | cPARP | 0 | 0 | 0 | N/A |
| 24 | Bid | 60000 | 0.02610 | 2.9E-6 | 0.288 |
| 25 | Caspase-8*:Bid | 0 | 0 | 2.9E-6 | N/A |
| 26 | tBid | 0 | 0 | 2.9E-6 | N/A |
| 27 | Mcl-1 | 20000 | 0.00870 | 0.0001 | 0.25 |
| 28 | tBid:Mcl-1 | 0 | 0 | 2.9E-6 | N/A |
| 29 | Bax | 80000 | 0.03480 | 2.9E-6 | 0.271 |
| 30 | tBid:Bax | 0 | 0 | 2.9E-6 | N/A |
| 31 | Bax* | 0 | 0 | 2.9E-6 | N/A |
| 32 | Bax*_m | 0 | 0 | 2.9E-6 | N/A |
| 33 | Bcl-2 | 30000 | 0.00870 | 2.9E-6 | 0.294 |
| 34 | Bax*_m:Bcl-2 | 0 | 0 | 2.9E-6 | N/A |
| 35 | Bax*2_m | 0 | 0 | 2.9E-6 | N/A |
| 36 | Bax*2_m:Bcl-2 | 0 | 0 | 2.9E-6 | N/A |
| 37 | Bax*4_m | 0 | 0 | 2.9E-6 | N/A |
| 38 | Bax*4_m:Bcl-2 | 0 | 0 | 2.9E-6 | N/A |
| 39 | Pore | 500000 | 0.21750 | 2.9E-6 | 0.25 |
| 40 | Bax*4:Pore | 0 | 0 | 2.9E-6 | N/A |
| 41 | Pore* | 0 | 0 | 0.0001 | N/A |
| 42 | CytoC_m | 500000 | 0.21750 | 2.9E-6 | 0.25 |
| 43 | M*:CytoC_m | 0 | 0 | 2.9E-6 | N/A |
| 44 | CytoC_r | 0 | 0 | 2.9E-6 | N/A |
| 45 | Smac | 100000 | 0.04350 | 2.9E-6 | 0.25 |
| 46 | M*:Smac | 0 | 0 | 2.9E-6 | N/A |
| 47 | Smac_r | 0 | 0 | 2.9E-6 | N/A |
| 48 | CytoC | 0 | 0 | 2.9E-6 | N/A |
| 49 | Apaf | 100000 | 0.04350 | 2.9E-6 | 0.25 |
| 50 | Apaf:CytoC | 0 | 0 | 2.9E-6 | N/A |
| 51 | Apaf* | 0 | 0 | 2.9E-6 | N/A |
| 52 | Caspase-9 | 100000 | 0.04350 | 2.9E-6 | 0.25 |
| 53 | Apoptosome | 0 | 0 | 2.9E-6 | N/A |
| 54 | Apoptosome:Caspase-3 | 0 | 0 | 2.9E-6 | N/A |
| 55 | Smac | 0 | 0 | 2.9E-6 | N/A |
| 56 | Apoptosome:XIAP | 0 | 0 | 2.9E-6 | N/A |
| 57 | Smac:XIAP | 0 | 0 | 2.9E-6 | N/A |
| 58 | Caspase-3*_Ub | 0 | 0 | 2.9E-6 | N/A |

Table 2: Kinetic rate parameters.

See (Albeck, Burke et al. 2008b) for reaction equations. * indicates units of 1/s.

| forward rates | 1/(s*molec/cell) | reverse rates | 1/s | catalytic rates | 1/s |
|---------------|------------------|---------------|----------|-----------------|-------|
| k1 | 4.00E-07* | kr1 | 1.00E-06 | kc1 | 1E-02 |
| k2 | 1.00E-06 | kr2 | 0.001 | kc2 | 0 |
| k3 | 1.00E-07 | kr3 | 0.001 | kc3 | 1 |
| k4 | 1.00E-06 | kr4 | 0.001 | kc4 | 0 |
| k5 | 1.00E-07 | kr5 | 0.001 | kc5 | 1 |
| k6 | 1.00E-07 | kr6 | 0.001 | kc6 | 1 |
| k7 | 1.00E-07 | kr7 | 0.001 | kc7 | 1 |
| k8 | 2.00E-06 | kr8 | 0.001 | kc8 | 0.1 |
| k9 | 1.00E-06 | kr9 | 0.001 | kc9 | 20 |
| k10 | 1.00E-07 | kr10 | 0.001 | kc10 | 1 |
| k11 | 1.00E-06 | kr11 | 0.001 | kc11 | 0 |
| k12 | 1.00E-07 | kr12 | 0.001 | kc12 | 1 |
| k13 | 0.01 | kr13 | 1 | kc13 | 0 |
| k14 | 1.00E-06 | kr14 | 0.001 | kc14 | 0 |
| k15 | 1.00E-06 | kr15 | 0.001 | kc15 | 0 |
| k16 | 1.00E-06 | kr16 | 0.001 | kc16 | 0 |
| k17 | 1.00E-06 | kr17 | 0.001 | kc17 | 0 |
| k18 | 1.00E-06 | kr18 | 0.001 | kc18 | 0 |
| k19 | 1.00E-06 | kr19 | 0.001 | kc19 | 1 |
| k20 | 2.00E-06 | kr20 | 0.001 | kc20 | 10 |
| k21 | 2.00E-06 | kr21 | 0.001 | kc21 | 10 |
| k22 | 1 | kr22 | 0.01 | kc22 | 0 |
| k23 | 5.00E-07 | kr23 | 0.001 | kc23 | 1 |
| k24 | 5.00E-08 | kr24 | 0.001 | kc24 | 0 |
| k25 | 5.00E-09 | kr25 | 0.001 | kc25 | 1 |
| k26 | 1 | kr26 | 0.01 | kc26 | 0 |
| k27 | 2.00E-06 | kr27 | 0.001 | kc27 | 0 |
| k28 | 7.00E-06 | kr28 | 0.001 | kc28 | 0 |
| k29 | 5.00E-08 | kr29 | 0.001 | kc29 | 1 |
| k30 | 6.00E-07 | kr30 | 0.001 | kc30 | 0 |
| k31 | 0.01 | kr31 | 0 | kc31 | 0 |

Chapter 3

3 Simulating a population of TRAIL-treated cells with a population of models

This chapter is based upon:

Computational analysis of variability in TRAIL-induced apoptosis

(In preparation)

Suzanne Gaudet*, Sabrina L. Spencer*, William W. Chen, and Peter K. Sorger

(* These authors contributed equally to this work.)

In TNF-related apoptosis inducing ligand (TRAIL)-mediated apoptosis, cells enter a long and variable delay period prior to sudden activation of effector caspases that rapidly kills the cell. We have previously shown that variability in death time largely results from cell-to-cell variability in the levels or activity states of protein regulators of apoptosis. Here we establish a method for modeling variability in cellular output caused by cell-to-cell variability in initial conditions. We also develop novel, intuitive forms of sensitivity analysis which can be directly tested experimentally. Modeling predicts, and experiments confirm, that a cell's response to

increasing Bcl-2 levels can be described as a step function where cells resist death entirely above a threshold level of the protein. We perform the simulations with and without measured covariance in initial conditions, revealing a moderate impact on variance in death time but a large impact on sensitivities. These differences underscore the need to consider cellular contexts, such as covariance in two antagonistic protein species, when building biological models.

3.1 Introduction

Mathematical modeling of complex signal transduction pathways is essential for understanding the highly non-linear and therefore non-intuitive behavior of signal propagation. Most models of induced signal transduction in mammalian cells use deterministic equations to mimic the average behavior of a population of cells (Hoffmann, Levchenko et al. 2002; Bentele, Lavrik et al. 2004; Hua, Cornejo et al. 2005; Legewie, Bluthgen et al. 2006; Chen, Schoeberl et al. 2009) or explicitly model a single representative cell from a population (Eissing, Conzelmann et al. 2004; Altan-Bonnet and Germain 2005; Geva-Zatorsky, Rosenfeld et al. 2006; Albeck, Burke et al. 2008b). With the exception of several studies that use stochastic simulations (Eissing, Allgower et al. 2005; Geva-Zatorsky, Rosenfeld et al. 2006; Toettcher, Loewer et al. 2009), variability from cell-to-cell has been largely ignored in modeling or treated as merely the standard deviation of an aggregate measurement. However, much can be learned from treating cell-to-cell variability not as noise or error, but rather as remarkable differences from cell-to-cell that can be modeled deterministically and can have an impact on cell fate.

Several recent papers have highlighted the consequences of variability in protein levels for biological processes ranging from differentiation (Chambers, Silva et al. 2007; Chang,

Hemberg et al. 2008) to drug-induced cell death (Cohen, Geva-Zatorsky et al. 2008), including a recent report from our group on TRAIL-mediated apoptosis (Spencer, Gaudet et al. 2009). The TRAIL signaling network represents an unusual variable delay, snap-action switch that forces an unequivocal and irreversible life-or-death decision (Albeck, Burke et al. 2008b). During the variable delay period, upstream initiator caspases are active, but mitochondrial outer membrane permeabilization (MOMP) has not occurred and downstream effector caspases are inactive (Albeck, Burke et al. 2008b). In many cell types, the decision period becomes a commitment to certain death once the MOMP threshold is crossed. This causes the release of pro-apoptotic proteins from the mitochondrial outer membrane; these proteins converge to rapidly activate effector caspases that destroy the cell.

The signaling pathway (Fig. 3.1a) that creates such a variable delay, all-or-none switch can be triggered by the binding of one of the TNF (tumor necrosis factor) family of ligands, which include TNF α , Fas ligand, and TRAIL. TRAIL ligand stimulation induces the trimerization of its receptors on the cell surface, DR4 and DR5. This initiates assembly of the death-inducing signaling complex (DISC), which activates initiator caspases-8 and -10 (hereafter C8). Activated C8 can directly cleave effector caspases-3 and -7 (hereafter C3), however complete activation of C3 requires activation of the mitochondrial pathway in most cells (the so-called 'Type II' cells). This step occurs because C8 also activates and cleaves Bid to tBid, which in turn activates Bax via conformational change. Active Bax translocates to the mitochondria, where it causes mitochondrial outer membrane permeabilization (MOMP) by the formation of pores in the outer membrane of the mitochondria. The pro-apoptotic activity of active Bax and tBid is antagonized, however, by the anti-apoptotic Bcl-2 family of proteins, which act as a buffer for active Bax and tBid. Upon permeabilization, the mitochondria release in an all-or-

none fashion a potent mixture of pro-apoptotic proteins, including cytochrome *c* and Smac. Cytochrome *c* forms the apoptosome complex with Apaf-1 and caspase-9 (C9), which activates additional C3. This activation is aided by Smac's inhibition of XIAP, which inhibits active C3. A positive feedback loop mediated by caspase-6 (C6) serves to amplify the death signal under certain conditions. C3 goes on to kill the cell by activating DNases that fragment the genome, cleaving DNA repair enzymes such as PARP, and cleaving structural proteins such as cytokeratins and nuclear lamins.

There are several features that describe the trajectory a cell can take from TRAIL stimulation to death (Fig. 3.1b). The 'decision' phase of the pathway lies upstream of MOMP and can be described as a variable rate of approach to a threshold of variable height (Spencer, Gaudet et al. 2009). The rate of approach (k_{IC}), the height of the MOMP threshold (θ), and the timing of MOMP (t_{MOMP}) can be measured in single cells using live-cell fluorescent reporters of initiator caspase activation (IC-RP) and MOMP (IMS-RP) (Albeck, Burke et al. 2008a, Spencer, Gaudet et al. 2009). After MOMP occurs, the cell is committed to apoptosis by means of effector caspase activation, which can be monitored using fluorescent reporter EC-RP (Albeck, Burke et al. 2008a). The time between exposure to TRAIL and the time of half-maximal cleavage of effector caspase substrates such as PARP is termed t_{PARP} . The cleavage of effector caspase substrates rapidly rises to a plateau, at which point the cell has died; the fraction of effector caspase substrate cleavage at this plateau is termed f . The switching time between initial and complete effector substrate cleavage is termed t_s . Together, these six features describe a cell's path through the pre-MOMP decision phase (k_{IC} , θ , t_{MOMP}) through to the death of the cell (t_{PARP} , f , t_s).

Here we develop a modeling methodology that accounts for the observed cell-to-cell variability in TRAIL signaling by modeling a population of cells using a population of deterministic models with distributions of initial conditions informed by our experimental measurements. Using this framework, we address the relative importance of proteins in the apoptosis network with novel types of sensitivity analysis that can be directly compared to single-cell experiments. The network is revealed as a complex landscape where various species can appear significant depending where its initial condition resides, underscoring the importance of knowledge of protein level mean and variance for meaningful sensitivity analysis. We find that the determination of death time is multifactorial, and that even perfect knowledge of the concentration of the most sensitive model species only returns partial predictability of a cell's death time in a background where all proteins' initial conditions are variable.

3.2 Results

3.2.1 Modeling a population of cells with a population of models

We have previously shown that variability in death time is in large part due to variability in protein levels. We therefore measured the spread in steady state levels of several apoptosis regulators in a clonal population of HeLa cells using immuno-fluorescence and flow cytometry (Fig. 3.1c-e). The antibodies used to measure total protein were validated by siRNA and overexpression (Supplementary Fig. 3.1 and 3.2). To ensure that antibody binding was not adding a substantial amount of variation to our total protein measurements, we assessed how well a signal from antibody binding matched a known amount of cellular GFP fluorescence (Fig. 3.1d). Variation extending along the diagonal represents real cell-to-cell differences in the level of protein, whereas off-diagonal variation reflects disagreement between the protein abundance measured by antibody and the known abundance as read out by GFP fluorescence. We found

that off-diagonal variation was much smaller than true cell-to-cell variation and could be safely ignored. All protein distributions measured were found to fit a log-normal distribution (Supplementary Fig. 3.3), with a coefficient of variation (CV, standard deviation/mean) of about 0.44 (Fig. 3.1c). Subsequently, we gated on a subset of cells with similar forward scatter and side scatter values in order to select a subpopulation of cells of similar size, and found that the CV of the protein distributions decreases to about 0.29, in accordance with similar measures of a different set of proteins made by live-cell microscopy (Sigal, Milo et al. 2006). The un-gated data measure dispersion in total protein amount, while the size-selected data measure dispersion in protein concentration. We also compared these measurements to ones made by immunofluorescence microscopy (where cell size was assessed by nuclear area) and found good agreement (data not shown).

Using a previously developed differential equation model of TRAIL-induced apoptosis describing a typical HeLa cell's response to TRAIL (Albeck, Burke et al. 2008b), we modeled a population of similarly sized HeLa cells with a population of models where cells vary in their initial proteins levels. We used the measured CV for the five proteins measured in Fig. 3.1c, or assumed a log-normal distribution with a CV of 0.25 for the 12 remaining initial conditions. To model a population of cells, we ran numerous deterministic simulations of this model, each time randomly and independently sampling from the log-normal protein distributions to pick the number of copies of each protein in that simulated cell. By plotting the distribution of t_{PARP} as a model output for a population of these simulated cells, we found that the variability in the model's initial conditions propagates through the pathway to recapitulate the experimentally observed variability in death time over a wide range of doses (Fig. 3.1h and ref. Spencer, Gaudet et al. 2009).

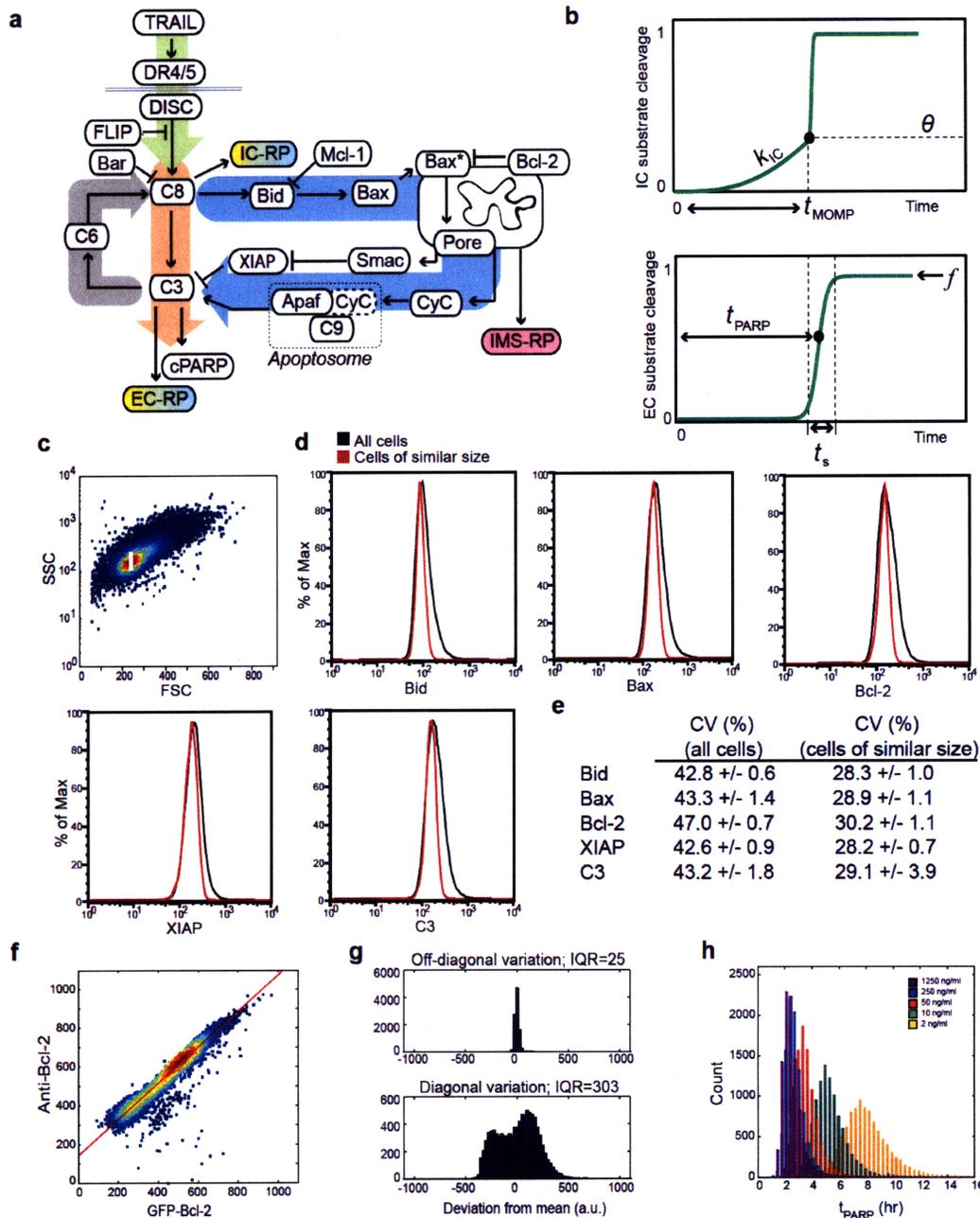


Figure 3.1. Measurements of variability in protein levels in the TRAIL-induced apoptosis network. **a**, The TRAIL-induced apoptosis pathway as described in the text. Fluorescent protein reporters IC-RP, EC-RP, and IMS-RP are indicated. **b**, Idealized IC-RP (top) and EC-RP (bottom) trajectories indicating the six features discussed in the text. **c**, Selection of cells of similar size by gating on side scatter (SSC) and forward scatter (FSC); white box marks the selected cells. **d**, Distribution of protein levels in a population of cells as measured by immunostaining and flow cytometry. **e**, Comparison of the coefficient of variation (CV) for the distributions of protein levels in (d). Error is the standard error of the mean from independent measurements. **f**, HeLa cells stably expressing GFP-Bcl-2 (x-axis) were stained with anti-Bcl-2 (SC7382) followed by a secondary antibody conjugated to Alexa Fluor 647 (y-axis). An increase in known Bcl-2 abundance (observable by the GFP tag) is matched by an increase in the measured amount of Bcl-2 using the antibody. **g**, Off-diagonal variation (mismatch in known Bcl-2 relative to measured Bcl-2 abundance) is small compared with diagonal variation (true variation in the amount of Bcl-2 from cell to cell). IQR, interquartile range. **h**, Distribution of t_{PARP} in populations of simulated cells for five doses of TRAIL. Each cell's initial protein levels were sampled independently from log-normal distributions.

3.2.2 Forward propagation of variability in initial conditions to timing of death

Given that all five proteins measured were found to be similarly log-normally distributed with CVs of about 0.29, we questioned whether variability in all proteins contributed equally to producing variability in t_{PARP} or whether variability in certain proteins was more influential than others. To determine which components of the apoptotic pathway provide the majority of the heterogeneity in t_{PARP} , we performed a computational scan of the effect of variability in single proteins on t_{PARP} . This involved running a set of simulations for each of the 17 initial conditions, with sampling from a log-normal distribution for the protein in question while all other proteins were held constant at their default level. We then compared the variance in t_{PARP} from the first set of simulations where all initial conditions are allowed to vary simultaneously, to these simulations where only one protein is varied at a time (Fig 3.2). We find that variability in several proteins at the top of the pathway controlling rate k_{IC} (namely Receptor, C8, and Bid) as well as the two main proteins controlling the MOMP threshold θ (namely Bax and Bcl-2) can each significantly contribute to variability in t_{PARP} . In contrast, proteins downstream of MOMP contribute little to variability in t_{PARP} . These findings are consistent with experiments showing that the majority of the variability in time-to-death lies upstream of MOMP (Spencer, Gaudet et al. 2009). We noted that the sum of variability in the individual network components did not equal the variability in output when all protein levels were allowed to vary simultaneously. This is a result of high nonlinearity in the model and the fact that the combined effect of individual contributions likely involves an operation more complex than simple addition.

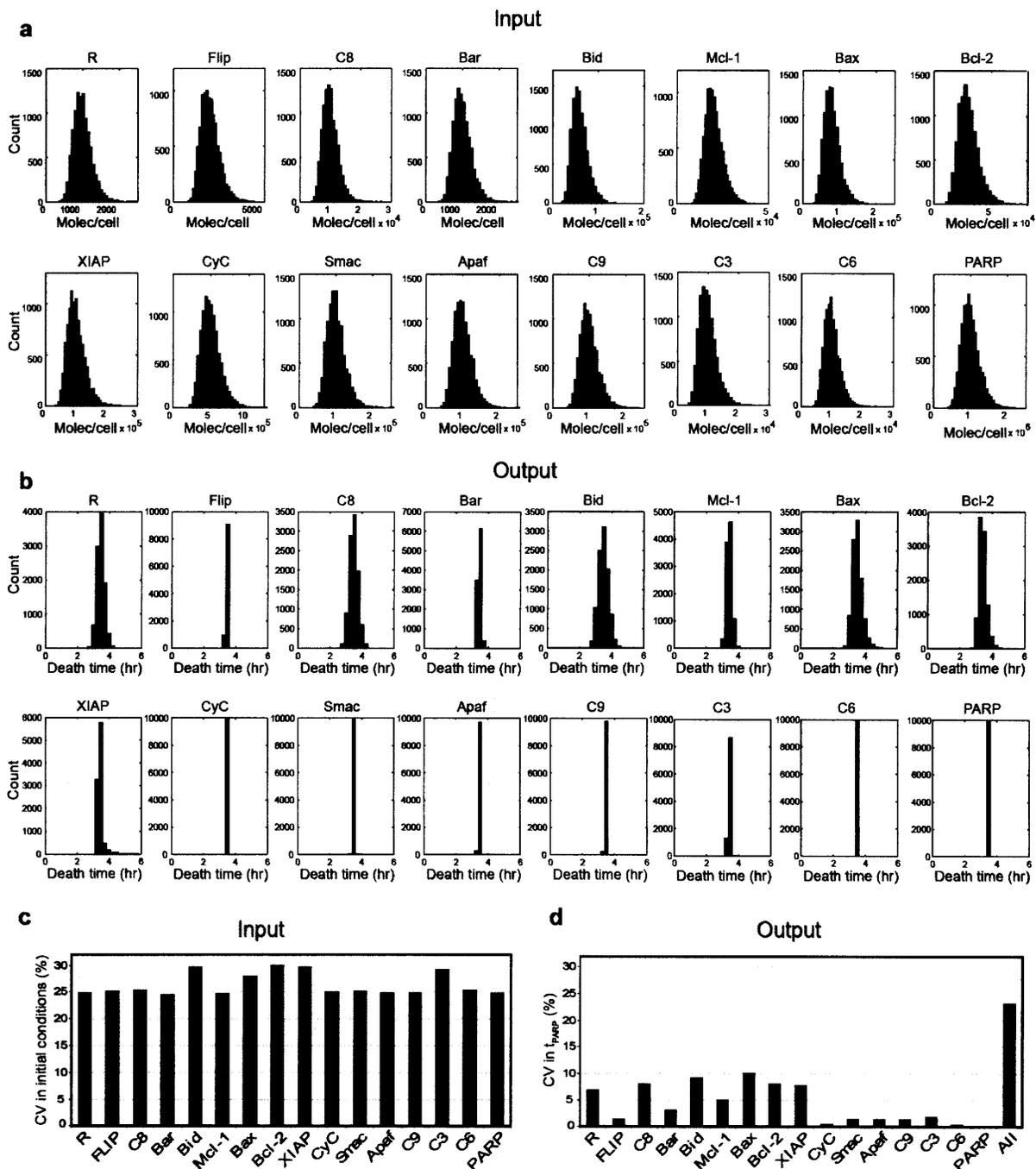


Figure 3.2. Propagation of variability in initial conditions to produce variability in t_{PARP} . **a**, Synthetic distributions of 16 of 17 initial protein species; omitted is the distribution from cell to cell in the number of possible pores in the mitochondrial outer membrane. Distributions are log-normal with CVs as measured (Fig. 2.1e), or set to 0.25 if unmeasured. **b**, Distribution of death times (measured by t_{PARP}) when the variation in one protein species at a time simulated, with all other species held constant at the mean value. **c**, Data from (a) plotted as a bar graph. **d**, Results from (b) plotted as a bar graph; the CV for simulations from Fig. 2.1h with all initial conditions varying simultaneously is included for comparison ("All"). Simulations were run with 50 ng/ml TRAIL.

3.2.3 Correlations in initial conditions reduce variance in death time

The simulations in Fig. 3.1h allowed all initial conditions to vary in an uncorrelated fashion. We next considered the effect of correlations in the levels of initial conditions. Using two color flow cytometry, we measured the degree of correlation in ten pairs of initial conditions using cells of similar size as described above. We found a range of linear correlation coefficients (R^2) ranging from an average of 0.15 for C3 and Bcl-2 to 0.53 for Bax and Bcl-2 (Fig. 3.4a,b). A positive control using two different Bcl-2 antibodies always produced the highest correlation among the pairs ($R^2=0.62$ – this correlation is less than one because the two antibodies have overlapping epitopes). This range of correlations is consistent with measures of different pairs of proteins made by microscopy (Sigal, Milo et al. 2006). We did not detect anti-correlation between any pairs of proteins. This could result from the fact that positive correlation in gene expression could be more easily achieved by a cell (via use of the same transcription factor, the same miRNA targeting mRNAs, or the same regulation of degradation) and thus more common than active negative correlation. In addition, some variability in cell size could be present even after our size selection process and could inflate positive correlations.

We next used the ten measured pair-wise correlations from Fig. 3.3b as inputs for a new set of simulations; proteins whose correlations were not measured were left uncorrelated (see Methods). We found that including knowledge of correlations in initial conditions reduced the variability in t_{PARP} by 18%, from a CV of 0.23 to a CV of 0.19 for 50 ng/ml TRAIL (Fig. 3.3c), providing a better match to experimental data (Fig. 3.3d). A similar reduction in CV was seen at all doses of TRAIL (Fig. 3.3d).

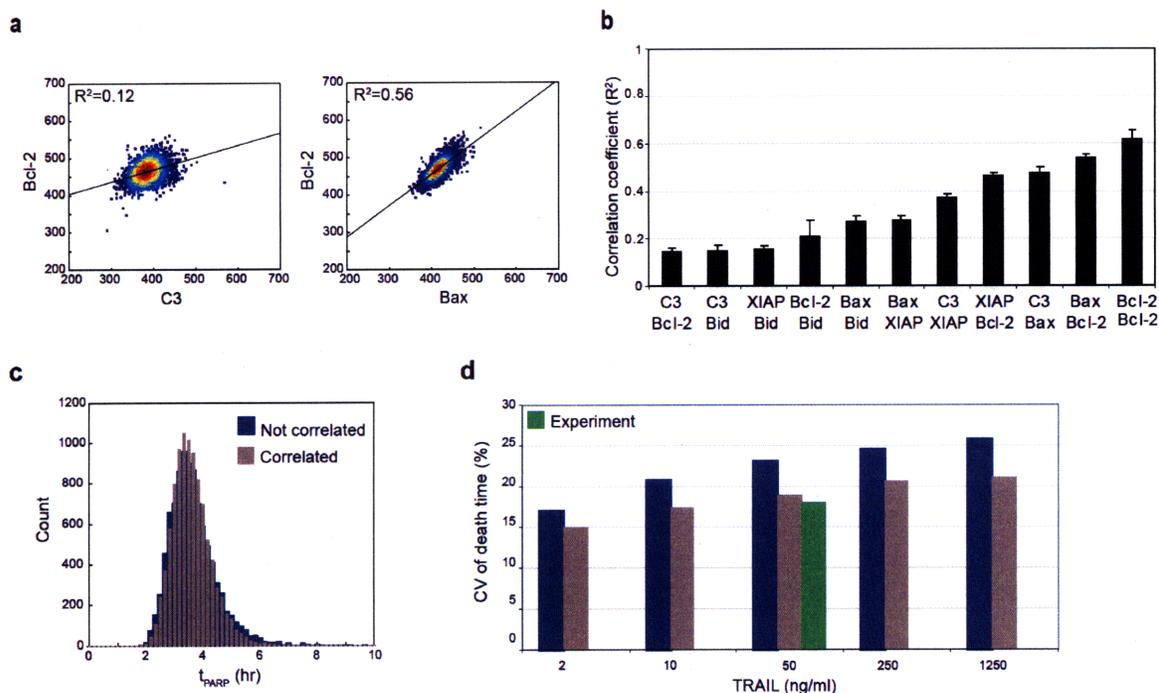


Figure 3.3. Correlations in protein levels affect the distribution of death times. **a**, Correlation between the levels of pairs of proteins in a population of cells measured by immunostaining and flow cytometry for the least correlated pair (left) and the most correlated pair (right) measured. The R^2 was calculated by linear regression. **b**, Measured correlation in the levels of ten protein pairs plus a positive control of Bcl-2 against itself using two different Bcl-2 antibodies. **c**, Comparison of the distribution of t_{PARP} with independent sampling of initial conditions (blue) or with the ten pair-wise correlations as measured in (b) and independent sampling of all other proteins. **d**, CV of death time for the two types of simulations in (c) as measured by t_{PARP} , or as measured experimentally by monitoring IMS-RP translocation using live cell microscopy.

3.2.4 A biologically driven sensitivity analysis

Thus far, we have addressed responses to measured *endogenous* variability in protein levels. However, additional features may be revealed by probing sensitivity outside the range of endogenous variation, as is commonly done by experimental knock-down and overexpression. For one protein at a time, we simulated a knock-down and an overexpression of each of the model species, allowing the initial conditions to vary in a uniform fashion from 10^2 - 10^7 proteins per cell and observing the effect on death time (Fig. 3.5a). In a first set of simulations, we predict the average cell behavior by holding all other 16 proteins constant at their mean value. Pro-apoptotic proteins upstream of the MOMP (Receptor, C8, Bid, Bax) have a negative slope

while anti-apoptotic proteins (FLIP, Bar, Mcl-2, Bcl-2) have a positive slope. Varying the levels of proteins downstream of the mitochondria has little effect on t_{MOMP} . Of note are the complex, nonlinear, and asymmetric sensitivities observed when a protein's level is increased or decreased, making intuition based on pictorial pathway representations unreliable. In general, pro-apoptotic proteins are more sensitive to having their levels decreased and anti-apoptotic proteins more sensitive to having their levels increased. By observing where a population's range of endogenous protein expression levels falls, we are able to understand why certain cells are very sensitive to some proteins' initial concentrations and not to others. For example, simulation predicts that HeLa cells sit very close to a threshold level of Bcl-2 above which the death time increases rapidly, to the extent that cells might actually survive the death stimulus. As these simulations can be directly compared with live-cell microscopy of TRAIL-treated cells overexpressing fluorescently tagged proteins, this type of simulation is a biologically testable form of sensitivity analysis.

To test this prediction, we forced a spread in the levels of Bcl-2 or its homolog Bcl-x_L by ectopic expression of GFP fusions. Live-cell microscopy yielded data on the levels of GFP in individual cells and quantitative immunoblotting yielded a population average for the number of molecules per cell (Supplementary Fig. 3.4 and 3.5); we combined this information to convert the *x*-axes of Fig. 3.4c,d into units of proteins/cell. We treated these cells with TRAIL and the protein synthesis inhibitor cycloheximide and scored the time of MOMP (t_{MOMP}) in each cell by monitoring IMS-RP translocation (Albeck, Burke et al. 2008a). When treated with TRAIL plus cycloheximide, 100% of wild-type HeLa cells die by apoptosis. However, when t_{MOMP} was plotted relative to the initial level of GFP-Bcl-2 or GFP- Bcl-x_L in individual HeLa cells overexpressing these proteins, we discovered a sharp threshold in the fate of these cells as

predicted by simulation (Fig 3.4b,c). At low fusion protein levels, MOMP occurred ~2-5 hr after TRAIL addition, while at high fusion protein levels, MOMP was blocked indefinitely. At intermediate levels (shaded yellow in Fig. 3.4b,c), cell fate was variable with a subset of cells undergoing MOMP and the others not. We presumed that cell-to-cell variability in the levels of other apoptotic proteins determines outcome in the variable region, whereas at very high levels of Bcl-2 and Bcl-x_L (protein levels above the yellow shading in Fig. 3.4b,c), pro-apoptotic factors never reach a concentration high enough to induce MOMP.

To study this region of variable fate more closely, we ran a second set of simulations. Here, we used correlated sampling as in Fig. 3.3c, and added a uniformly distributed overexpressed amount of Bcl-2 ranging from endogenous levels to 10⁶ proteins/cell to match the experimental data. This additional realism allows us to reproduce the region of variable fate in simulation and provides a reasonable match between model and experiment (Fig. 3.4d). We can now ask why, for a fixed amount of GFP-Bcl-2, one cell lives while another dies. We found that variability in the levels of other proteins controlled the fate of the cell, but there was no single protein that was primarily responsible for the bifurcation in fate (Fig. 3.4e,f). Close to a sharp threshold, small changes can have a large impact. This appears to be such a case – small differences in the levels of many other proteins combine to change the cell's fate.

Another noteworthy feature of these overexpression experiments is the observation that increasing Bcl-2 and Bcl-x_L levels cause only a very minor increase in t_{MOMP} for levels below the region of variable fate (Fig. 3.4b,c and Supplementary Fig 3.6). Consistent with these two proteins contributing to θ (the threshold height), they have less impact on the timing of death compared to proteins involved in k_{IC} . A small increase in θ can slightly delay MOMP (Spencer, Gaudet et al. 2009), but the effect of a large increase in θ is to prevent a cell from crossing the

threshold for MOMP entirely. Thus, k_{IC} primarily affects the timing of death, while θ primarily affects whether a cell lives or dies (with a minor effect on timing).

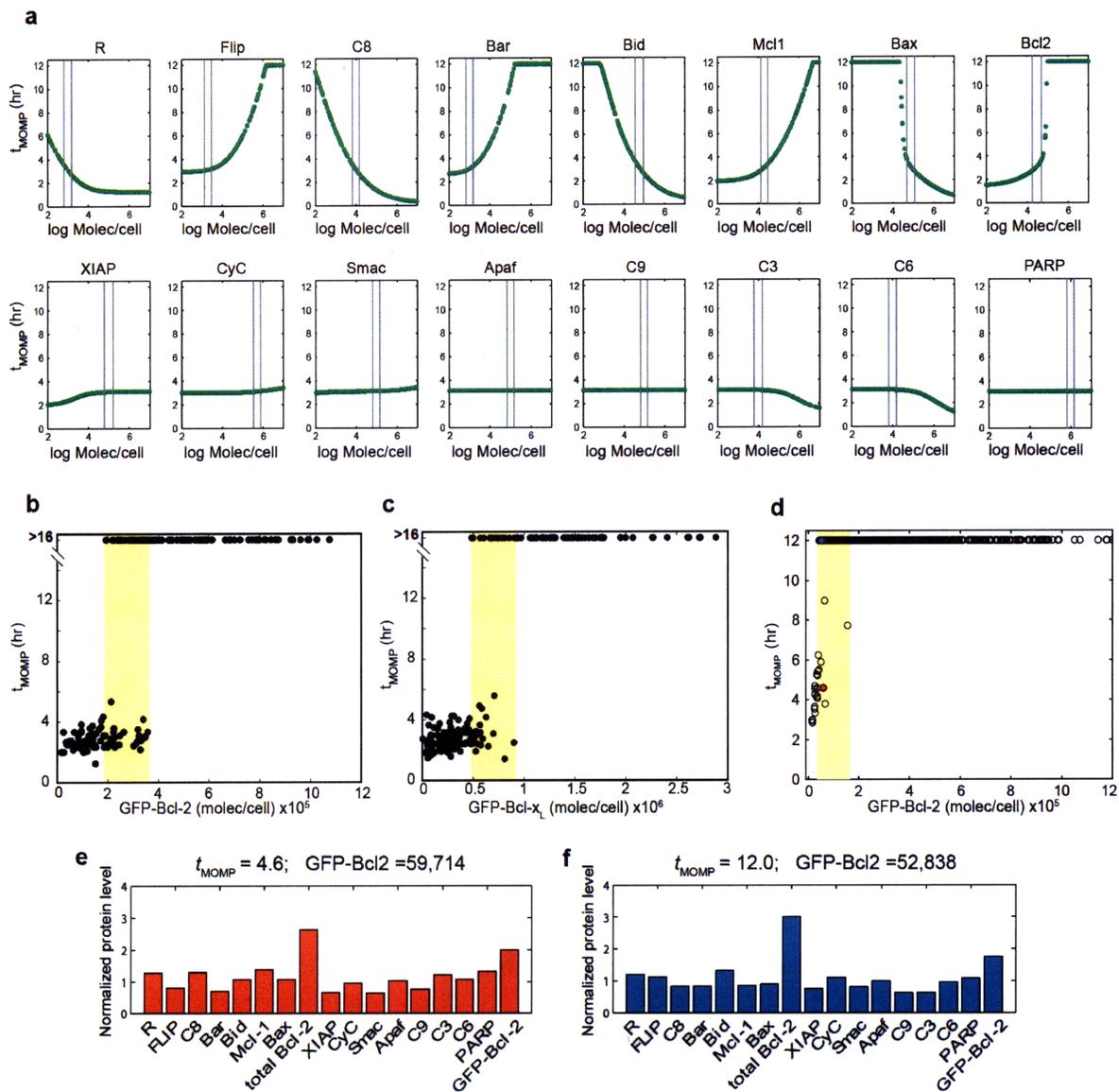


Figure 3.4. Effect of knock-down and overexpression of protein levels on t_{MOMP} . **a**, The 16 initial conditions from Fig. 3.2a were varied one at a time over five orders of magnitude and the effect on t_{MOMP} plotted; all other proteins were held constant at the default value. Double grey bars indicate the 5th and 95th percentiles of the endogenous distribution. **b**, Experimental analysis of the effect on t_{MOMP} of overexpressing GFP-Bcl-2 in HeLa cells on a cell-by-cell basis. MOMP was scored using IMS-RP. Cells remaining alive at the end of the 16 hr movie are indicated at >16 hr. Yellow shading indicates the region of variable fate. **c**, Same as (b) but for the Bcl-2 homolog Bcl-x_L. **d**, Effect on t_{MOMP} of increasing Bcl-2 levels in simulation on a background of variability to reproduce the region of variable fate. Simulations were run with correlated sampling from log-normal distributions as in Fig. 3.3 but with an additional uniform amount of overexpressed Bcl-2. Two cells with similar levels of overexpressed Bcl-2 but with different fates are indicated in orange and blue and are described in (e) and (f). **e**, Initial conditions of the orange cell indicated in (d) with 59,714 GFP-Bcl-2 proteins per cell and $t_{MOMP} = 4.6$ hr. **f**, Initial conditions of the blue cell indicated in (d) with 52,838 GFP-Bcl-2 proteins per cell and no MOMP by the end of the 12 hr simulation. Initial protein levels in the two cells have been normalized to the average (default level) of that species.

A third aspect of these overexpression data is that ~360,000 GFP-Bcl-2 proteins/cell (~13 fold over endogenous Bcl-2) versus ~900,000 GFP-Bcl-x_L proteins/cell (~120 fold over endogenous Bcl-x_L) are required to prevent MOMP (Fig. 3.4b,c). However, we note that the number of copies needed to reach a point where all of the cells survive is not necessarily a function of the fold overexpression over endogenous, but rather a function of the absolute number of copies sufficient to overwhelm variability in all other determinants of cell fate. The difference in the total number of Bcl-2 proteins (~360,000 + ~30,000 endogenous) or Bcl-x_L proteins (~900,000 + ~8,000 endogenous) needed to prevent MOMP leads us to predict that in HeLa cells, Bcl-2 is a more potent inhibitor of death than Bcl-x_L. This could be due to the number of pro-apoptotic partners that Bcl-2 is able to buffer and/or its relative affinity for these targets. The relative affinities of Bcl-2 and Bcl-x_L for a protein like Bax are as yet impossible to measure *in vivo* (for Bax in its activated conformation), but we are potentially observing their effects in these experiments.

3.2.5 Reverse prediction of death time given incomplete knowledge of initial conditions

Given the importance of Bid, Bax, and Bcl-2 in the forward simulations, and the availability of validated antibodies to these three proteins, we asked whether knowledge of the levels one or two of these proteins would be sufficient to distinguish experimentally between cells that would die quickly after treatment with TRAIL and cells that would take longer to die.

Using simulations with correlated initial conditions as in Fig. 3.3c, we compared the levels of Bid, Bax, and Bcl-2 in ‘untreated’ cells (the full population of initial conditions) with cells that were still alive after 2.5 hr of treatment with TRAIL plus cycloheximide. We saw only a slight reduction of cells with high Bid and Bax levels in the population of cells that remained alive after 2.5 hr of treatment (Fig 3.5a). Based on these results, we predicted that these differences would be too small to measure in a corresponding flow cytometry experiment, which we found to be the case (Fig. 3.5b). Furthermore, simultaneous knowledge of the levels of two proteins in a single cell also failed to distinguish untreated cells from cells that remained alive after 2.5 hr of treatment. In the experiments, one could attribute this negative finding to error in the experimental methods that prevent such subtle differences from being measurable (Supplementary Fig. 3.8). However, even in our deterministic simulations where we know that variability in Bid, Bax, and Bcl-2 propagates forward through the pathway to produce variability in death time, we are unable to detect in reverse the differences in protein levels that cause the variability in death time.

A more time-consuming but nevertheless feasible experimental approach would be to endogenously label proteins corresponding to sensitive model species with a fluorescent tag and then to ask whether knowledge of a protein’s level is predictive of a cell’s death time. As was demonstrated for four proteins contributing to k_{IC} in simulations with independently sampled initial conditions (Spencer, Gaudet et al. 2009), and shown here for all proteins in the model with correlated initial conditions (as in Fig. 3.3c), the answer was no (Fig. 3.6a). Variability in other proteins obscured the contribution from any individual protein. However, the extent to which the rank ordering of sensitivities changes when the simulations are run with and without correlated initial conditions is noteworthy (Fig. 3.6b). The sensitivity of Bcl-2 changes the most

dramatically – Bcl-2 is the second most sensitive protein when the simulations are performed with independent sampling, but is second to last in sensitivity when initial conditions are sampled using the measured covariance. Thus, although knowledge of correlations in initial conditions had only a moderate impact on the CV of t_{PARP} , it has a large impact on the rank ordering of sensitivities.

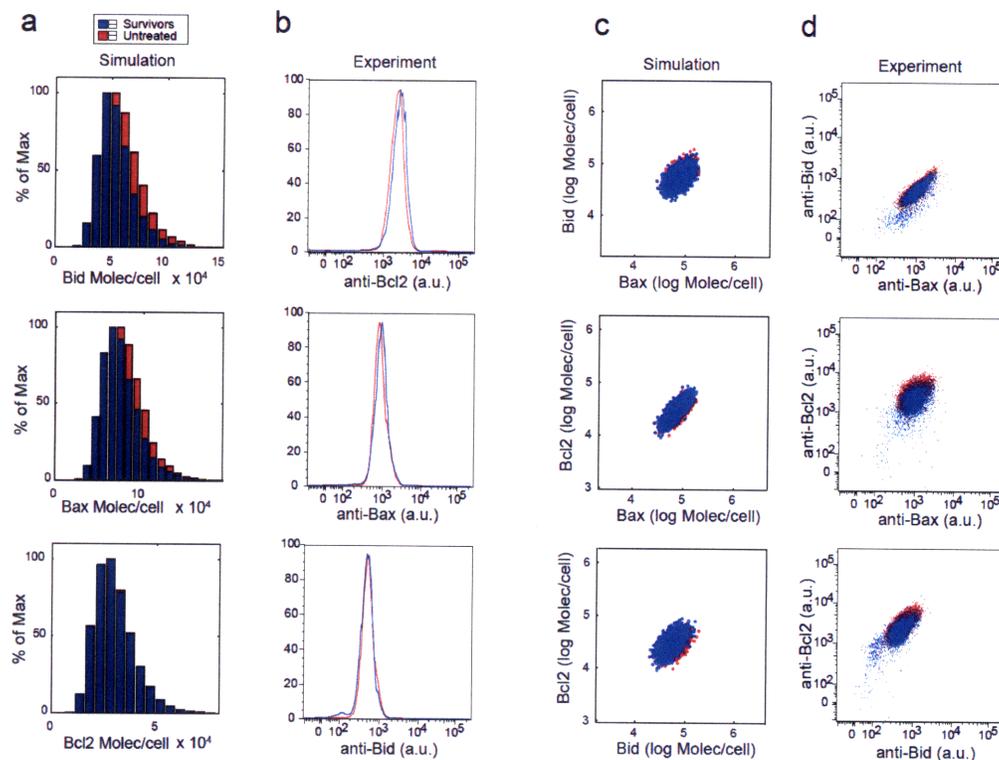


Figure 3.5. The levels of single or double proteins are not detectably different in untreated cells and TRAIL survivors. **a**, Levels of Bid, Bax, and Bcl-2 in untreated cells (the total population, red) versus cells remaining alive after 2.5 hr of treatment with 50 ng/ml TRAIL (“survivors”, blue) using simulations run with correlated initial conditions as in Fig. 3.3c. **b**, Same as (a) but via experimental analysis of immunostained cells and flow cytometry (see also Supplementary Fig. 3.8). **c**, Same as (a), but now examining whether the levels of a pair of proteins is significantly different in untreated cells versus “survivors” using simulation. **d**, Same as (c) but via experimental analysis of immunostained cells and flow cytometry.

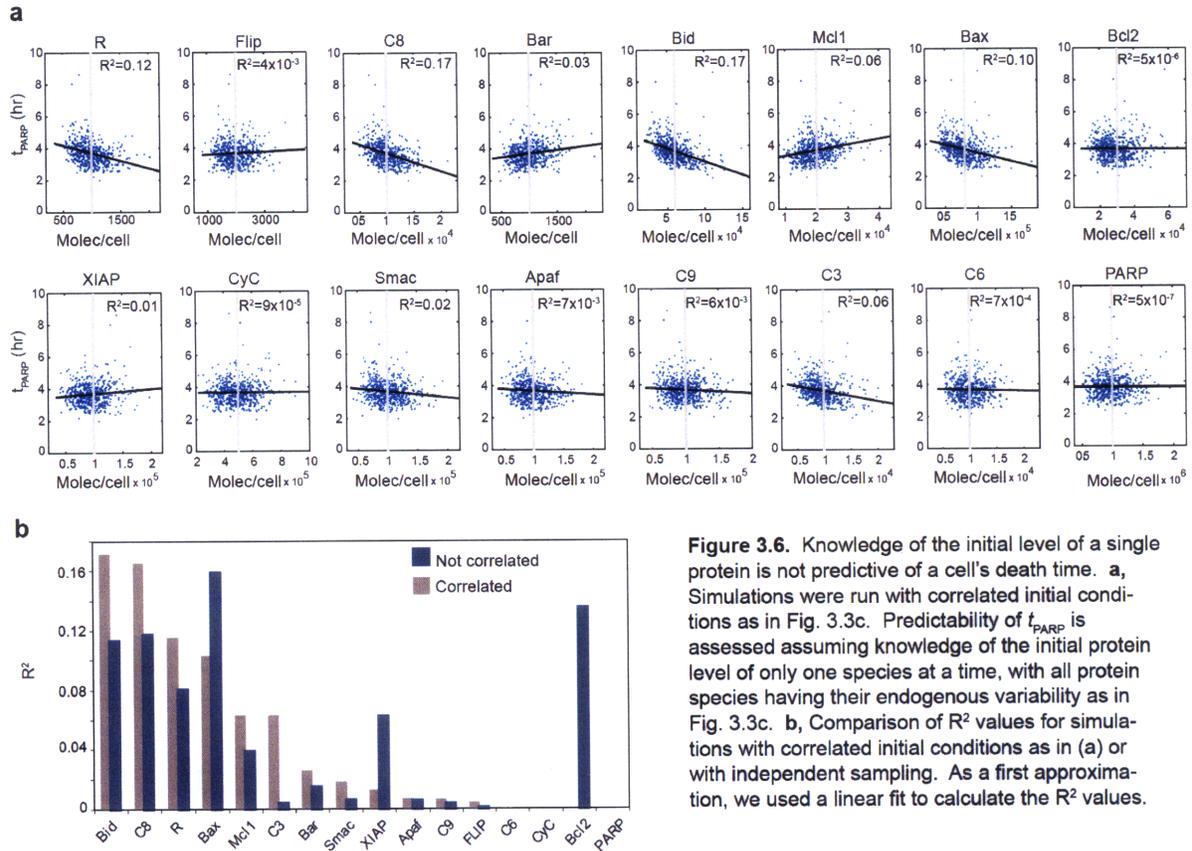


Figure 3.6. Knowledge of the initial level of a single protein is not predictive of a cell's death time. **a**, Simulations were run with correlated initial conditions as in Fig. 3.3c. Predictability of t_{PARP} is assessed assuming knowledge of the initial protein level of only one species at a time, with all protein species having their endogenous variability as in Fig. 3.3c. **b**, Comparison of R^2 values for simulations with correlated initial conditions as in (a) or with independent sampling. As a first approximation, we used a linear fit to calculate the R^2 values.

3.3 Discussion

In this work, we develop methods for modeling variability in cell behavior that results from variability in initial conditions. The idea that variability in cellular response can be modeled by variability in protein levels has been suggested previously (Eissing, Conzelmann et al. 2004; Wilkinson 2009), but we are the first to implement such a modeling effort. The primary source of heterogeneity in the timing of apoptosis induced by TRAIL in the presence of cycloheximide was recently shown to be a result of cell-to-cell variability in protein levels that exists prior to treatment (Spencer, Gaudet et al. 2009). As pairs of sister cells had very similar death times, stochasticity in the TRAIL-induced protein signaling cascade, as is typically simulated using the Gillespie algorithm, plays a minimal role. We therefore are able to use a deterministic framework with random sampling from measured distributions of protein levels to

simulate a population of cells. We develop three novel forms of sensitivity analysis in Fig. 3.2, 3.4, and 3.6 that should be much more intuitive for biologists than a classical sensitivity analysis. Moreover, two of these analyses (Fig. 3.4 and 3.6) are analogs of experiments that can be performed using live-cell microscopy.

Our primary biological discovery relates to the extreme nonlinearity in a cell's response to Bcl-2 and Bcl-x_L levels, a finding that was predicted by our model. The ability of Bcl-2 and Bcl-x_L to prevent apoptosis has been known for some time (Vaux, Cory et al. 1988; Hockenbery, Nunez et al. 1990; Boise, Gonzalez-Garcia et al. 1993). However, our single-cell analysis provides a precise mapping between a cell's Bcl-2 or Bcl-x_L overexpression level and its death time. We note that MOMP can be blocked indefinitely by a 13-fold overexpression of Bcl-2 in HeLa cells, a fold increase reached in acute lymphoblastic leukemias (Coustan-Smith, Kitanaka et al. 1996). Bcl-2 is a more potent inhibitor than Bcl-x_L of TRAIL-induced apoptosis in HeLa cells. The difference in Bcl-2 and Bcl-x_L levels required to block MOMP may reflect differences in the relative affinities of these proteins for their pro-apoptotic binding partners that are not currently measurable in living cells.

We highlight two key computational findings pertaining to the creation of accurate biological models. First, we find that while including knowledge of correlations in initial conditions had a moderate impact on variance in death time, it had a large impact on the sensitivities of initial conditions. Correlations can change the apparent importance of proteins, especially when a protein's level is correlated with the level of its direct antagonist, as is the case for Bcl-2 and Bax. A cell with high Bcl-2 may have had a delayed death time in the case of independent sampling of initial conditions, but if high Bcl-2 results in the cell simultaneously having high Bax, the anti-apoptotic effect of Bcl-2 will be negated. Thus, knowledge of the

biochemistry must be supplemented by knowledge of cellular context, as co-variation in a highly non-linear model can produce surprising results.

Second, our simulations underscore the need for accurate knowledge of the mean and variance of key protein levels when modeling – a small error in the estimates of sensitive species' mean levels can result in large inaccuracies in the distribution of death times or in estimations of sensitivity. For example, we found that doubling the initial condition for Bcl-2 from our measured level of 3×10^4 Bcl-2 proteins/cell (Supplementary Fig. 3.4) to 6×10^4 had a significant impact on the CV of t_{MOMP} and on the relative importance of pathway proteins, to the extent that Bax and Bcl-2 become the most dominant species (Supplementary Fig. 3.7). This inflated sensitivity is inconsistent with experimental data showing the importance of k_{IC} in determining time-to-death (Spencer, Gaudet et al. 2009) and highlights the need for accuracy in assigning the initial conditions of sensitive model species.

While we have measured the absolute levels of several of the most important species using quantitative immunoblotting (Supplementary Fig. 3.4 and 3.5 and ref. Spencer, Gaudet et al. 2009), our manually calibrated model could reside in a local minimum. However, the mean as well as the variance in cell responses measured in various single-cell experiments can be used for automated parameter estimation and model calibration. Future model calibration efforts should therefore consider cell-to-cell variability as valuable data that can constrain the calibration of a model.

The biologically driven way of viewing species' sensitivities described in this paper reveals why slight variations in the levels of certain proteins can have a huge impact on a cell's death time. HeLa cells are tuned such that their initial protein levels fall in sensitive regions of initial condition space, guaranteeing variability in response to TRAIL. Cells can evolve toward

optimal protein expression levels (Dekel and Alon 2005), suggesting that there may be an evolutionary advantage for cells to have a high level of tunability. During development or adult homeostasis, variability in sensitivity to apoptosis provides a way to bring about a graded response at a cell population or tissue level, despite a binary output at the single cell level. However, we have thus far only modeled variability in the *timing* of death in cells treated with TRAIL plus cycloheximide. A next step will be to examine cells treated with TRAIL alone to determine whether, in the limit, variability in timing becomes variability in fate. Such modeling awaits additional biological knowledge surrounding which survival pathways are most influential in producing variability in cell fate.

3.4 Methods

Transfections. HeLa cells expressing IMS-RP (Albeck, Burke et al. 2008a) were stably transfected using FuGENE 6 (Roche) with pExchange vectors (Stratagene) into which we cloned cDNAs for EGFP-Bcl-2 or EGFP-Bcl-x_L. Stable transfectants were isolated by neomycin and sorted on a FACSaria (BD Biosciences) to sample expression levels across a wide range.

Live-cell microscopy. HeLa cells expressing IMS-RP and GFP-Bcl-2 or GFP-Bcl-x_L were plated in a 96-well glass bottom plate (Matrical). Cells were treated with 50 ng/ml TRAIL and 2.5 ug/ml cycloheximide and imaged on a Nikon TE2000E at 20x magnification with frames every 5 min in a 37°C chamber in phenol-red free CO₂-independent medium (Invitrogen) supplemented with 1% fetal bovine serum (Mediatech), L-Glutamine (Gibco) and Penicillin/Streptomycin (Gibco). GFP-Bcl-2 or GFP-Bcl-x_L fluorescence was quantified at $t = 0$ (time of treatment) by manually outlining the cell and measuring the average fluorescence intensity within the outline. MOMP was scored by monitoring cytosolic translocation of IMS-RP. To

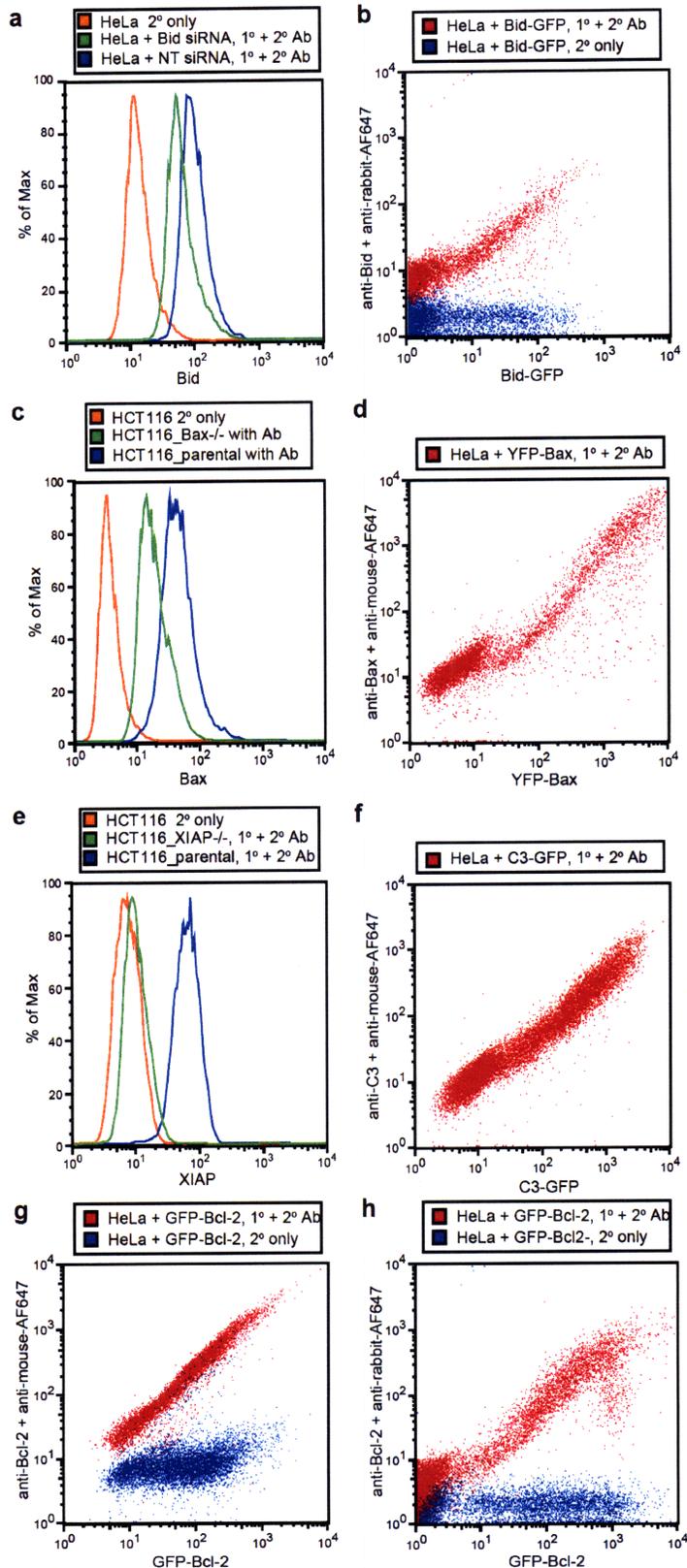
convert the x -axes in Fig. 3.4b,c to proteins/cell, the average GFP fluorescence intensity from these movies was set equal to the average number of GFP-tagged proteins per cell as measured by quantitative immunoblotting (Supplementary Fig. 3.4 and 3.5).

Flow cytometry. The distributions of initial protein levels were measured in untreated HeLa cells (fixed with paraformaldehyde and permeabilized with methanol) on a FACSCalibur in Fig. 3.1 and 3.3 or on a FACSCanto in Fig. 3.5 (BD Biosciences). The antibodies were carefully validated as described in Supplementary Fig. 3.1 and 3.2. The following antibodies were used to measure total protein levels: α -Bid (HPA000722, Atlas Antibodies), α -Bax (MAB4601, Chemicon International), α -Bcl-2 (SC7382 or SC783, Santa Cruz Biotechnology), α -XIAP (610717, BD Biosciences), α -C3 (SC7272, Santa Cruz Biotechnology). Correlations in protein levels were measured by combining pairs of antibodies of different species or using the primary antibodies listed above conjugated to differing fluorophores (C3-AF488, Bax-PE, XIAP-AF647). In Fig. 3.6, “survivors” were cells negative for cleaved PARP (51-9000017, BD Biosciences) or cleaved C3 (559565, BD Biosciences) at 2.5 hr of treatment.

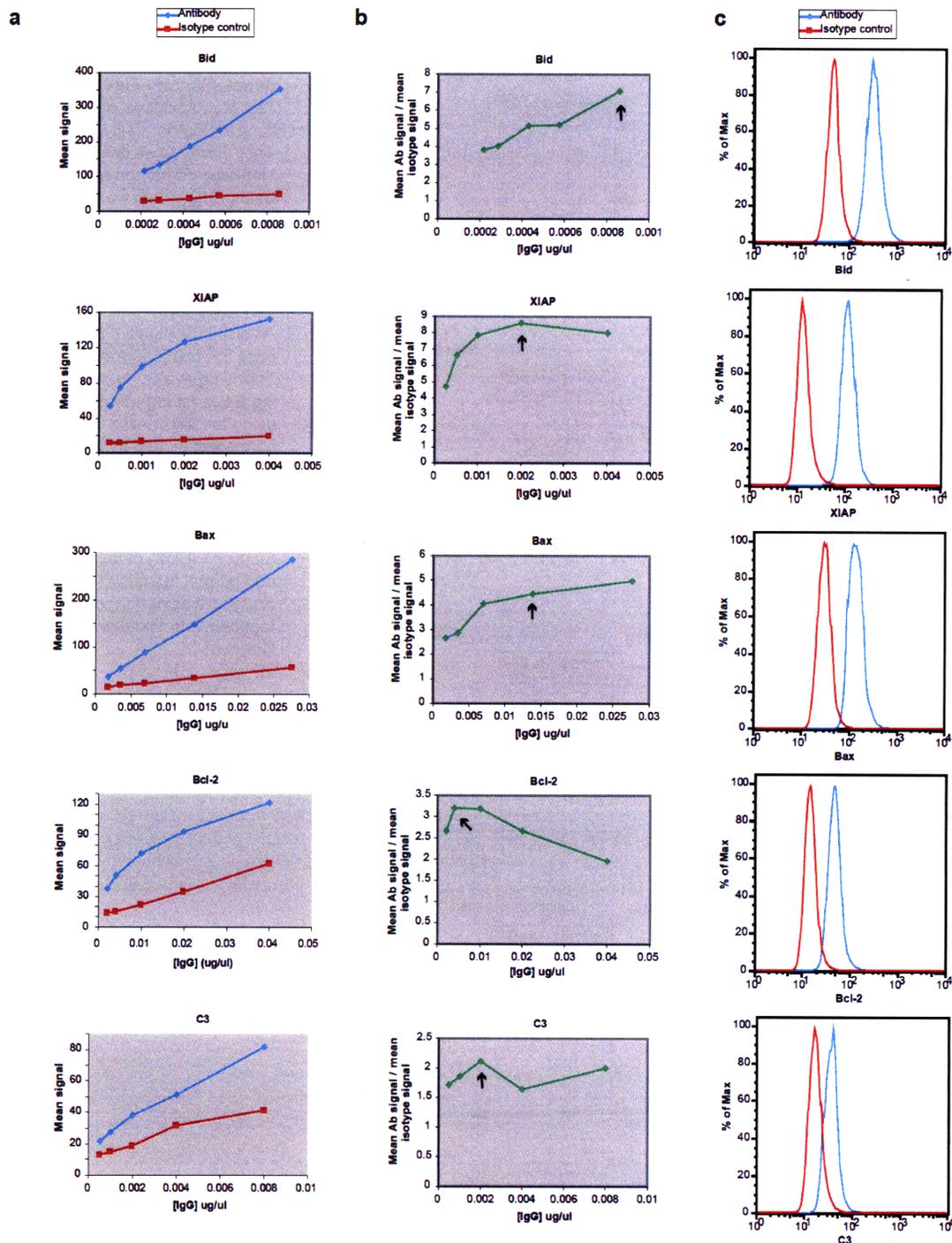
Modeling. The first most basic set of simulations in Fig. 3.1h was performed as in (Spencer, Gaudet et al. 2009) using the EARMv1.1 ordinary differential equation model (Albeck, Burke et al. 2008b). This model was manually calibrated to represent the response of a single HeLa cell to TRAIL treatment. To model a population of HeLa cells, we ran a series of 10^4 simulations of the model (modified to include general protein synthesis and degradation) in Jacobian (Numerica Technology). For each run of the model (representing one cell), all 17 initial conditions were independently sampled from log-normal distributions having mean values as in Supplementary Table 1 and coefficient of variation as measured by flow cytometry (Fig. 3.1) or set to 0.25 for proteins that were not measured. The second set of simulations in Fig. 3.2

was performed by sampling from only one protein distribution at a time while holding all others constant at their default mean value and assessing the impact on t_{PARP} . The third set of simulations (Fig. 3.3c,d, brown) was performed similarly to the first set, but included the measured pair-wise correlations in the ten pairs of initial conditions from Fig. 3.3a,b. This was done by creating synthetic sets of initial conditions with correlations according to the measured R values. All other initial conditions were assumed to be independent. The fourth set of simulations (Fig. 3.4a) involved uniformly sampling one initial condition from 10^2 to 10^7 proteins per cell, holding all others constant at the default value (no variability was simulated here). In Fig. 3.4d, GFP-Bcl-2 (an experimental observable) was added to the level of endogenous Bcl-2 (experimentally unobservable), which followed a lognormal distribution; simulations were performed with correlated initial conditions as in Fig. 3.3c (brown). The simulated GFP-Bcl-2 levels were selected to match experimental GFP-Bcl-2 levels in Fig. 3.4b. Simulations in Fig. 3.5 and 3.6 were performed as described above for Fig. 3.3c (brown). All experiments and simulations were performed in the presence of 2.5 $\mu\text{g/ml}$ cycloheximide or the modeled equivalent (80% reduction in protein synthesis rates).

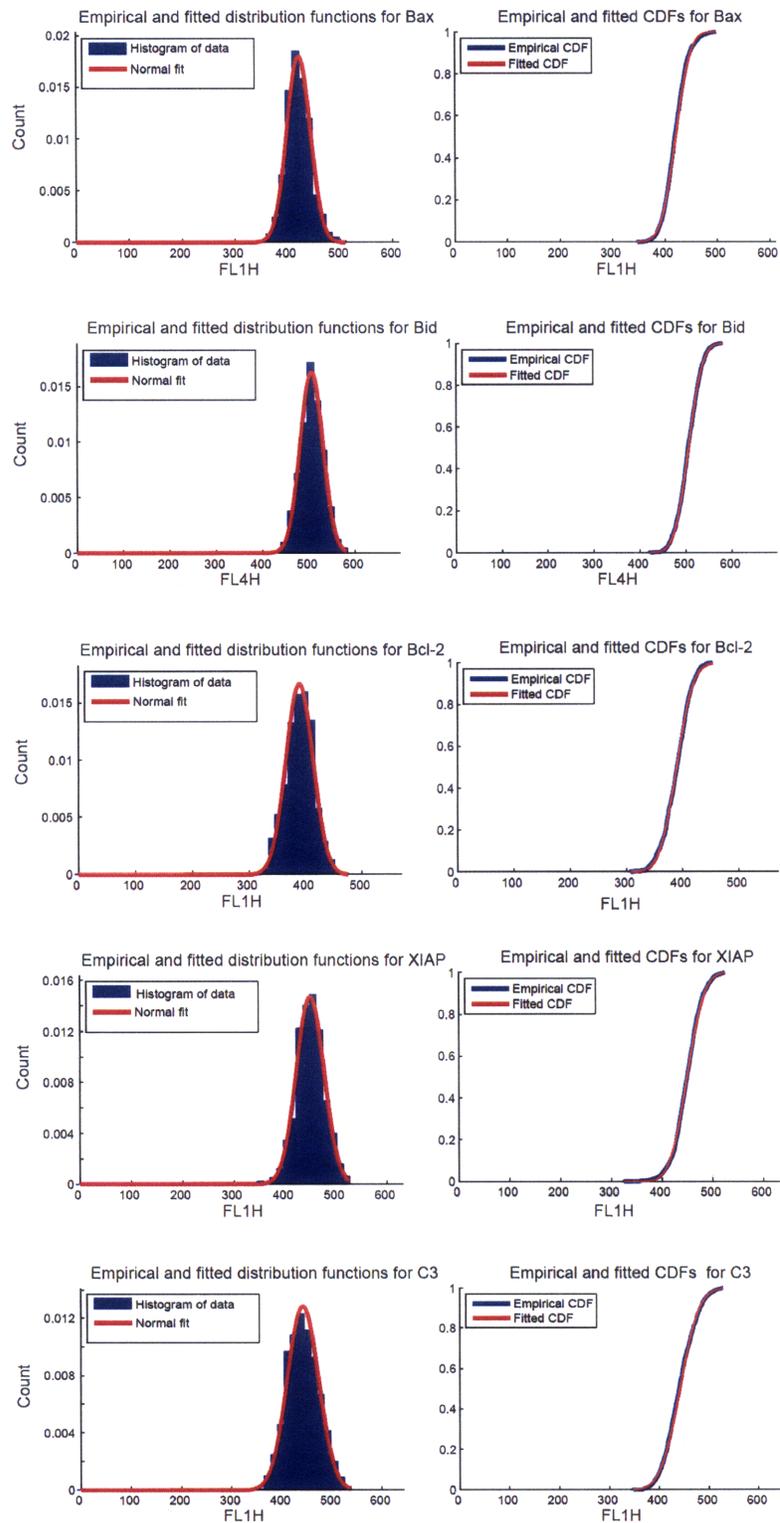
3.5 Supplementary figures



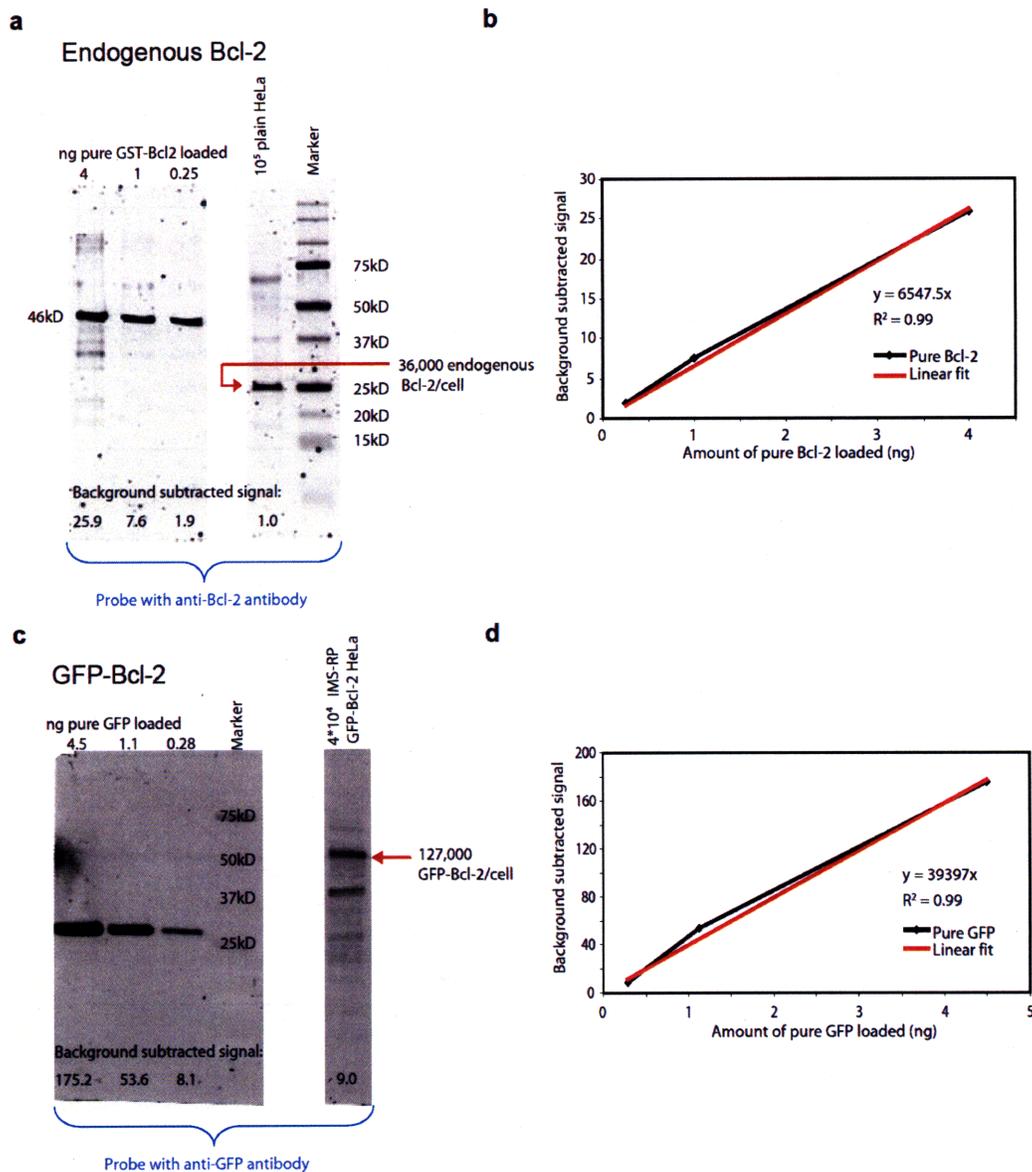
Supplementary Figure 3.1. Validation of antibodies used for measuring protein distributions by flow cytometry. **a** and **b**, The rabbit anti-Bid antibody (Atlas Antibodies HPA000722) was validated using two methods. **a**, HeLa cells were treated with an siRNA for Bid or with a non-targeting (NT) siRNA and stained with anti-Bid followed by a secondary antibody or with secondary antibody alone. **b**, HeLa cells were transiently transfected with Bid-GFP and stained with anti-Bid followed by a secondary antibody conjugated to Alexa Fluor 647 (AF647), or stained with AF647-conjugated secondary antibody only. **c** and **d**, The mouse anti-Bax antibody (Chemicon International MAB4601) was validated using two methods. **c**, Parental HCT116 cells that express Bax and HCT116 Bax^{-/-} derivatives were stained with anti-Bax followed by a secondary antibody or with secondary antibody alone. **d**, HeLa cells were transiently transfected with YFP-Bax and stained with anti-Bax followed by a secondary antibody conjugated to AF647. **e**, The mouse anti-XIAP antibody (BD Biosciences 610717) was validated by one method. Parental HCT116 cells that express XIAP and HCT116 XIAP^{-/-} derivatives were stained with anti-XIAP followed by a secondary antibody or with secondary antibody alone. **f**, The mouse anti-C3 antibody (Santa Cruz Biotechnology SC7272) was validated by one method. HeLa cells were transiently transfected with C3-GFP and stained with anti-C3 followed by a secondary antibody conjugated to AF647. **g**, The mouse anti-Bcl-2 antibody (Santa Cruz Biotechnology SC7382) was validated by one method. HeLa cells stably expressing GFP-Bcl-2 were stained with anti-Bcl-2 followed by a secondary antibody conjugated to AF647 or stained with AF647-conjugated secondary antibody alone. **h**, The rabbit anti-Bcl-2 antibody (Santa Cruz Biotechnology SC783) was validated by one method. HeLa cells were transiently transfected with GFP-Bcl-2 and stained with anti-Bcl-2 followed by a secondary antibody conjugated to AF647 or stained with AF647-conjugated secondary antibody alone.



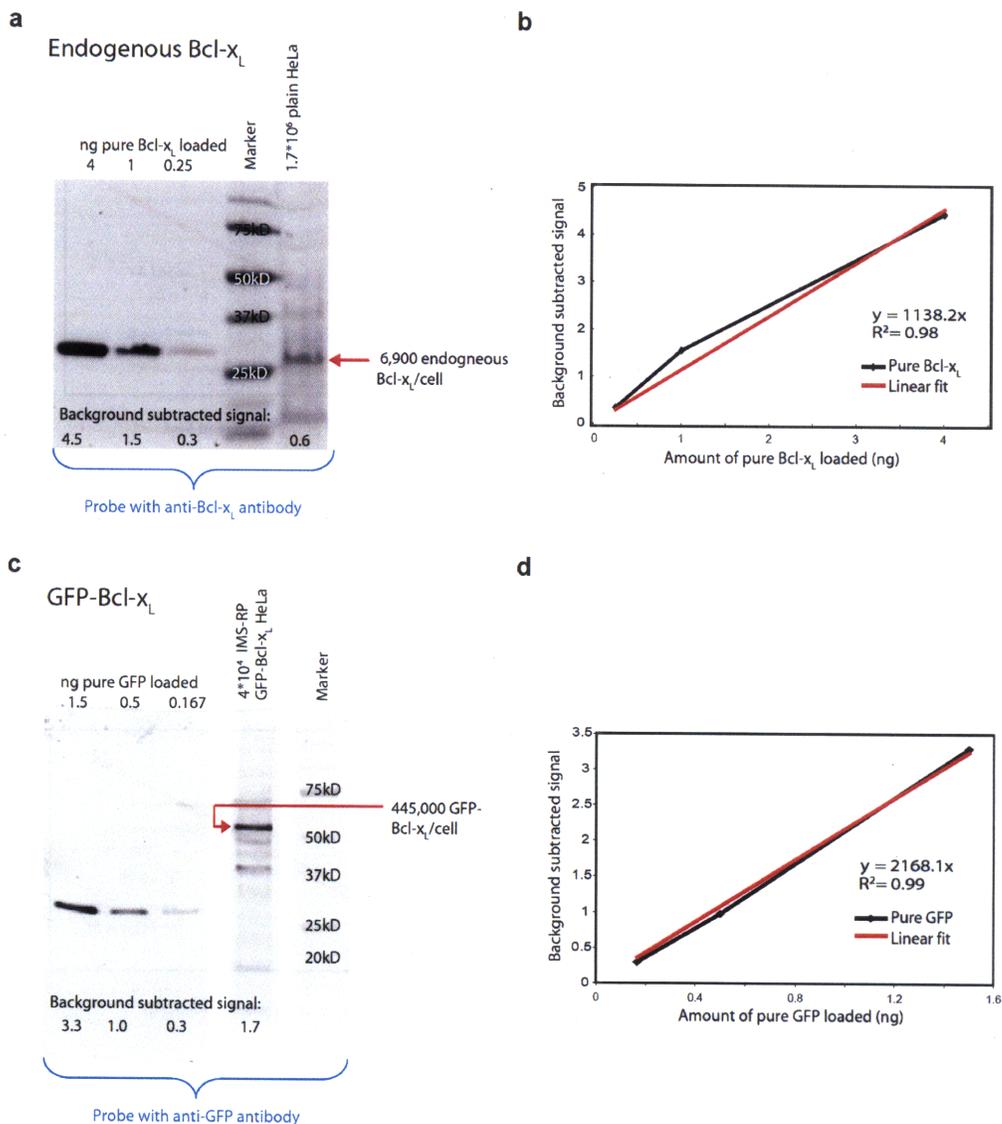
Supplementary Figure 3.2. Comparison of antibodies to the five proteins described in Methods with their relevant isotype controls. **a**, Mean signal as a function of increasing concentrations of antibody and isotype control. For Bid, the matched isotype control used was rabbit IgG; for XIAP, Bax, and Bcl2, mouse IgG₁; for C3, mouse IgG_{2a}. All isotype controls were purchased from Santa Cruz Biotechnology. **b**, Fold increase in signal from antibody staining versus background isotype control staining. Arrows indicate the concentrations of antibodies used in future experiments whose distributions are plotted in (c). **c**, Assessment of the degree of overlap of distributions of isotype control- and antibody-stained cells. Cells were fixed and permeabilized as in Methods and run on a FACSCalibur (BD Biosciences).



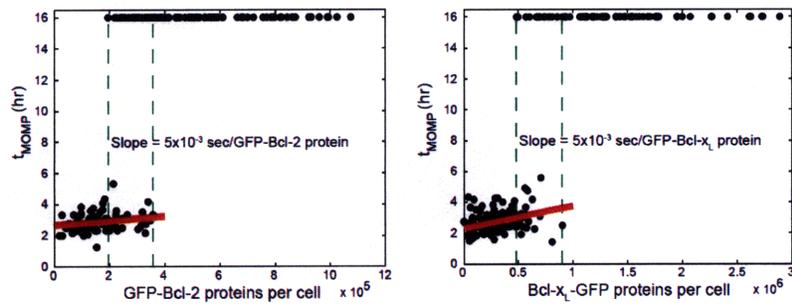
Supplementary Figure 3.3. Test of protein level distributions for log-normality. Cells were prepared as described in Methods and run on a FACS-Calibur. The data were read into MATLAB in linear form, gated to select cells of similar size as described in Methods, and tested for normality using the Kolmogorov-Smirnov test. All distributions were found to pass the test for normality. This is equivalent to performing a test for log-normality using the log transformed data commonly plotted by the software FlowJo. a, Distribution of data (blue) compared with a normal fit (red). b, Cumulative distribution functions (CDF) of data (blue) and normal fit (red). This analysis was performed together with Thomas Norman.



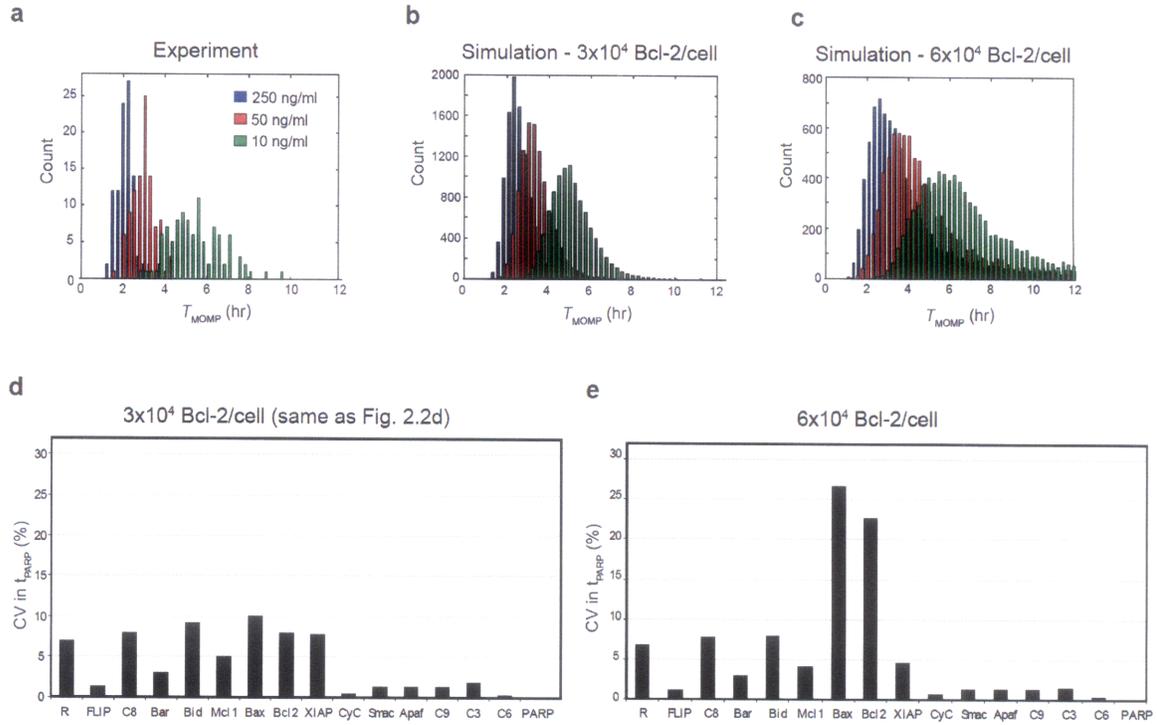
Supplementary Figure 3.4. Quantitative immunoblots for endogenous Bcl-2 and GFP-Bcl-2 in HeLa cells. Pure protein and HeLa cell lysate were loaded on a 10% Tricine SDS-PAGE gel. After transfer to a PVDF membrane, blots were probed, scanned on a LI-COR Odyssey scanner, and quantified digitally. **a**, The membrane was probed with rabbit anti-Bcl-2 (Santa Cruz Biotechnology SC783) followed by AF680-conjugated anti-rabbit. The pure Bcl-2 is a 46kD fusion protein (Santa Cruz Biotechnology SC4096). **b**, From the standard curve, we calculate that a single HeLa cell has 1.57×10^{-15} g Bcl-2. Using 26,135 as the molecular weight of Bcl-2, we find 36,000 Bcl-2/cell. The average of 14 such measurements yields 30,000 Bcl-2/HeLa cell; s.e.m = 10,000. **c**, The membrane was probed with mouse anti-GFP (Roche #11814460001) followed by IRDye 800-conjugated anti-mouse. The pure GFP was purchased from Biovision (#4999-100). **d**, From the standard curve, we calculate that a single IMS-RP GFP-Bcl-2 HeLa cell has 5.68×10^{-15} g GFP-Bcl-2. Using 27,000 as the molecular weight of GFP, we find 127,000 GFP-Bcl-2/cell. The average of 5 such measurements yields 133,000 GFP-Bcl-2/HeLa cell s.e.m = 18,000. We set the average (background subtracted) GFP-Bcl-2 fluorescence intensity of the population of cells in the first frame of the movie used in Figure 3.4b equal to the average number of GFP-Bcl-2 in the HeLa cells used for the movie (calculated above) and rescaled the x-axis of Figure 3.4b into units of GFP-Bcl-2 proteins per cell.



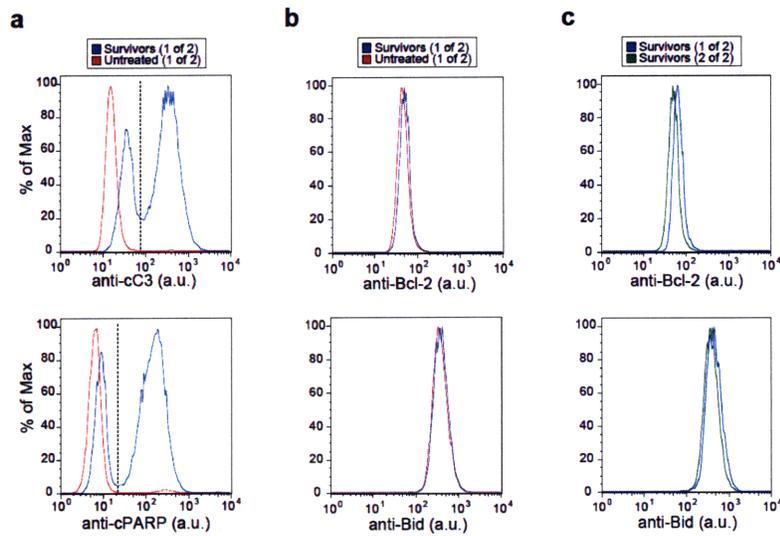
Supplementary Figure 3.5. Quantitative immunoblots for endogenous Bcl-x_L and GFP-Bcl-x_L in HeLa cells. Pure protein and HeLa cell lysate were loaded on a 10% Tricine SDS-PAGE gel. After transfer to a PVDF membrane, blots were probed, scanned on a LI-COR Odyssey scanner, and quantified digitally. **a**, The membrane was probed with rabbit anti-Bcl-x_L (CST #2762) followed by AF680-conjugated anti-rabbit. The pure Bcl-x_L was a gift from Emiko Fire (MIT). **b**, From the standard curve, we calculate that a single HeLa cell has 2.96×10^{-16} g Bcl-x_L. Using 25,918 as the molecular weight of Bcl-x_L, we find 6,900 Bcl-x_L/cell. The average of 7 such measurements yields 7,700 Bcl-x_L/HeLa cell; s.e.m = 1,300. **c**, The membrane was probed with mouse anti-GFP (Roche #11814460001) followed by IRDye 800-conjugated anti-mouse. The pure GFP was purchased from Biovision (#4999-100). **d**, From the standard curve, we calculate that a single IMS-RP GFP-Bcl-x_L HeLa cell has 1.99×10^{-14} g GFP-Bcl-x_L. Using 27,000 as the molecular weight of GFP, we find 445,000 GFP-Bcl-x_L/cell. The average of 6 such measurements yields 579,000 GFP-Bcl-x_L/HeLa cell; s.e.m = 200,000. We set the average (background subtracted) GFP-Bcl-x_L fluorescence intensity of the population of cells in the first frame of the movie in used in Figure 3.4c equal to the average number of GFP-Bcl-x_L in the HeLa cells used for the movie (calculated above) and rescaled the x-axis of Figure 3.4c into units of GFP-Bcl-x_L proteins per cell.



Supplementary Figure 3.6. Increasing Bcl-2 and Bcl-x_L levels cause a slight increasing in t_{MOMP} . Plot are reproduced from Fig. 3.4b and 3.4c and the cells undergoing MOMP fit via linear regression (red line). t_{MOMP} increases by 0.005 seconds for each additional Bcl-2 or Bcl-x_L protein in the cell.



Supplementary Figure 3.7. Sensitivity to doubling the level of Bcl-2. **a**, Distribution of death times as measured experimentally by IMS-RP translocation for three doses of TRAIL plus cycloheximide. **b**, Distribution of death times as measured in simulation with independent sampling of initial conditions and Bcl-2 levels set to the default 30,000 per cell. (a) and (b) are reproduced from Spencer et al. 2009. **c**, Same as (b) but with Bcl-2 levels set to 60,000 per cell. **d**, Simulation results from Fig. 2.2d are reproduced. **e**, Simulation as in (d) except that the Bcl-2 level was set to 60,000 per cell. Bcl-2 and Bax now become the most sensitive species in the model.



Supplementary Figure 3.8. Selection of cells that survive a 2.5 hr treatment with 50 ng/ml TRAIL plus cycloheximide and comparison of duplicate samples. Cells were fixed with paraformaldehyde/methanol, stained, and run on a BD FACSCalibur flow cytometer. **a**, Surviving cells were distinguished from dead cells using rabbit anti-cleaved C3 (BD #559565) or mouse anti-cleaved PARP (BD #51-9000017). Cells negative for cleaved C3 or cleaved PARP (to the left of the dashed line) after 2.5 hr of treatment were gated and labeled "survivors". **b**, Levels of Bcl-2 and Bid in "survivors" compared with untreated cells. **c**, Measurement differences between duplicates can be as large or larger than differences between "survivors" and untreated samples. a.u., arbitrary units.

Chapter 4

4 Crossing the threshold for mitochondrial outer membrane permeabilization

Section 4.1 will become part of a future manuscript involving observation of cells' approach to the MOMP threshold as well as modulation of this threshold.

Section 4.2 is adapted from Flusberg D., Spencer S.L., Sorger P.K. "TRAIL-induced transient resistance and heterogeneity in drug response", *in preparation*. The section contains my contribution to the paper, which involved the initial observation and measurement of transient TRAIL resistance in cells that survive an initial TRAIL challenge. These experiments were performed together with D. Flusberg.

Section 4.3 is an excerpt from ref. Albeck, Burke et al. 2008b containing my contribution to the paper, which involved the experimental measurements and analyses of GFP-Bax and GFP-Bak puncta at the threshold for MOMP.

Mitochondrial outer membrane permeabilization (MOMP) is considered the point of no return in cell death (Keeble and Gilmore 2007). Cells that cross the MOMP threshold die rapidly thereafter. However, even in a population of genetically identical cells treated with TRAIL, there are cells that do not cross this threshold and survive indefinitely. Here I investigate the differences between a cell that dies and a cell that survives, as well as what happens to these surviving cells upon re-treatment with TRAIL. In cells that survive, I find that the rate of cleavage of initiator caspase substrates plateaus before reaching the threshold level required to kill the cell. These surviving cells are then transiently resistant to re-treatment with TRAIL, but this resistance decays over the course of several days, confirming that the resistance is not genetic in origin. Lastly, I show that formation of Bax and Bak containing pores in the mitochondrial outer membrane is the point at which a gradual buildup of pro-apoptotic signal is converted to a switch-like commitment to death.

4.1 Observation and modulation of the threshold for MOMP

Diverse stimuli, from oncogene activation to death receptor signals and DNA damage, converge at the mitochondria where pro-apoptotic and anti-apoptotic signals are integrated by members of the Bcl-2 family. Here, moderate changes in the levels of key regulators controlling the MOMP threshold can potentially change the fate of a cell. In this section, I examine the initiator caspase cleavage dynamics of cells that die and cells that survive TRAIL treatment, and show that co-drugging acts to lower the MOMP threshold.

4.1.1 Monitoring the approach to the MOMP threshold in surviving and dying cells

The dynamics of initiator caspase substrate cleavage and the onset of MOMP can be monitored in single cells treated with TRAIL using fluorescent reporter proteins IC-RP and IMS-

RP, respectively (Albeck, Burke et al. 2008a). A population of genetically identical cells contains a transient mixture of resistant and sensitive cells with the result that individual cells will survive or eventually succumb to TRAIL treatment (Spencer, Gaudet et al. 2009). By combining IC-RP and IMS-RP in single cells, a measure of the rate of accumulation of cleaved C8 substrates and a measure of the height of the MOMP threshold can be obtained (Spencer, Gaudet et al. 2009).

The rate of initiator caspase substrate cleavage in cells treated with TRAIL cannot easily be fit mathematically as is possible for cells treated with TRAIL plus cycloheximide. This is at least partly due to the ability of induced protein synthesis to change the dynamics of initiator caspase substrate cleavage, an event not captured by our current mathematical model of TRAIL-induced apoptosis (Albeck, Burke et al. 2008b). Nonetheless, IC-RP trajectories in HeLa cells can be classified into three general families of cellular behaviors. First are the cells with rapid to moderate rates of IC-RP cleavage resulting in early to intermediate MOMP times (Fig. 4.1a, first two rows). These cells commonly show a steady rise in IC-RP signal leading to MOMP.

Second are cells whose IC-RP signal plateaus for some time before the cell undergoes MOMP. Among single cells, the onset of the plateau phase can occur as early as 3.6 hr after TRAIL treatment and as late as 10.5 hr, with a median time of 7 hr (Fig. 4.1a, third row, and Fig. 4.1b). An intriguing biological explanation is that TRAIL causes the transcriptional induction of a signal that turns off the upstream response via negative feedback, creating the plateau phase. One potential candidate for this role is FLIP, which can be transcriptionally induced by NF- κ B and can compete for caspase-8 activation at the DISC (Micheau, Lens et al. 2001). FLIP upregulation could be measured by immunoblot in HeLa cells. However, it is possible that FLIP upregulation does not occur in cells that do not reach a plateau phase, and the aggregate nature of

immunoblotting would obscure these cell-to-cell differences. A lung cancer cell line (H1299) is available from the Kahn Dynamic Proteomics Project that contains FLIP tagged with YFP at the endogenous locus (Spencer, Gaudet et al. 2009). FLIP levels were found to be upregulated at 8 hr in H1299 cells that survived a treatment with 50 ng/ml TRAIL; FLIP levels were constant in untreated control cells (Fig 4.1c). However, it is not known whether these cells show the same plateau in initiator caspase substrate cleavage observed in HeLa cells.

There are also two alternative explanations for the plateau phase. First, it is possible that the TRAIL present in the media degrades after several hours at 37° C, resulting in the slowing of IC-RP cleavage. It is also possible that the plateau phase is an artifact, due to depletion of IC-RP. Arguing against this second possibility is the sudden increase in the IC-RP signal seen in some cells after MOMP, suggesting that the cell contains reporter that remains to be cleaved. However, up to 40% of total IC-RP signal can be caused by the change in cell morphology associated with apoptosis, as measured with an uncleavable initiator caspase FRET reporter (Albeck, Burke et al. 2008a). Degradation of TRAIL could be tested with an ELISA. Possible depletion of IC-RP could be tested by treating cells with 50 ng/ml TRAIL for ~7 hours so that many cells will have entered the plateau phase. The concentration of TRAIL could then be increased to 250 ng/ml and cells could be monitored for an increase in the rate of IC-RP cleavage, indicative of remaining IC-RP.

The third category of cellular behavior is survival (Fig. 4.1a, fourth row) – these are cells that have not undergone MOMP at the end of the 23 hr observation period. A great majority of these cells survive indefinitely, as the number of surviving cells growing the following day is large. All surviving cells reach a plateau phase in IC-RP signal. A distribution of the dynamics of a larger set of surviving and dying cells can be seen in Fig. 4.1d.

Do any features of the IC-RP trajectories differ between surviving and dying cells? One candidate feature is the height of the threshold for MOMP. In cells that die, this threshold can be scored as the amount of IC-RP cleaved at the time of MOMP (referred to as θ in ref. Spencer, Gaudet et al. 2009). In cells that do not undergo MOMP and survive, this can be scored as either the amount of IC-RP cleaved at the end of the imaging period (Fig. 4.1e) or as the maximum IC-RP signal observed (data not shown). When this threshold height was compared in surviving and dying cells, we found that threshold heights could be grouped into three levels. A “safe” region contained only cells that survived, whereas a region of “certain death” was bounded to include only cells that die. An intermediate region of variable fate lay in between (yellow shading), containing dying cells with IC-RP cleavage heights that are also reached by some surviving cells. As a side note, the fact that surviving cells reach lower IC-RP plateau values than dying cells argues for the plateau being a result of a true negative feedback response. Put another way, if the IC-RP plateau were merely due to depletion of the reporter, both surviving and dying cells should reach the same plateau height.

The difference between death and survival is not binary at the level of initiator caspase substrate cleavage. Rather, a continuum of IC-RP cleavage rates and threshold heights can be seen among cells that die early, cells that die late, and cells that survive. Nevertheless, IC-RP trajectories can be monitored for features that aid in distinguishing the fate of a cell. Two features are partially informative – the height of the threshold for MOMP, and the presence or absence of a plateau phase. It remains to be seen whether the plateau phase is an artifact due to depletion of IC-RP, but if it represents a true feedback mechanism, the identity of the protein(s) responsible for this feedback could be elucidated.

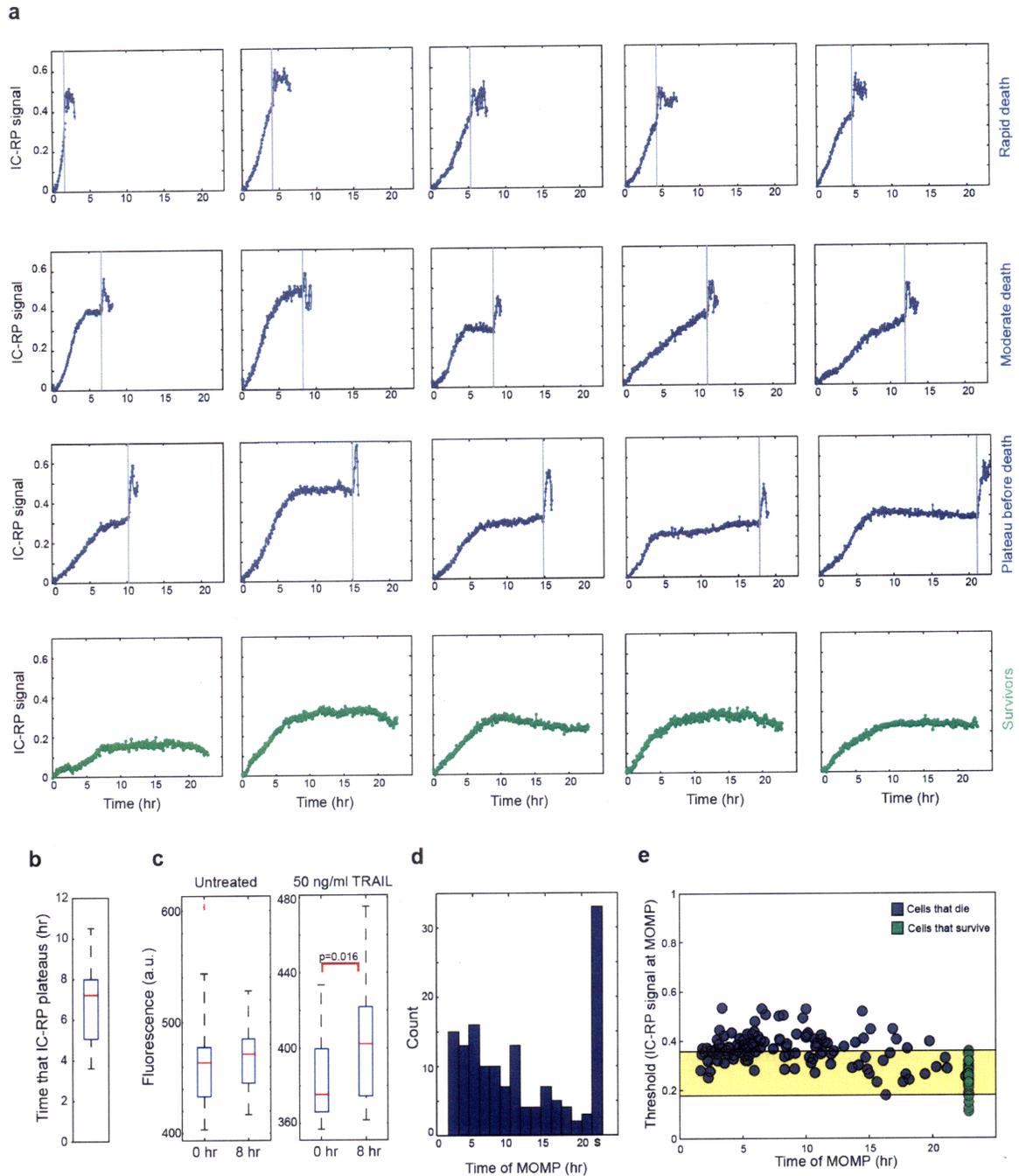


Figure 4.1. The approach to the MOMP threshold in surviving and dying cells. **a**, Single cell IC-RP trajectories of HeLa cells that die at various rates (gray, top three rows) and cells that survive (green, bottom row) after treatment with 50 ng/ml TRAIL. The vertical gray bar indicates the time of MOMP in each cell. A photobleaching control from untreated cells has been subtracted from all trajectories. Trajectories are not normalized. **b**, Boxplot of time of plateau onset for HeLa cells whose IC-RP trajectories plateau (dying or surviving). **c**, Comparison of FLIP-YFP levels in H1299 cells left untreated (left) or treated with 50 ng/ml TRAIL (right). Fluorescence intensity was measured by manually outlining 16-18 individual cells at 0 hr (start of imaging, and time of TRAIL treatment) or 8 hr later. In TRAIL-treated cells, only cells remaining alive at 8 hr were considered. Mean fluorescence intensity is statistically different (by t-test) in TRAIL-treated cells at 0 hr compared with 8 hr; means in untreated cells are not statistically different. **d**, Distribution of MOMP times for cells shown in (a). "S" indicates cells that survive through the end of the movie. **e**, Height of the MOMP threshold for cells shown in (a) that die (gray), as measured by IC-RP signal at the time of MOMP. For surviving cells (green), the IC-RP signal at the end of the movie is plotted. Yellow shading indicates the region of variable fate. a.u., arbitrary units.

4.1.2 Co-drugging lowers the threshold for MOMP

TRAIL is being evaluated in clinical trials not only as a single agent, but in combination with other targeted cancer therapies (Ashkenazi and Herbst 2008). TRAIL receptor agonists can synergize with other drugs, as measured by aggregate methods. However, perhaps equally important is synergy that acts to reduce heterogeneity in TRAIL response. Although not used clinically, cycloheximide, a protein synthesis inhibitor, is one drug that has powerful synergy with TRAIL. No matter how high the TRAIL dose, no treatment with TRAIL alone can kill all cells in a population. However, when TRAIL is combined with 2.5 $\mu\text{g/ml}$ cycloheximide (a non-lethal cycloheximide dose over the time period considered), 100% of the cells will be killed, even with low doses of TRAIL. Since cycloheximide can have many effects on the cell, it is not known which are responsible for this synergy. However, live-cell imaging using IC-RP and IMS-RP shows that the synergy is at least in part due to the fact that cycloheximide dramatically lowers the threshold for MOMP (Fig. 4.2), bringing the threshold from an average normalized value of 0.71 to a value of 0.46. This lowered threshold then results in a decrease in the time-to-death because less pro-apoptotic signal is required for a cell to cross the threshold.

Synergy via lowering the threshold for MOMP has also been observed between TRAIL and several other clinically used cancer drugs, including Gefitinib (an epidermal growth factor receptor (EGFR) inhibitor), and Sorafenib (an inhibitor of kinases in the Raf/Mek/Erk pathway) (D. Flusberg, unpublished observations). Future experiments on this topic will involve using IC-RP and IMS-RP to profile the mechanisms of synergy when cells are treated with TRAIL plus a second cancer drug. Of particular interest is Cetuximab (another EGFR inhibitor), currently in trials as a combination therapy with TRAIL, and the promising clinical inhibitor of Bcl-2 family proteins, ABT-737, which is thought to act by lowering the MOMP threshold.

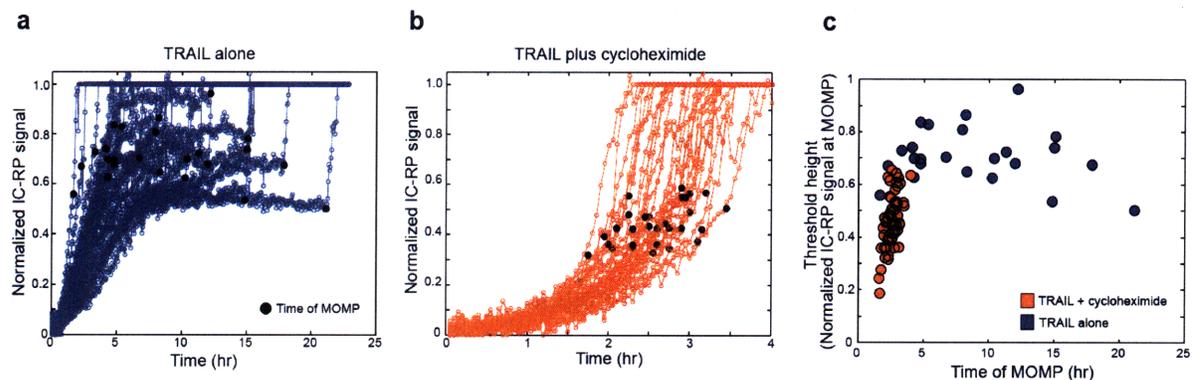


Figure 4.2. Cycloheximide lowers the MOMP threshold in HeLa cells treated with TRAIL. **a**, Normalized IC-RP trajectories in cells treated with 50 ng/ml TRAIL alone. Black dot indicates time of MOMP in each cell. **b**, Same as (a) but for cells co-treated with 50 ng/ml TRAIL plus 2.5 ug/ml cycloheximide. **c**, Comparison of height of the MOMP threshold in cells treated with TRAIL alone or TRAIL plus cycloheximide.

4.2 Memory of TRAIL treatment in surviving cells and induced transient resistance

We have previously shown that some cells in a TRAIL-treated population live while other cells die (Spencer, Gaudet et al. 2009). Here we show that cells which survive an initial treatment with TRAIL are resistant to a subsequent challenge by TRAIL, but that this resistance fades with time. Transient resistance does not appear to reflect down-regulation or adaptation of TRAIL receptors, but rather induction of a survival response acting downstream whose effects decay over time.

4.2.1 TRAIL treatment induces transient resistance in surviving cells

What is the difference between cells that survive TRAIL treatment and those that die? To begin to answer this question, a clonal population of MCF10A cells was exposed to sufficient TRAIL (50 ng/ml TRAIL for 6 hr) to kill ~80% of the cells. At this time, referred to as Day 0, the surviving cells were then recovered by trypsinization and re-plated in fresh medium. The recovered cells divided at approximately the same rate as untreated cells. These cells were then exposed to TRAIL a second time one to nine days after re-plating (Fig. 4.3a) and the fraction of

cells undergoing apoptosis was scored by flow cytometry using an antibody to the cleaved form of PARP (cPARP; Albeck, Burke et al. 2008a). When TRAIL was added to re-plated cells at Day 1, we observed the cells to be 5-6-fold less likely to undergo apoptosis compared to the starting cell population: whereas ~70-80% of naïve cells become cPARP positive 6 hr after treatment with 50 ng/ml TRAIL, only ~10-20% of re-plated survivors exhibited a similar response. Insensitivity to TRAIL decreased steadily thereafter, so that by Day 6, re-plated cells were indistinguishable from the starting cell population (Fig. 4.3b). Thus, cells that survive initial exposure to TRAIL are resistant to a second exposure, but resistance decreases over several days so that the initial response profile is re-established. The transient heritability of TRAIL resistance rules out genetic mutation as a cause, and the rapidity of the return to the pre-treatment state argues against epigenetic effects (which typically last for 10^4 - 10^5 cell generations (Rando and Verstrepen 2007)). Instead, the data are most consistent with non-genetic effects.

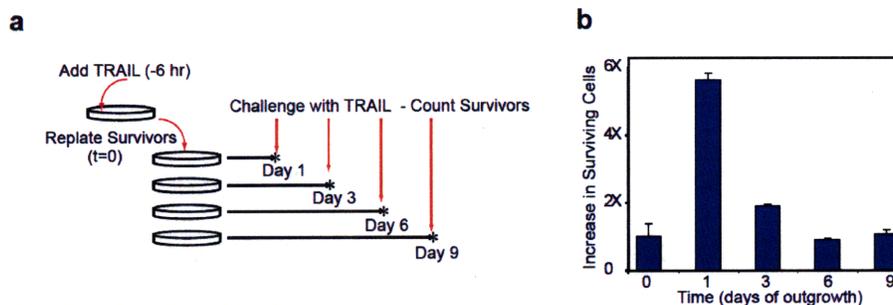


Figure 4.3. Transient resistance to TRAIL-induced apoptosis in cells which survive an initial challenge. **a**, Schematic of the experimental design. MCF10A cells were treated with TRAIL for 6h. Survivors of the treatment (10-20% of the total population) were collected, re-plated, and re-challenged with TRAIL (50ng/ml, 6h) on subsequent days in parallel with naïve cells. **b**, Fold-increase in surviving cells among TRAIL survivors relative to naïve cells treated in parallel.

4.2.2 Transient resistance is due to changes downstream of receptors and initiator caspases but upstream of effector caspases.

Possible explanations for transient insensitivity to TRAIL include internalization, down-regulation or adaptation of TRAIL receptors, phenomena that are common among other transmembrane receptors (Ferguson and Caron 1998; Le Roy and Wrana 2005; Sorkin and Goh 2008), as well as down regulation of DISC assembly or activity. To assess these possibilities, we monitored initiator caspase activation using flow cytometry and an antibody to the cleaved form of caspase-3 (cC3), a direct substrate of initiator caspases. When naïve MCF10A cells were exposed to 50 ng/ml TRAIL for 6 hr, 97% stained positive for cC3 and 68% for cPARP (Fig. 4.4a). When surviving cells were recovered and re-plated (as described above), 55% retained cC3 on Day 1, even prior to TRAIL treatment. This fraction increased to 98% following a second exposure to 50 ng/ml TRAIL. However, only 10% of cells stained positive for cPARP, consistent with very low levels of apoptosis (Fig. 4.4b). Thus, TRAIL-insensitive survivors on Day 1 efficiently activate initiator caspases, even though effector caspases remain largely inactive. We therefore conclude that the insensitivity of the surviving cells to a second TRAIL treatment is not a consequence of receptor or DISC inactivation, but instead involves decoupling between initiator and effector caspases: high levels of active initiator caspases are unable to activate effector caspases. Insensitivity must therefore arise in part of the pathway that is downstream of initiator caspases and upstream of effector caspases. This would appear to implicate regulators of MOMP, which is blocked in the transiently resistant cells.

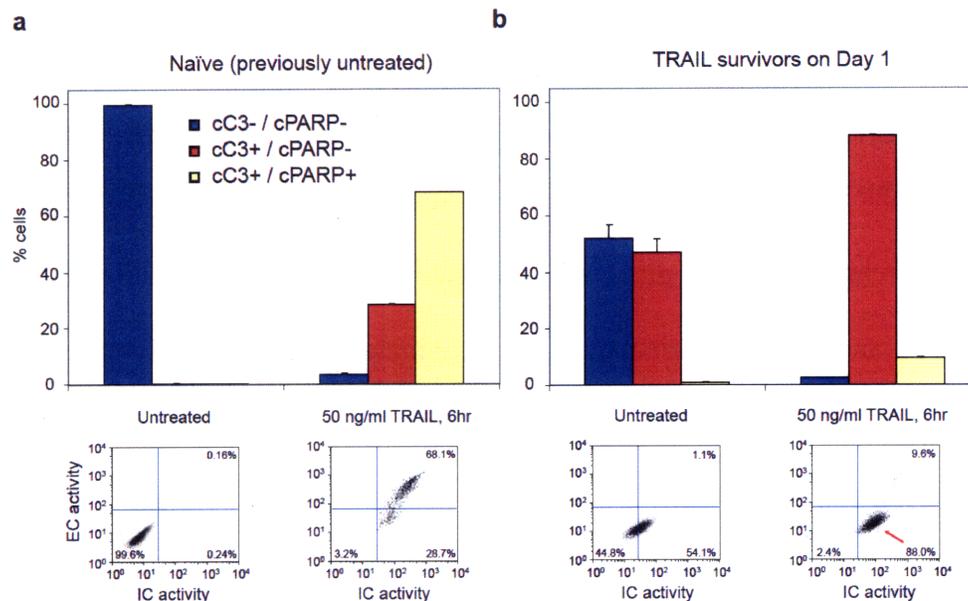


Figure 4.4. Transient TRAIL resistance is not due to receptor desensitization. **a** and **b**, Initiator and effector caspase substrate cleavage in naive cells (**a**) and Day 1 survivors (**b**) treated with TRAIL for 6h. The double-negative fraction represents live cells without initiator or effector caspase activity (blue). The cC3-positive, cPARP-negative fraction (red) represents live cells positive for initiator caspase activity but negative for effector caspase activity; the double-positive fraction represents dead cells (yellow).

4.3 Pore formation converts a gradual buildup of pro-apoptotic signal into a switch-like commitment to death

Our group has previously shown that cells enter a protracted and variable delay period in which upstream initiator caspases are active but downstream effector caspases are inactive (Albeck, Burke et al. 2008b). A subsequent sudden transition marks activation of the downstream effector caspases that rapidly dismantle the cell. To understand how the extrinsic apoptosis switch functions in quantitative terms, a mathematical model was constructed based on a mass-action representation of known reaction pathways. The trained model accurately reproduces the behavior of normal and perturbed cells exposed to TRAIL, making it possible to study switching mechanisms in detail. Model analysis shows that the snap-action control of

effector caspase activation is achieved by reactions involved in permeabilization of the mitochondrial membrane and consequent relocalization of proteins such as Smac.

4.3.1 MOMP is complete by the time dying cells have assembled relatively few pores

Two testable predictions arise from the simulations described in (Albeck, Burke et al. 2008b) (i) Smac release should begin nearly simultaneously with the formation of the first Bax-containing pores, and (ii) pore formation should continue long after Smac release is complete. To test these predictions, cells expressing GFP-Bax and IMS-RP were treated with TRAIL (50 ng/ml) and imaged at 60x resolution at 30 sec intervals for 1 hour before and after MOMP. The rate of release of IMS-RP was estimated using an edge-detection algorithm sensitive to the transition from clustered IMS-RP signals diagnostic of mitochondrial localization to diffuse signals diagnostic of cytosolic localization. In agreement with previous studies (Wolter, Hsu et al. 1997) and the assumptions in EARMv1.0, GFP-Bax had a diffuse cytosolic localization prior to MOMP but, in dying cells, formed bright puncta that co-localized with mitochondria (as marked by IMS-RP; Fig. 4.5a). Moreover, GFP-Bax puncta appear to be identical to puncta detected by immunofluorescence microscopy (not shown), suggesting that GFP-Bax is representative of endogenous Bax. Appearance of the first GFP-Bax puncta coincided with IMS-RP translocation, which appeared to be complete within 1-2 frames (~ 1 min), after which puncta continued to form for 20-30 min more, typically rising to >100 per cell by the time cells began to fragment (at which point further observation was unreliable; Fig. 4.5b). Live-cell studies by others using similar methods have also demonstrated a close temporal link between initial formation of Bax puncta and MOMP (D.R. Green, personal communication). We often observed that the timing of MOMP varied with location in a cell, such that IMS-RP release from some mitochondria preceded release from other mitochondria by ~1 frame (30 seconds; Fig.

4.5c). In these cases, the first observable Bax punctum was associated with the earliest-releasing subset of mitochondria.

A similar relationship was observed between aggregation of Bak-GFP (a second pore-forming protein involved in MOMP) and IMS-RP translocation, with the exception that Bak-GFP was found on the mitochondrial membrane prior to MOMP (Nechushtan, Smith et al. 2001). The first appearance of Bak-GFP puncta was coincident with IMS-RP translocation and puncta once again continued to form for >20 min thereafter (Fig. 4.5d). In contrast, GFP-Bcl-2 and GFP-Bcl-X_L exhibited diffuse mitochondrial localization throughout, with no apparent changes during MOMP (data not shown). Bid-GFP remained in the cytosol before, during, and after MOMP, suggesting that tBid dissociates from Bax and Bak prior to pore formation (some Bid-GFP aggregates were visible once membrane blebbing and cell shrinkage had begun but only long after MOMP was complete; data not shown).

The precise relationship between functional translocation pores and visible GFP-Bax/Bak puncta is not known, and puncta visible by live-cell imaging almost certainly contain more than the 4-8 Bax or Bak subunits thought to comprise functional pores (Nechushtan, Smith et al. 2001). However, the close temporal and spatial association between puncta and IMS-RP release (particularly at different locations in a single cell) implies that puncta may be clusters of pores. Regardless, experiments clearly confirm our two model based predictions (i) that cytosolic translocation of mitochondrial intermembrane proteins is complete by the time a small number of pores have formed and (ii) that pores continue to form long afterward. Modeling also provides a possible explanation for this latter phenomenon: overshoot in pore forming reactions guarantees that the release of intermembrane proteins is sudden and complete regardless of variations in the rate of initial pore formation.

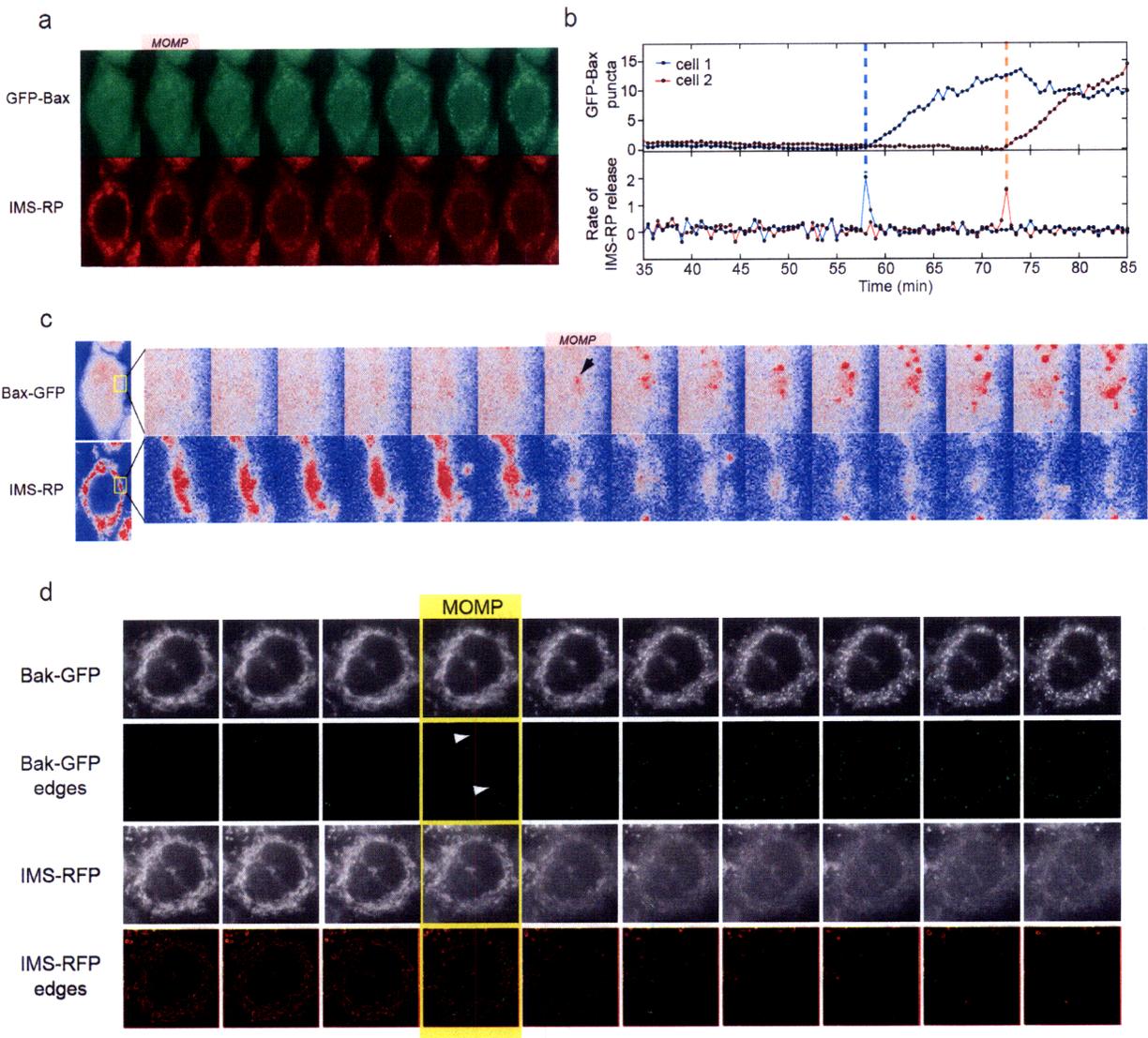


Figure 4.5. Formation of GFP-Bax and GFP-Bak puncta in synchrony with MOMP in HeLa cells. **a**, Live-cell imaging of IMS-RP (red) and GFP-Bax (green) in the same cell. Frames correspond to 30-second intervals, with the first frame of MOMP denoted by a pink box. Partial mitochondrial localization of IMS-RP following MOMP is an artifact of the over-expressed reporter; endogenous cytochrome c is fully cytosolic at this point, as determined by immunofluorescence (not shown). **b**, Quantitation of Bax pores (top) and rate of IMS-RP release (bottom) for two cells (orange curves correspond to the cell shown in (a)); puncta and rate of release were quantified as described in Materials and Methods. **c**, Live-cell images for the cell in (a) shown at higher zoom and with pseudo-coloring to highlight the temporal and spatial relationship between Bax puncta and IMS-RP release. Frames correspond to 30-second intervals; the magnified region (yellow box) encompasses the area of the cell in which both GFP-Bax puncta and IMS-RP release are first visible. **d**, The localization of Bak-GFP and IMS-RFP are shown as raw images and as processed images after the application of an edge-detection filter. The first frame in which IMS-RP is detected is highlighted by a yellow border; in the same frame, the first GFP-Bak puncta appear (arrow heads). As expected for functionally redundant proteins involved in pore formation, GFP-Bax and GFP-Bak both form oligomeric clusters simultaneous with Smac release and continue to form clusters long after Smac release has been completed.

4.4 Future directions

The observations in Section 4.1 represent progress toward understanding the biochemical differences in cells that undergo MOMP and cells that do not. However, knowledge of the rate of cleavage of initiator caspase substrates and the amount cleaved at the time of MOMP only partially distinguish surviving and dying cells. This is likely because induced survival pathways also play a role in determining the fate of the cell. A cell's fate can be thought of as a race between the post-translational caspase cascade and survival pathways transcriptionally induced by NF- κ B. Such a race could be monitored using IC-RP and NF- κ B tagged with mCherry to monitor NF- κ B translocation. Alternatively, the effects of NF- κ B translocation could be monitored by imaging fluorescent protein production driven by a κ B promoter (Nelson, Ihekwa et al. 2004).

A more basic method of understanding the upstream dynamics of cells treated with TRAIL involves immunoblotting of cleaved initiator caspase substrates after treatment. Modeling suggests that in cells that survive TRAIL stimulation, most of the Bid has been processed to tBid before MOMP is able to occur. Conversion of all Bid to tBid combined with rapid degradation of tBid could delay MOMP indefinitely, as a certain amount of tBid is needed to overwhelm the anti-apoptotic buffer at the mitochondria. Thus, cells on the low end of the endogenous Bid protein distribution (mean = 60,000 proteins/cell; 5th - 95th percentile = 36,000 - 90,000) could potentially exhaust their supply of uncleaved Bid before the cell nears the MOMP threshold. The conversion of Bid to tBid can be monitored in aggregate by immunoblotting to determine the average time at which all of the Bid has been cleaved. Cells remaining alive after that point will be much less likely to die, as any further signal from the receptor will be unable to be transmitted to the mitochondria, at least via Bid. Indeed, a strong knockdown of Bid can

prevent MOMP (Albeck, Burke et al. 2008a). Perhaps cells that undergo MOMP at late times upregulate other Bid homologs, such as Bim.

Overexpression of anti-apoptotic Bcl-2 family members is associated with an array of cancers. Various anti-cancer therapies, such as the BH3 mimetic ABT-737, therefore target the mitochondrial apoptosis pathway in an effort to lower the barrier for MOMP. Cell-permeable BH3 peptides can also be used to modulate the MOMP threshold. The combination of IC-RP and IMS-RP provides a means to measure the height of the MOMP threshold in single dying cells to address the critical issue of how such drugs alter the MOMP threshold. Additionally, in ‘primed’ cancer cells that are sensitive to ABT-737 as a single agent, monitoring MOMP simultaneously with pore formation using Bax-GFP and Bak-GFP will provide insight into its mechanism of action in living cells.

The MOMP threshold can also be modulated in living cells by overexpressing fluorescently tagged pro- and anti-apoptotic proteins to different degrees. In Chapter 3, I demonstrated the existence of a very sharp threshold in Bcl-2 and Bcl-x_L protein levels above which cells completely resist MOMP. A next step will be to concomitantly express, at varying levels, different pro-apoptotic proteins to determine how many of each protein is required to neutralize Bcl-2 and Bcl-x_L, thereby allowing MOMP. Of particular interest will be the comparison between “activator” proteins such as Bid, “effector” proteins such as Bax and Bak, and “sensitizer” proteins such as Noxa and Bad, whose purpose seems to involve the fine-tuning of the MOMP threshold (Letai, Bassik et al. 2002).

Chapter 5

5 Conclusions

5.1 Summary of major contributions

The goal of this thesis was to understand the origins of variability in both the timing and the probability of death in TRAIL-induced apoptosis. To this end, I employed both experimental and computational methods to show that natural variability in protein levels can be a major contributor to variability in sensitivity to TRAIL within a clonal population of cells.

In Chapter 2, I experimentally addressed the sources of cell-to-cell variability in the timing of TRAIL-induced apoptosis. The sister cell studies provide strong causal evidence for variability in initial conditions and argue against other possible causes of variability (cell cycle, genetic mutation, stochasticity in the signaling reactions activated by TRAIL). I then demonstrated the short-term heritability of this phenotype and measured its rate of decay in the presence and absence of protein translation. Last, I performed a detailed analysis of the relative contributions of three pieces of the TRAIL pathway (upstream, downstream, and at MOMP) to variability in death time. This included analysis of the rate of initiator caspase product accumulation in single cells, which I found to be highly predictive of a cell's death time.

In Chapter 3, I used a differential equation model for TRAIL-induced apoptosis (Albeck, Burke et al. 2008b) to examine the impact of variability in protein levels on variability in the timing of death. These simulations showed that the endogenous variability in apoptotic regulators was sufficient to produce the observed variability in death time. A sensitivity analysis followed by experimentation revealed that moderate changes in the levels of protein regulators of MOMP, such as Bcl-2, can have a large impact on the fate of a cell. Finally, despite the fact that variability in protein levels is the cause of variability in death time in our simulations, knowing the concentration of any single protein in the pathway has minimal value in predicting a cell's death time because variation in all other proteins masks the underlying trends.

In Chapter 4, I examined the differences between cells that resist MOMP to survive TRAIL treatment and cells that die, within a genetically identical population. Cells that survive an initial TRAIL treatment are immune to a subsequent challenge with TRAIL, but this resistance decays over time. I found that the height of the MOMP threshold could partially differentiate between cells that were susceptible and cells that were resistant to death. Lastly, I measured a close temporal and spatial association between the initial appearance Bax and Bak puncta (presumably clusters of pores) and the onset of MOMP, narrowing in on the reactions that convert a gradual buildup of pro-apoptotic signal to a switch-like commitment to death.

5.2 Relevance of this work

5.2.1 Evolutionary advantages and disadvantages of variability

One can imagine non-genetic variability as an advantageous characteristic that cells can exploit or as a disadvantage for cells trying to achieve robust behavior. In unicellular organisms, noise could be useful in allowing isogenic populations of cells to attain heterogeneity in

phenotype, which they cannot otherwise do. In stressful or fluctuating environments, such as food shortage, two options exist – cells can either sense a new food source in the environment and then activate the required metabolic networks, or they can pre-commit a fraction of the population to have this metabolic network active constitutively (Raj and van Oudenaarden 2008). The tradeoff in the first strategy is slow response time, whereas the second strategy sacrifices a subset of cells to suboptimal growth (Raj and van Oudenaarden 2008). A striking example of this bet-hedging is bacterial persistence. Persistent cells grow at a slower rate than other cells, but tend to be more resistant to antibiotic exposure. Using live-cell imaging, one group found that a small fraction of *E. coli* always survive an antibiotic treatment; these persistent cells were not genetically resistant mutants, as cells re-grown from this population were sensitive to antibiotics (Balaban, Merrin et al. 2004). Instead, persistence was linked to pre-existing (as opposed to induced) heterogeneity in the population and could be clearly detected before treatment due to the reduced growth rate of persistent cells (Balaban, Merrin et al. 2004). The fact that slow-growing persistent cells and rapidly-growing non-persistent cells can stochastically interconvert suggests a possible role for noise in gene expression. A better understanding of this switching process has medical relevance for the antibiotic treatment of *Mycobacterium tuberculosis*, where persistence is a treatment obstacle (Stewart, Robertson et al. 2003).

In the case of TRAIL-mediated apoptosis addressed in this thesis, cells have not been observed to exist in such noticeably discrete susceptible and resistance states prior to treatment. Nevertheless, cells treated with TRAIL alone subdivide neatly into cells that die and cells that survive with no visible trauma - survivors continue to divide at the same rate as untreated cells (S.L.S. unpublished observations). This is a testament to the “stiff trigger”, “all-or-nothing” nature of the apoptotic switch – cells that cross the threshold for MOMP are fully committed to

die, while cells that do not must be able reset to their healthy pre-treatment state. Yet the question remains why the system has evolved such that only a fraction of cells respond to TRAIL treatment. Is there any possible benefit to such a variable response? For normal cells during development or adult homeostasis, variability in sensitivity to apoptosis provides a way to bring about a graded response at a cell population or tissue level, despite a binary output at the single cell level. In the case of cancer, since a tumor cell's apoptotic program can be triggered by oncogene overexpression, increased variability in sensitivity to apoptosis may allow a few cells to survive this anti-cancer defense mechanism and expand to form a tumor. In a population with no phenotypic variability, a sudden environmental fluctuation could kill the entire population, whereas in a phenotypically diverse population, a few members might survive the insult (e.g. due to transient, higher than average levels of some protective factor). Indeed, two studies that used flow cytometry to monitor the levels of many GFP-tagged proteins in yeast revealed that proteins that respond to stress have unusually large cell-to-cell variability (Bar-Even, Paulsson et al. 2006; Newman, Ghaemmaghami et al. 2006). If a population of isogenic cells contains members that are significantly better suited to a new environment than the population average, and if these advantageous traits are at least transiently heritable due to slow mixing rates, these traits can be temporarily selected for in a process similar to Darwinian selection. Although the cells may lose their fitness advantage over time due to the non-genetic nature of trait, this fitter subpopulation can temporarily expand and increase the chances of acquiring permanent genetic mutations. Perhaps it is in these cells that advantageous genetic changes first arise and become fixed.

In situations where variability is disadvantageous, organisms may have developed mechanisms to suppress this variability. For example, these same two flow cytometry studies in yeast found that genes involved in protein synthesis and degradation exhibited much less

variability than the stress response genes, raising the possibility that genes that are essential for cellular function require higher precision in their protein levels (Bar-Even, Paulsson et al. 2006; Newman, Ghaemmaghami et al. 2006). Additionally, the presence of negative feedback loops may reveal situations where an otherwise variable output (in the absence of negative feedback) would be deleterious. In the case of receptor-mediated apoptosis, the presence of a dose-dependent variable delay period preceding MOMP followed by a dose-independent and nearly invariant post-MOMP period likely reflects the evolutionary advantages of such a system. The advantage of a rapid and nearly invariant switch should be to prevent cells from initiating but not completing apoptosis, thereby preventing the formation of “undead” pre-cancerous cells with partially cleaved genomes and resulting chromosomal rearrangements (Albeck, Burke et al. 2008a).

5.2.2 Cancer stem cells

Variability in the tumorigenicity of cancer cells is a commonly observed phenomenon. In many studies, individual cells or subpopulations of cells obtained from tumors are assayed for tumorigenicity, revealing large variability in the malignancy of individual cancer cells (Brock, Chang et al. 2009). These observations have traditionally been explained by genetic differences among cells within a tumor. More recently, such observations have been considered evidence for the existence of cancer stem cells. Cancer stem cells have been defined as “rare cells with indefinite potential for self-renewal that drive tumorigenesis” (Reya, Morrison et al. 2001). The existence of such rare cells has important implications for cancer therapy, as normal stem cells tend to be more resistant to chemotherapy than mature cells from the same tissue (Reya, Morrison et al. 2001). If the same were true of cancer stem cells, these cells might also have

increased resistance to chemotherapy, and new therapies would need to be developed to specifically target these cells.

The evidence for cancer stem cells relies on findings that only a small subset of cancer cells is capable of extensive proliferation (Reya, Morrison et al. 2001). The creation of immunodeficient mice that can tolerate the growth of human cancer cells allowed researchers to address experimentally whether all cancer cells have the ability to form tumors, or whether this property is restricted to a unique subset (the cancer stem cells). A series of studies performed in non-obese diabetic/severe combined immunodeficiency (NOD/SCID) mice showed that only a small fraction of cells (0.0001-0.1%) have the ability to produce a tumor (Bonnet and Dick 1997; Al-Hajj, Wicha et al. 2003; Singh, Hawkins et al. 2004; O'Brien, Pollett et al. 2007; Ricci-Vitiani, Lombardi et al. 2007; Eaves 2008; Schatton, Murphy et al. 2008). These studies found that the cells with tumorigenic potential have cell surface markers similar to those on normal stem cells of the same tissue. These findings supported the notion that the cancer cells that could actually populate a tumor represent a distinct subset having similarity to stem cells.

However, a recent report using even more highly immunocompromised mice demonstrated the formation of tumors from single-cell transplants of unselected melanoma cells (Quintana, Shackleton et al. 2008). The authors found that 27% or about one in four individual melanoma cells formed tumors under these more permissive conditions, indicating that cells with tumorigenic potential are more common than the cancer stem cell hypothesis originally proposed (Quintana, Shackleton et al. 2008). The authors then assessed whether the tumorigenic melanoma cells were phenotypically distinct from melanoma cells that failed to form tumors. Many proteins shown to mark cancer stem cell populations in other studies were tested, but in

every case, tumors arose from all fractions of cells despite heterogeneous expression of these proteins.

One protein tested was CD133, a cell surface marker commonly expressed on stem cells whose presence was previously shown to increase tumorigenicity 200-fold (O'Brien, Pollett et al. 2007). Interestingly, tumors derived from either CD133⁺ or CD133⁻ cells were later found to contain both CD133⁺ and CD133⁻ cells, irrespective of the pool of cells from which they were derived (Quintana, Shackleton et al. 2008). The time-scale of such “re-mixing” has been examined for 20 proteins (Sigal, Milo et al. 2006); remixing has also been independently observed for two stem cell markers, Nanog and Sca-1 (Chambers, Silva et al. 2007; Chang, Hemberg et al. 2008). These results raise the possibility that cancer cells that are capable of forming tumors are not necessarily genetically or epigenetically distinct, static entities. Rather, noise in gene expression could transiently create subpopulations of cells that express a specific set of initial conditions that favors tumor formation. Indeed, a report from 25 years ago found that the majority of melanoma cells were non-metastatic, but the cells that did possess metastatic potential were unstable and lost at very high rates (Hill, Chambers et al. 1984; Ling, Chambers et al. 1984). The authors dubbed such rapid variations “dynamic heterogeneity”, which could be due to genomic instability or possibly non-genetic cell-to-cell variability.

5.2.3 Fractional killing of tumors

Understanding the sensitivity and resistance of tumors to drug treatment, both across cancer types and within a single tumor, is critical for effective treatment. It is well known clinically that one round of chemotherapy does not kill all the cells in a tumor, a poorly understood phenomenon known as “fractional cell kill.” The fractional kill hypothesis states that a defined chemotherapy concentration applied for a defined time period will kill a constant

fraction of the cells in a population, independent of the absolute number of cells (Berenbaum 1972; Skipper 1979; Chabner and Longo 2006). In solid tumors, access of the drug to the tumor can limit the fraction of tumor cells killed, but the validity of the fractional kill hypothesis has been established in animal models of leukemia as well as in human leukemia and lymphoma, where drug access is less of an issue (Chabner and Longo 2006). Because only a fraction of the cells die with each treatment, repeated doses must be administered to continue to reduce the size of the tumor (Skeel 2003). Current chemotherapy regimens apply drug treatment in cycles, with the frequency and duration of treatments limited by toxicity to the patient (Chabner and Longo 2006). The goal is to reduce the tumor population to zero with successive fractional kills (Chabner and Longo 2006). For example, assuming a 99% kill per cycle of chemotherapy, a tumor of 10^{11} cells would be reduced to less than one cell with six treatment cycles: $10^{11} * 0.01^6 < 1$ (Chabner and Longo 2006). However, the tumor can also re-grow during the intervals between treatments, limiting the net reduction of each fractional kill (Skeel 2003).

The fractional killing of tumors in response to treatment is assumed to be due to the cell cycle specificity of chemotherapy drugs (Skeel 2003; Chabner and Longo 2006). Cytarabine, a DNA-synthesis inhibitor also known as ara-C, is cited as the classic cell cycle phase-specific agent (Skeel 2003). Chemotherapy dosing schedules have been optimized based on the fact that cytarabine is only expected to be effective in the DNA synthesis (S) phase of the cell cycle (Skeel 2003). Consistent with this, leukemia patients respond better to cytarabine treatments given every 12 hours rather than every 24 hours. This finding that can be explained by the fact that S-phase in these leukemia cells lasts 18-20 hours, allowing some cells to escape the cytotoxic effect of the drug if it is given every 24 hours (Skeel 2003). However, alternative explanations are possible, as described below. A trace through the literature on the S-phase

specificity of cytarabine leads to literature that simply assumes S-phase specificity based on cytarabine's reported site of biochemical action (Skipper, Schabel et al. 1970), which the later papers reference.

Very little direct information is available on whether cells undergo apoptosis from a certain point in the cell cycle (Cotter, Glynn et al. 1992). One study which did address this topic used flow cytometry or elutriation of synchronized cells treated with actinomycin D1, camptothecin, or aphidicolin, each of which had been documented to exert its effects in a particular phase of the cell cycle (Cotter, Glynn et al. 1992). Surprisingly, the authors found that each of the agents was able to induce apoptosis in all phases of the cell cycle, suggesting that the mechanism through which the drugs induce apoptosis may be independent of the drugs' biochemical targets (Cotter, Glynn et al. 1992). The lack of cell cycle effect for camptothecin has been confirmed recently in a live-cell microscopy study (Cohen, Geva-Zatorsky et al. 2008). To my knowledge, a concerted effort has not been undertaken to prove the phase specificity of classic chemotherapy drugs, upon which explanations of fractional kill currently rely. These assumptions would be worth testing using modern cell biology methods, for example with time-lapse imaging of the recently published cell cycle phase reporters (Sakaue-Sawano, Kurokawa et al. 2008).

Indeed, this thesis raises the possibility that cell-to-cell variability in protein concentrations may contribute to fractional killing in the case of TRAIL treatment. I have observed fractional killing at a single cell level in every cell line examined, even in genetically identical populations grown in homogenous environments, and have ruled out the conventional explanation (cell cycle effects) in two of these lines. Variability in the timing and probability of death is not simply a feature of TRAIL treatment, as variability in response has been observed in

cells treated with both ionizing radiation and many other cancer drugs in clinical use including camptothecin and taxol (Lahav, Rosenfeld et al. 2004; Geva-Zatorsky, Rosenfeld et al. 2006; Cohen, Geva-Zatorsky et al. 2008; Gascoigne and Taylor 2008). More likely, variability in cell fate will eventually be regarded as a general feature of apoptotic response. A better understanding of the determinants of fractional kill in the controlled environment of a cell culture system should contribute to the understanding of fractional killing in tumors, and could ultimately have ramifications for the dosing and timing of chemotherapy treatment in patients.

5.3 Future Directions

A number of possible lines of future study stem from this thesis. A priori prediction of which cells will live and which cells will die in response to TRAIL as well as other drugs remains elusive. In the continued quest to understand this non-genetic variability in cell fate, two lines of experimentation using time-lapse microscopy could be informative. In the context of TRAIL-induced apoptosis, endogenously tagging (for example, using adeno-associated virus technology) (Rago, Vogelstein et al. 2007) the most sensitive species in the pathway with fluorescent proteins would be valuable. This would facilitate measurement of the timescales of fluctuations in key proteins such as Bid, Bax, and Bcl-2 and could potentially enable prediction of cell fate. If successful, variability in cell fate could be definitively demonstrated to be a function of transient fluctuations in protein levels. A second set of fruitful live-cell microscopy experiments would involve using the newly published fluorescent cell cycle reporters (Sakaue-Sawano, Kurokawa et al. 2008) to screen a panel of cancer drugs for potential cell cycle phase dependence. As discussed above, cell cycle effects on variability in drug response are likely to be less prominent than currently assumed.

Currently, the time between chemotherapy treatments is determined largely by toxicity to the patient; the next dose is given as soon as the patient is able to tolerate an additional dose of the drug. However, given my observations of fractional killing by TRAIL and the timescales of transient resistance to re-treatment, perhaps the commonly used dosing regimen is sub-optimal. For example, this thesis suggests that tumor cells that survive an initial treatment with TRAIL one day may be completely resistant to treatment one or two days later. In this case, re-treating the tumor too soon could waste expensive drugs and cause unnecessary toxicity to the patient; conversely, allowing too much time to elapse between treatments would permit the surviving cells to replenish the tumor, negating any progress in tumor eradication. The data gathered in this thesis could be used to build and calibrate a mathematical model that would take into consideration a particular cancer cell type's rate of decay of transient resistance, the cancer cell type's doubling rate, and a drug's fractional kill to forecast the optimal chemotherapy dosing scheme. Perhaps a lower concentration and more frequent dosing based on model predictions would be more effective than a maximally tolerated dose given at the shortest possible interval. Model predictions could be tested in cancer cell lines and later in mice carrying xenografts of human tumors.

The identification of biomarkers to select patients whose cancers will be sensitive to TRAIL would be clinically valuable (Ashkenazi and Herbst 2008). Many studies have examined possible causes of sensitivity or resistance to TRAIL across cancer cell lines in experiments that measure one or a few nodes in the pathway. However, even among genetically identical cells grown in a homogenous environment, the response to TRAIL is complex and heterogeneous. As this thesis shows, single gene measurements are not likely to predict sensitivity or resistance to death-inducing agents. The life-or-death decision is made by a complex network of interacting

proteins whose levels and states govern the fate of the cell. Therefore, simultaneous measurement of many network nodes to assess the state of the cell will be necessary for prediction of a particular cell type's susceptibility to TRAIL. One approach that is currently underway in our lab involves the use of Luminex's xMAP technology to multiplex measurements of up to 17 protein levels or states of apoptotic regulators.

Our model of TRAIL-induced apoptosis contains several estimated parameter values, such as initial conditions and reaction rates. Thus, there may be multiple parameter sets that could produce the basic dynamics of the signaling pathway. An important future direction for parameter estimation and model calibration involves using single cell experimental data to constrain parameter values. Our group now has a large collection of dynamic single cell data of perturbed and wild-type cells that can be used for automated calibration of the model. The measurements of cell-to-cell variability described in this thesis are optimal for a Bayesian statistical approach using Markov Chain Monte Carlo techniques. This approach combines prior information regarding model parameters with information in the data to produce a distribution of possible parameter values (Wilkinson 2009). These resulting distributions should anticipate future measurements of heterogeneity in protein levels, a key contributor to variability in apoptosis.

5.4 Closing thoughts

I hope that this thesis brings awareness of the potential of non-genetic variability to influence many diverse processes, including apoptosis. The findings described here have relevance to understanding the dynamics of natural selection, the malignant potential of individual cancer cells, as well as fractional killing in cancer treatment. In general, my work

suggests that non-genetic factors can have an unanticipated role in explaining sensitivity and resistance to chemotherapy

6 References

- Al-Hajj, M., M. S. Wicha, et al. (2003). "Prospective identification of tumorigenic breast cancer cells." Proc Natl Acad Sci U S A **100**(7): 3983-8.
- Albeck, J. G., J. M. Burke, et al. (2008a). "Quantitative analysis of pathways controlling extrinsic apoptosis in single cells." Mol Cell **30**(1): 11-25.
- Albeck, J. G., J. M. Burke, et al. (2008b). "Modeling a snap-action, variable-delay switch controlling extrinsic cell death." PLoS Biol **6**(12): 2831-52.
- Alberts, B., A. Johnson, et al. (2002). Molecular Biology of the Cell, Garland Science.
- Altan-Bonnet, G. and R. N. Germain (2005). "Modeling T cell antigen discrimination based on feedback control of digital ERK responses." PLoS Biol **3**(11): e356.
- Arkin, A., J. Ross, et al. (1998). "Stochastic kinetic analysis of developmental pathway bifurcation in phage lambda-infected Escherichia coli cells." Genetics **149**(4): 1633-48.
- Ashkenazi, A. and R. S. Herbst (2008). "To kill a tumor cell: the potential of proapoptotic receptor agonists." J Clin Invest **118**(6): 1979-90.
- Austin, D. W., M. S. Allen, et al. (2006). "Gene network shaping of inherent noise spectra." Nature **439**(7076): 608-11.
- Balaban, N. Q., J. Merrin, et al. (2004). "Bacterial persistence as a phenotypic switch." Science **305**(5690): 1622-5.

- Bar-Even, A., J. Paulsson, et al. (2006). "Noise in protein expression scales with natural protein abundance." Nat Genet **38**(6): 636-43.
- Barkai, N. and S. Leibler (1997). "Robustness in simple biochemical networks." Nature **387**(6636): 913-7.
- Becskei, A., B. B. Kaufmann, et al. (2005). "Contributions of low molecule number and chromosomal positioning to stochastic gene expression." Nat Genet **37**(9): 937-44.
- Becskei, A. and L. Serrano (2000). "Engineering stability in gene networks by autoregulation." Nature **405**(6786): 590-3.
- Bentele, M., I. Lavrik, et al. (2004). "Mathematical modeling reveals threshold mechanism in CD95-induced apoptosis." J Cell Biol **166**(6): 839-51.
- Berenbaum, M. C. (1972). "In vivo determination of the fractional kill of human tumor cells by chemotherapeutic agents." Cancer Chemother Rep **56**(5): 563-71.
- Blake, W. J., G. Balazsi, et al. (2006). "Phenotypic consequences of promoter-mediated transcriptional noise." Mol Cell **24**(6): 853-65.
- Blake, W. J., K. A. M, et al. (2003). "Noise in eukaryotic gene expression." Nature **422**(6932): 633-7.
- Boatright, K. M., C. Deis, et al. (2004). "Activation of caspases-8 and -10 by FLIP(L)." Biochem J **382**(Pt 2): 651-7.
- Boatright, K. M., M. Renatus, et al. (2003). "A unified model for apical caspase activation." Mol Cell **11**(2): 529-41.
- Boise, L. H., M. Gonzalez-Garcia, et al. (1993). "bcl-x, a bcl-2-related gene that functions as a dominant regulator of apoptotic cell death." Cell **74**(4): 597-608.
- Bonnet, D. and J. E. Dick (1997). "Human acute myeloid leukemia is organized as a hierarchy that originates from a primitive hematopoietic cell." Nat Med **3**(7): 730-7.

- Bose, K., C. Pop, et al. (2003). "An uncleavable procaspase-3 mutant has a lower catalytic efficiency but an active site similar to that of mature caspase-3." Biochemistry **42**(42): 12298-310.
- Bouralexis, S., D. M. Findlay, et al. (2005). "Death to the bad guys: targeting cancer via Apo2L/TRAIL." Apoptosis **10**(1): 35-51.
- Brock, A., H. Chang, et al. (2009). "Non-genetic heterogeneity - a mutation-independent driving force for the somatic evolution of tumours." Nat Rev Genet.
- Chabner, B. and D. L. Longo (2006). Cancer Chemotherapy and Biotherapy: Principles and Practice. Philadelphia, Lippincott Williams & Wilkins.
- Chambers, I., J. Silva, et al. (2007). "Nanog safeguards pluripotency and mediates germline development." Nature **450**(7173): 1230-4.
- Chang, D. W., Z. Xing, et al. (2003). "Interdimer processing mechanism of procaspase-8 activation." Embo J **22**(16): 4132-42.
- Chang, D. W., Z. Xing, et al. (2002). "c-FLIP(L) is a dual function regulator for caspase-8 activation and CD95-mediated apoptosis." Embo J **21**(14): 3704-14.
- Chang, H. H., M. Hemberg, et al. (2008). "Transcriptome-wide noise controls lineage choice in mammalian progenitor cells." Nature **453**(7194): 544-7.
- Chaudhary, P. M., M. Eby, et al. (1997). "Death receptor 5, a new member of the TNFR family, and DR4 induce FADD-dependent apoptosis and activate the NF-kappaB pathway." Immunity **7**(6): 821-30.
- Chen, W. W., B. Schoeberl, et al. (2009). "Input-output behavior of ErbB signaling pathways as revealed by a mass action model trained against dynamic data." Mol Syst Biol **5**: 239.
- Cheng, E. H., M. C. Wei, et al. (2001). "BCL-2, BCL-X(L) sequester BH3 domain-only molecules preventing BAX- and BAK-mediated mitochondrial apoptosis." Mol Cell **8**(3): 705-11.
- Chubb, J. R., T. Trcek, et al. (2006). "Transcriptional pulsing of a developmental gene." Curr Biol **16**(10): 1018-25.

- Clarke, P. G. and S. Clarke (1995). "Historic apoptosis." Nature **378**(6554): 230.
- Cohen, A. A., N. Geva-Zatorsky, et al. (2008). "Dynamic proteomics of individual cancer cells in response to a drug." Science **322**(5907): 1511-6.
- Colman-Lerner, A., A. Gordon, et al. (2005). "Regulated cell-to-cell variation in a cell-fate decision system." Nature **437**(7059): 699-706.
- Cotter, T. G., J. M. Glynn, et al. (1992). "The induction of apoptosis by chemotherapeutic agents occurs in all phases of the cell cycle." Anticancer Res **12**(3): 773-9.
- Coustan-Smith, E., A. Kitanaka, et al. (1996). "Clinical relevance of BCL-2 overexpression in childhood acute lymphoblastic leukemia." Blood **87**(3): 1140-6.
- Cretney, E., K. Takeda, et al. (2002). "Increased susceptibility to tumor initiation and metastasis in TNF-related apoptosis-inducing ligand-deficient mice." J Immunol **168**(3): 1356-61.
- Debnath, J., S. K. Muthuswamy, et al. (2003). "Morphogenesis and oncogenesis of MCF-10A mammary epithelial acini grown in three-dimensional basement membrane cultures." Methods **30**(3): 256-68.
- Degli-Esposti, M. A., W. C. Dougall, et al. (1997). "The novel receptor TRAIL-R4 induces NF-kappaB and protects against TRAIL-mediated apoptosis, yet retains an incomplete death domain." Immunity **7**(6): 813-20.
- Degli-Esposti, M. A., P. J. Smolak, et al. (1997). "Cloning and characterization of TRAIL-R3, a novel member of the emerging TRAIL receptor family." J Exp Med **186**(7): 1165-70.
- Dekel, E. and U. Alon (2005). "Optimality and evolutionary tuning of the expression level of a protein." Nature **436**(7050): 588-92.
- Deveraux, Q. L., R. Takahashi, et al. (1997). "X-linked IAP is a direct inhibitor of cell-death proteases." Nature **388**(6639): 300-4.
- Donepudi, M., A. Mac Sweeney, et al. (2003). "Insights into the regulatory mechanism for caspase-8 activation." Mol Cell **11**(2): 543-9.

- Du, C., M. Fang, et al. (2000). "Smac, a mitochondrial protein that promotes cytochrome c-dependent caspase activation by eliminating IAP inhibition." Cell **102**(1): 33-42.
- Dublanche, Y., K. Michalodimitrakis, et al. (2006). "Noise in transcription negative feedback loops: simulation and experimental analysis." Mol Syst Biol **2**: 41.
- Eaves, C. J. (2008). "Cancer stem cells: Here, there, everywhere?" Nature **456**(7222): 581-2.
- Eggert, A., M. A. Grotzer, et al. (2001). "Resistance to tumor necrosis factor-related apoptosis-inducing ligand (TRAIL)-induced apoptosis in neuroblastoma cells correlates with a loss of caspase-8 expression." Cancer Res **61**(4): 1314-9.
- Eissing, T., F. Allgower, et al. (2005). "Robustness properties of apoptosis models with respect to parameter variations and intrinsic noise." Syst Biol (Stevenage) **152**(4): 221-8.
- Eissing, T., H. Conzelmann, et al. (2004). "Bistability analyses of a caspase activation model for receptor-induced apoptosis." J Biol Chem **279**(35): 36892-7.
- Ellis, H. M. and H. R. Horvitz (1986). "Genetic control of programmed cell death in the nematode *C. elegans*." Cell **44**(6): 817-29.
- Elowitz, M. B., A. J. Levine, et al. (2002). "Stochastic gene expression in a single cell." Science **297**(5584): 1183-6.
- Emery, J. G., P. McDonnell, et al. (1998). "Osteoprotegerin is a receptor for the cytotoxic ligand TRAIL." J Biol Chem **273**(23): 14363-7.
- Fadeel, B., S. Orrenius, et al. (1999). "Apoptosis in human disease: a new skin for the old ceremony?" Biochem Biophys Res Commun **266**(3): 699-717.
- Feinerman, O., J. Veiga, et al. (2008). "Variability and robustness in T cell activation from regulated heterogeneity in protein levels." Science **321**(5892): 1081-4.
- Ferguson, S. S. and M. G. Caron (1998). "G protein-coupled receptor adaptation mechanisms." Semin Cell Dev Biol **9**(2): 119-27.
- Fischer, U., R. U. Janicke, et al. (2003). "Many cuts to ruin: a comprehensive update of caspase substrates." Cell Death Differ **10**(1): 76-100.

- Fisher, M. J., A. K. Virmani, et al. (2001). "Nucleotide substitution in the ectodomain of trail receptor DR4 is associated with lung cancer and head and neck cancer." Clin Cancer Res **7**(6): 1688-97.
- Fuentes-Prior, P. and G. S. Salvesen (2004). "The protein structures that shape caspase activity, specificity, activation and inhibition." Biochem J **384**(Pt 2): 201-32.
- Fulda, S., M. U. Kufer, et al. (2001). "Sensitization for death receptor- or drug-induced apoptosis by re-expression of caspase-8 through demethylation or gene transfer." Oncogene **20**(41): 5865-77.
- Gascoigne, K. E. and S. S. Taylor (2008). "Cancer cells display profound intra- and interline variation following prolonged exposure to antimetabolic drugs." Cancer Cell **14**(2): 111-22.
- Geva-Zatorsky, N., N. Rosenfeld, et al. (2006). "Oscillations and variability in the p53 system." Mol Syst Biol **2**: 2006 0033.
- Gillespie, D. T. (1977). "Exact Stochastic Simulation of Coupled Chemical Reactions." The Journal of Physical Chemistry **81**(25): 2340-2361.
- Golding, I., J. Paulsson, et al. (2005). "Real-time kinetics of gene activity in individual bacteria." Cell **123**(6): 1025-36.
- Goldstein, J. C., R. M. Kluck, et al. (2000). "A single cell analysis of apoptosis. Ordering the apoptotic phenotype." Ann N Y Acad Sci **926**: 132-41.
- Goldstein, J. C., C. Munoz-Pinedo, et al. (2005). "Cytochrome c is released in a single step during apoptosis." Cell Death Differ **12**(5): 453-62.
- Goldstein, J. C., N. J. Waterhouse, et al. (2000). "The coordinate release of cytochrome c during apoptosis is rapid, complete and kinetically invariant." Nat Cell Biol **2**(3): 156-62.
- Griffith, T. S., S. R. Wiley, et al. (1999). "Monocyte-mediated tumoricidal activity via the tumor necrosis factor-related cytokine, TRAIL." J Exp Med **189**(8): 1343-54.
- Hanahan, D. and R. A. Weinberg (2000). "The hallmarks of cancer." Cell **100**(1): 57-70.

- Hill, R. P., A. F. Chambers, et al. (1984). "Dynamic heterogeneity: rapid generation of metastatic variants in mouse B16 melanoma cells." Science **224**(4652): 998-1001.
- Hinz, S., A. Trauzold, et al. (2000). "Bcl-XL protects pancreatic adenocarcinoma cells against CD95- and TRAIL-receptor-mediated apoptosis." Oncogene **19**(48): 5477-86.
- Hockenbery, D., G. Nunez, et al. (1990). "Bcl-2 is an inner mitochondrial membrane protein that blocks programmed cell death." Nature **348**(6299): 334-6.
- Hoffmann, A., A. Levchenko, et al. (2002). "The IkappaB-NF-kappaB signaling module: temporal control and selective gene activation." Science **298**(5596): 1241-5.
- Hopkins-Donaldson, S., A. Ziegler, et al. (2003). "Silencing of death receptor and caspase-8 expression in small cell lung carcinoma cell lines and tumors by DNA methylation." Cell Death Differ **10**(3): 356-64.
- Hua, F., M. G. Cornejo, et al. (2005). "Effects of Bcl-2 levels on Fas signaling-induced caspase-3 activation: molecular genetic tests of computational model predictions." J Immunol **175**(2): 985-995.
- Hutchins, J. B. and S. W. Barger (1998). "Why neurons die: cell death in the nervous system." Anat Rec **253**(3): 79-90.
- Ichikawa, K., W. Liu, et al. (2001). "Tumoricidal activity of a novel anti-human DR5 monoclonal antibody without hepatocyte cytotoxicity." Nat Med **7**(8): 954-60.
- Inohara, N., T. Koseki, et al. (1999). "Identification of regulatory and catalytic domains in the apoptosis nuclease DFF40/CAD." J Biol Chem **274**(1): 270-4.
- Irmeler, M., M. Thome, et al. (1997). "Inhibition of death receptor signals by cellular FLIP." Nature **388**(6638): 190-5.
- Jo, M., T. H. Kim, et al. (2000). "Apoptosis induced in normal human hepatocytes by tumor necrosis factor-related apoptosis-inducing ligand." Nat Med **6**(5): 564-7.
- Johnstone, R. W., A. J. Frew, et al. (2008). "The TRAIL apoptotic pathway in cancer onset, progression and therapy." Nat Rev Cancer **8**(10): 782-98.

- Kaufmann, B. B., Q. Yang, et al. (2007). "Heritable stochastic switching revealed by single-cell genealogy." PLoS Biol **5**(9): e239.
- Kaufmann, S. H. (1989). "Induction of endonucleolytic DNA cleavage in human acute myelogenous leukemia cells by etoposide, camptothecin, and other cytotoxic anticancer drugs: a cautionary note." Cancer Res **49**(21): 5870-8.
- Kaufmann, S. H. and W. C. Earnshaw (2000). "Induction of apoptosis by cancer chemotherapy." Exp Cell Res **256**(1): 42-9.
- Keeble, J. A. and A. P. Gilmore (2007). "Apoptosis commitment--translating survival signals into decisions on mitochondria." Cell Res **17**(12): 976-84.
- Kerr, J. F., A. H. Wyllie, et al. (1972). "Apoptosis: a basic biological phenomenon with wide-ranging implications in tissue kinetics." Br J Cancer **26**(4): 239-57.
- Kim, H. E., F. Du, et al. (2005). "Formation of apoptosome is initiated by cytochrome c-induced dATP hydrolysis and subsequent nucleotide exchange on Apaf-1." Proc Natl Acad Sci U S A **102**(49): 17545-50.
- Kim, K., M. J. Fisher, et al. (2000). "Molecular determinants of response to TRAIL in killing of normal and cancer cells." Clin Cancer Res **6**(2): 335-46.
- Kischkel, F. C., S. Hellbardt, et al. (1995). "Cytotoxicity-dependent APO-1 (Fas/CD95)-associated proteins form a death-inducing signaling complex (DISC) with the receptor." Embo J **14**(22): 5579-88.
- Kuwana, T., M. R. Mackey, et al. (2002). "Bid, Bax, and lipids cooperate to form supramolecular openings in the outer mitochondrial membrane." Cell **111**(3): 331-42.
- Lahav, G., N. Rosenfeld, et al. (2004). "Dynamics of the p53-Mdm2 feedback loop in individual cells." Nat Genet **36**(2): 147-50.
- Le Roy, C. and J. L. Wrana (2005). "Clathrin- and non-clathrin-mediated endocytic regulation of cell signalling." Nat Rev Mol Cell Biol **6**(2): 112-26.
- Lee, S. H., M. S. Shin, et al. (1999). "Alterations of the DR5/TRAIL receptor 2 gene in non-small cell lung cancers." Cancer Res **59**(22): 5683-6.

- Lee, S. H., M. S. Shin, et al. (2001). "Somatic mutations of TRAIL-receptor 1 and TRAIL-receptor 2 genes in non-Hodgkin's lymphoma." Oncogene **20**(3): 399-403.
- Legewie, S., N. Bluthgen, et al. (2006). "Mathematical modeling identifies inhibitors of apoptosis as mediators of positive feedback and bistability." PLoS Comput Biol **2**(9): e120.
- Leist, M. and M. Jaattela (2001). "Four deaths and a funeral: from caspases to alternative mechanisms." Nat Rev Mol Cell Biol **2**(8): 589-98.
- Letai, A., M. C. Bassik, et al. (2002). "Distinct BH3 domains either sensitize or activate mitochondrial apoptosis, serving as prototype cancer therapeutics." Cancer Cell **2**(3): 183-92.
- Letai, A. G. (2008). "Diagnosing and exploiting cancer's addiction to blocks in apoptosis." Nat Rev Cancer **8**(2): 121-32.
- Li, H., H. Zhu, et al. (1998). "Cleavage of BID by caspase 8 mediates the mitochondrial damage in the Fas pathway of apoptosis." Cell **94**(4): 491-501.
- Li, P., D. Nijhawan, et al. (1997). "Cytochrome c and dATP-dependent formation of Apaf-1/caspase-9 complex initiates an apoptotic protease cascade." Cell **91**(4): 479-89.
- Ling, V., A. F. Chambers, et al. (1984). "Dynamic heterogeneity and metastasis." J Cell Physiol Suppl **3**: 99-103.
- Liu, X., P. Li, et al. (1998). "The 40-kDa subunit of DNA fragmentation factor induces DNA fragmentation and chromatin condensation during apoptosis." Proc Natl Acad Sci U S A **95**(15): 8461-6.
- Lowe, S. W., E. Cepero, et al. (2004). "Intrinsic tumour suppression." Nature **432**(7015): 307-15.
- Luo, X., I. Budihardjo, et al. (1998). "Bid, a Bcl2 interacting protein, mediates cytochrome c release from mitochondria in response to activation of cell surface death receptors." Cell **94**(4): 481-90.
- McAdams, H. H. and A. Arkin (1997). "Stochastic mechanisms in gene expression." Proc Natl Acad Sci U S A **94**(3): 814-9.

- Medema, J. P., C. Scaffidi, et al. (1997). "FLICE is activated by association with the CD95 death-inducing signaling complex (DISC)." Embo J **16**(10): 2794-804.
- Meier, P., A. Finch, et al. (2000). "Apoptosis in development." Nature **407**(6805): 796-801.
- Micheau, O., S. Lens, et al. (2001). "NF-kappaB signals induce the expression of c-FLIP." Mol Cell Biol **21**(16): 5299-305.
- Miyashita, T. and J. C. Reed (1995). "Tumor suppressor p53 is a direct transcriptional activator of the human bax gene." Cell **80**(2): 293-9.
- Munoz-Pinedo, C., A. Guio-Carrion, et al. (2006). "Different mitochondrial intermembrane space proteins are released during apoptosis in a manner that is coordinately initiated but can vary in duration." Proc Natl Acad Sci U S A **103**(31): 11573-8.
- Nechushtan, A., C. L. Smith, et al. (2001). "Bax and Bak coalesce into novel mitochondria-associated clusters during apoptosis." J Cell Biol **153**(6): 1265-76.
- Nelson, D. E., A. E. Ihekweba, et al. (2004). "Oscillations in NF-kappaB signaling control the dynamics of gene expression." Science **306**(5696): 704-8.
- Newman, J. R., S. Ghaemmaghami, et al. (2006). "Single-cell proteomic analysis of *S. cerevisiae* reveals the architecture of biological noise." Nature **441**(7095): 840-6.
- Ng, C. P. and B. Bonavida (2002). "X-linked inhibitor of apoptosis (XIAP) blocks Apo2 ligand/tumor necrosis factor-related apoptosis-inducing ligand-mediated apoptosis of prostate cancer cells in the presence of mitochondrial activation: sensitization by overexpression of second mitochondria-derived activator of caspase/direct IAP-binding protein with low pl (Smac/DIABLO)." Mol Cancer Ther **1**(12): 1051-8.
- Ng, C. P., A. Zisman, et al. (2002). "Synergy is achieved by complementation with Apo2L/TRAIL and actinomycin D in Apo2L/TRAIL-mediated apoptosis of prostate cancer cells: role of XIAP in resistance." Prostate **53**(4): 286-99.
- O'Brien, C. A., A. Pollett, et al. (2007). "A human colon cancer cell capable of initiating tumour growth in immunodeficient mice." Nature **445**(7123): 106-10.

- Okano, H., K. Shiraki, et al. (2003). "Cellular FLICE/caspase-8-inhibitory protein as a principal regulator of cell death and survival in human hepatocellular carcinoma." Lab Invest **83**(7): 1033-43.
- Oltvai, Z. N., C. L. Milliman, et al. (1993). "Bcl-2 heterodimerizes in vivo with a conserved homolog, Bax, that accelerates programmed cell death." Cell **74**(4): 609-19.
- Ozbudak, E. M., M. Thattai, et al. (2002). "Regulation of noise in the expression of a single gene." Nat Genet **31**(1): 69-73.
- Pan, G., J. Ni, et al. (1997). "An antagonist decoy receptor and a death domain-containing receptor for TRAIL." Science **277**(5327): 815-8.
- Pedraza, J. M. and A. van Oudenaarden (2005). "Noise propagation in gene networks." Science **307**(5717): 1965-9.
- Pop, C., Y. R. Chen, et al. (2001). "Removal of the pro-domain does not affect the conformation of the procaspase-3 dimer." Biochemistry **40**(47): 14224-35.
- Quintana, E., M. Shackleton, et al. (2008). "Efficient tumour formation by single human melanoma cells." Nature **456**(7222): 593-8.
- Rago, C., B. Vogelstein, et al. (2007). "Genetic knockouts and knockins in human somatic cells." Nat Protoc **2**(11): 2734-46.
- Raj, A. and A. van Oudenaarden (2008). "Nature, nurture, or chance: stochastic gene expression and its consequences." Cell **135**(2): 216-26.
- Rando, O. J. and K. J. Verstrepen (2007). "Timescales of genetic and epigenetic inheritance." Cell **128**(4): 655-68.
- Raser, J. M. and E. K. O'Shea (2004). "Control of stochasticity in eukaryotic gene expression." Science **304**(5678): 1811-4.
- Rehm, M., H. Dussmann, et al. (2002). "Single-cell fluorescence resonance energy transfer analysis demonstrates that caspase activation during apoptosis is a rapid process. Role of caspase-3." J Biol Chem **277**(27): 24506-14.

- Rehm, M., H. Dussmann, et al. (2003). "Real-time single cell analysis of Smac/DIABLO release during apoptosis." J Cell Biol **162**(6): 1031-43.
- Reya, T., S. J. Morrison, et al. (2001). "Stem cells, cancer, and cancer stem cells." Nature **414**(6859): 105-11.
- Ricci-Vitiani, L., D. G. Lombardi, et al. (2007). "Identification and expansion of human colon-cancer-initiating cells." Nature **445**(7123): 111-5.
- Rodriguez, J. and Y. Lazebnik (1999). "Caspase-9 and APAF-1 form an active holoenzyme." Genes Dev **13**(24): 3179-84.
- Rosenfeld, N., J. W. Young, et al. (2005). "Gene regulation at the single-cell level." Science **307**(5717): 1962-5.
- Sakaue-Sawano, A., H. Kurokawa, et al. (2008). "Visualizing spatiotemporal dynamics of multicellular cell-cycle progression." Cell **132**(3): 487-98.
- Schatton, T., G. F. Murphy, et al. (2008). "Identification of cells initiating human melanomas." Nature **451**(7176): 345-9.
- Sheridan, J. P., S. A. Marsters, et al. (1997). "Control of TRAIL-induced apoptosis by a family of signaling and decoy receptors." Science **277**(5327): 818-21.
- Shin, M. S., H. S. Kim, et al. (2001). "Mutations of tumor necrosis factor-related apoptosis-inducing ligand receptor 1 (TRAIL-R1) and receptor 2 (TRAIL-R2) genes in metastatic breast cancers." Cancer Res **61**(13): 4942-6.
- Sigal, A., R. Milo, et al. (2006). "Variability and memory of protein levels in human cells." Nature **444**(7119): 643-6.
- Singh, S. K., C. Hawkins, et al. (2004). "Identification of human brain tumour initiating cells." Nature **432**(7015): 396-401.
- Skeel, R. T. (2003). Handbook of Cancer Chemotherapy, Lippincott Williams & Wilkins.
- Skipper, H. E. (1979). "Historic milestones in cancer biology: a few that are important in cancer treatment (revisited)." Semin Oncol **6**(4): 506-14.

- Skipper, H. E., F. M. Schabel, Jr., et al. (1970). "Implications of biochemical, cytokinetic, pharmacologic, and toxicologic relationships in the design of optimal therapeutic schedules." Cancer Chemother Rep **54**(6): 431-50.
- Smyth, M. J., E. Cretny, et al. (2001). "Tumor necrosis factor-related apoptosis-inducing ligand (TRAIL) contributes to interferon gamma-dependent natural killer cell protection from tumor metastasis." J Exp Med **193**(6): 661-70.
- Sorkin, A. and L. K. Goh (2008). "Endocytosis and intracellular trafficking of ErbBs." Exp Cell Res **314**(17): 3093-106.
- Spencer, S. L., S. Gaudet, et al. (2009). "Non-genetic origins of cell-to-cell variability in TRAIL-induced apoptosis." Nature **advance online publication**.
- Spudich, J. L. and D. E. Koshland, Jr. (1976). "Non-genetic individuality: chance in the single cell." Nature **262**(5568): 467-71.
- Stewart, G. R., B. D. Robertson, et al. (2003). "Tuberculosis: a problem with persistence." Nat Rev Microbiol **1**(2): 97-105.
- Suel, G. M., J. Garcia-Ojalvo, et al. (2006). "An excitable gene regulatory circuit induces transient cellular differentiation." Nature **440**(7083): 545-50.
- Suel, G. M., R. P. Kulkarni, et al. (2007). "Tunability and noise dependence in differentiation dynamics." Science **315**(5819): 1716-9.
- Suzuki, Y., Y. Nakabayashi, et al. (2001). "Ubiquitin-protein ligase activity of X-linked inhibitor of apoptosis protein promotes proteasomal degradation of caspase-3 and enhances its anti-apoptotic effect in Fas-induced cell death." Proc Natl Acad Sci U S A **98**(15): 8662-7.
- Takeda, K., Y. Hayakawa, et al. (2001). "Involvement of tumor necrosis factor-related apoptosis-inducing ligand in surveillance of tumor metastasis by liver natural killer cells." Nat Med **7**(1): 94-100.
- Takeda, K., M. J. Smyth, et al. (2002). "Critical role for tumor necrosis factor-related apoptosis-inducing ligand in immune surveillance against tumor development." J Exp Med **195**(2): 161-9.

- Teitz, T., T. Wei, et al. (2000). "Caspase 8 is deleted or silenced preferentially in childhood neuroblastomas with amplification of MYCN." Nat Med **6**(5): 529-35.
- Tepper, C. G. and M. F. Seldin (1999). "Modulation of caspase-8 and FLICE-inhibitory protein expression as a potential mechanism of Epstein-Barr virus tumorigenesis in Burkitt's lymphoma." Blood **94**(5): 1727-37.
- Tewari, M., L. T. Quan, et al. (1995). "Yama/CPP32 beta, a mammalian homolog of CED-3, is a CrmA-inhibitable protease that cleaves the death substrate poly(ADP-ribose) polymerase." Cell **81**(5): 801-9.
- Thattai, M. and A. van Oudenaarden (2001). "Intrinsic noise in gene regulatory networks." Proc Natl Acad Sci U S A **98**(15): 8614-9.
- Toettcher, J. E., A. Loewer, et al. (2009). "Distinct mechanisms act in concert to mediate cell cycle arrest." Proc Natl Acad Sci U S A **106**(3): 785-90.
- Tyas, L., V. A. Brophy, et al. (2000). "Rapid caspase-3 activation during apoptosis revealed using fluorescence-resonance energy transfer." EMBO Rep **1**(3): 266-70.
- Vaux, D. L., S. Cory, et al. (1988). "Bcl-2 gene promotes haemopoietic cell survival and cooperates with c-myc to immortalize pre-B cells." Nature **335**(6189): 440-2.
- Vaux, D. L. and S. J. Korsmeyer (1999). "Cell death in development." Cell **96**(2): 245-54.
- Verhagen, A. M., P. G. Ekert, et al. (2000). "Identification of DIABLO, a mammalian protein that promotes apoptosis by binding to and antagonizing IAP proteins." Cell **102**(1): 43-53.
- Volfson, D., J. Marciniak, et al. (2006). "Origins of extrinsic variability in eukaryotic gene expression." Nature **439**(7078): 861-4.
- Vousden, K. H. and X. Lu (2002). "Live or let die: the cell's response to p53." Nat Rev Cancer **2**(8): 594-604.
- Wagner, K. W., E. A. Punnoose, et al. (2007). "Death-receptor O-glycosylation controls tumor-cell sensitivity to the proapoptotic ligand Apo2L/TRAIL." Nat Med **13**(9): 1070-7.

- Walczak, H., R. E. Miller, et al. (1999). "Tumoricidal activity of tumor necrosis factor-related apoptosis-inducing ligand in vivo." Nat Med **5**(2): 157-63.
- Wang, X. (2001). "The expanding role of mitochondria in apoptosis." Genes Dev **15**(22): 2922-33.
- Wang, Y., I. H. Engels, et al. (2004). "Synthetic lethal targeting of MYC by activation of the DR5 death receptor pathway." Cancer Cell **5**(5): 501-12.
- Wei, M. C., T. Lindsten, et al. (2000). "tBID, a membrane-targeted death ligand, oligomerizes BAK to release cytochrome c." Genes Dev **14**(16): 2060-71.
- Wei, M. C., W. X. Zong, et al. (2001). "Proapoptotic BAX and BAK: a requisite gateway to mitochondrial dysfunction and death." Science **292**(5517): 727-30.
- Wilkinson, D. J. (2009). "Stochastic modelling for quantitative description of heterogeneous biological systems." Nat Rev Genet **10**(2): 122-33.
- Wolter, K. G., Y. T. Hsu, et al. (1997). "Movement of Bax from the cytosol to mitochondria during apoptosis." J Cell Biol **139**(5): 1281-92.
- Yang, X., M. S. Merchant, et al. (2003). "Induction of caspase 8 by interferon gamma renders some neuroblastoma (NB) cells sensitive to tumor necrosis factor-related apoptosis-inducing ligand (TRAIL) but reveals that a lack of membrane TR1/TR2 also contributes to TRAIL resistance in NB." Cancer Res **63**(5): 1122-9.
- Yang, Y., S. Fang, et al. (2000). "Ubiquitin protein ligase activity of IAPs and their degradation in proteasomes in response to apoptotic stimuli." Science **288**(5467): 874-7.
- Youle, R. J. and A. Strasser (2008). "The BCL-2 protein family: opposing activities that mediate cell death." Nat Rev Mol Cell Biol **9**(1): 47-59.
- Zerfa, N., J. A. Westwood, et al. (2005). "Cutting edge: TRAIL deficiency accelerates hematological malignancies." J Immunol **175**(9): 5586-90.
- Zhang, L. and B. Fang (2005). "Mechanisms of resistance to TRAIL-induced apoptosis in cancer." Cancer Gene Ther **12**(3): 228-37.

Zhang, X. D., X. Y. Zhang, et al. (2001). "Tumor necrosis factor-related apoptosis-inducing ligand-induced apoptosis of human melanoma is regulated by smac/DIABLO release from mitochondria." Cancer Res **61**(19): 7339-48.

Zou, H. and L. Niswander (1996). "Requirement for BMP signaling in interdigital apoptosis and scale formation." Science **272**(5262): 738-41.

Zuzarte-Luis, V. and J. M. Hurle (2002). "Programmed cell death in the developing limb." Int J Dev Biol **46**(7): 871-6.